

STRESS ANALYSIS OF WEBS WITH ECCENTRIC HOLES

by

  
Peter W.K. Chan, B. Eng.

A thesis submitted to the  
Faculty of Graduate Studies and Research  
McGill University  
in partial fulfillment for the degree of  
Master of Engineering

Department of Civil Engineering  
and Applied Mechanics

March, 1975.

TO

MY WIFE, PARENTS AND IN-LAWS

STRESS ANALYSIS OF WEBS WITH ECCENTRIC HOLES

Peter W.K. Chan

Department of Civil Engineering  
and Applied Mechanics,  
McGill University,  
Montreal, Canada.

M.Eng. Thesis  
March, 1975.

ABSTRACT

Methods of analysis for beams with circular holes, both mid-depth and eccentric, are investigated for both unreinforced and circularly reinforced holes. An approximate method of analysis is developed in which regions of a beam around a hole are analysed as curved beam sections and the stresses are calculated accordingly. In applying this approximation to circularly reinforced holes, modified cross-sections are used in calculating the stresses because of secondary bending of the curved reinforcement flanges. The application of the theory of elasticity method is discussed for the case of unreinforced holes. Experiments are described and it is shown that in the case of unreinforced holes, the curved beam approximation is more accurate than the theory of elasticity solution in predicting hole edge stresses for large holes and under high shear-to-moment ratios. This method is also found to be suitable for use in design of circular

reinforcements for the type of holes considered.

Design aids in the form of moment-shear interaction curves for unreinforced holes, and a computer program for reinforced holes are presented.

L'ANALYSE DES CONTRAINTES DE L'ÂME AVEC TROUS EXCENTRIQUES

Peter W.K. Chan

Département de génie civil  
et de mécanique appliquée,  
Université McGill,  
Montréal, Canada.

Thèse de maîtrise  
Mars, 1975.

RESUME

Les méthodes analytiques pour des poutres aux trous circulaires, à demi-profondeur et excentriques, sont étudiées pour des trous non-renforcés et circulairement renforcés. Une méthode approximative d'analyse est développée dans laquelle les régions d'une poutre autour d'un trou sont analysées comme des sections de poutres courbées et les contraintes sont calculées en conséquence. En appliquant cette approximation aux trous circulairement renforcés, les sections transversales modifiées sont utilisées dans le calcul des contraintes à cause de flexions secondaires des collets de renforcement courbés. L'application de la théorie des méthodes d'élasticité est discutée pour le cas des trous non-renforcés. Les essais sont décrits et il est montré que dans le cas des trous non-renforcés l'approximation pour les poutres courbées est plus précise que la solution de la théorie d'élasticité pour la prédiction des contraintes aux bords des trous pour des gros trous avec des rapports élevés de cisaillement au moment. Cette méthode peut

être aussi appliquée dans la conception de renforcements circulaires pour les types de trous considérés.

Des supports à la conception sous la forme de courbes d'interaction de moment-cisaillement pour des trous non-renforcés et un programme d'ordinateur pour les trous renforcés sont attachés.

TABLE OF CONTENTS

ABSTRACT		i
RESUME		iii
TABLE OF CONTENTS		v
LIST OF FIGURES		vii
FOREWORD		xi
ACKNOWLEDGEMENT		xiii
NOTATION		xv
CHAPTER 1	INTRODUCTION	1
	1.1 General	1
	1.2 Previous Work	3
	1.3 Scope	7
CHAPTER 2	UNREINFORCED HOLES	11
	2.1 Introduction	11
	2.2 Analysis	13
	2.2.1 Mid-Depth Holes	14
	2.2.2 Eccentric Holes	18
	2.3 Test Program and Results	20
	2.4 Conclusions	24
CHAPTER 3	REINFORCED HOLES	37
	3.1 Introduction	37
	3.2 Analysis	38
	3.2.1 Mid-Depth Holes	38
	3.2.2 Eccentric Holes	41

	3.3 Test Program and Results	42
	3.4 Conclusions	45
CHAPTER 4	EXPERIMENTAL PROGRAM	61
	4.1 Test Specimens	61
	4.2 Instrumentation	62
	4.3 Testing Procedure	63
	4.4 Analysis of Data	65
	4.5 Experimental Results	66
CHAPTER 5	DESIGN OF UNREINFORCED HOLES	70
	5.1 Derivation of Design Aids	70
	5.2 Example	73
	5.3 Conclusions	75
CHAPTER 6	SUMMARY AND CONCLUSIONS	91
APPENDIX I	SHEAR FORCE DIVISION	93
APPENDIX II	THEORY OF ELASTICITY SOLUTION	100
APPENDIX III	CURVED BEAM METHOD	105
APPENDIX IV	EQUATIONS OF CURVED BEAM METHOD IN NON-DIMENSIONAL FORM	111
APPENDIX V	COMPUTER PROGRAMS - EXPERIMENTS	115
APPENDIX VI	COMPUTER PROGRAM - THEORY OF ELASTICITY METHOD	128
APPENDIX VII	COMPUTER PROGRAM - CURVED BEAM METHOD	133
APPENDIX VIII	SUPPLEMENTAL RESULTS	142
BIBLIOGRAPHY		155

LIST OF FIGURES

Figure 1.1	Vierendeel Method	9
Figure 1.2	Equivalent Rectangular Hole	10
Figure 2.1	Curved Beam Idealisation	26
Figure 2.2	Typical Inclined Tee-Section	27
Figure 2.3	Details Of Test Beams	28
Figure 2.4	Instrumentation Of Beams	29
Figure 2.5	Hole Edge Stresses For Hole 1, Beam A	30
Figure 2.6	Hole Edge Stresses For Hole 2, Beam A	31
Figure 2.7	Hole Edge Stresses For Hole 3, Beam B	32
Figure 2.8	Hole Edge Stresses For Hole 4, Beam B	33
Figure 2.9	Shear Stresses At Hole Centreline For Hole 3, Beam B	34
Figure 2.10	Flange Stresses For Hole 2, Beam A	35
Figure 2.11	Flange Stresses For Hole 3, Beam B	35
Figure 2.12	Comparison Of Analytical Methods	36
Figure 3.1	Curved Beam Idealisation	47
Figure 3.2	Deflection Of Curved Reinforcement Flange	48
Figure 3.3	Details Of Test Beam	49
Figure 3.4	Instrumentation of Beam	50
Figure 3.5	Hole Edge Stresses For Hole 6, Beam C (M/V = 48")	51
Figure 3.6	Hole Edge Stresses For Hole 6, Beam C (M/V = 24")	52
Figure 3.7	Hole Edge Stresses For Hole 5, Beam C (M/V = 48")	53

Figure 3.8	Hole Edge Stresses For Hole 5, Beam C (M/V = 24")	54
Figure 3.9	Flange Stresses For Hole 5, Beam C (M/V = 48")	55
Figure 3.10	Flange Stresses For Hole 5, Beam C (M/V = 24")	56
Figure 3.11	Flange Stresses For Hole 6, Beam C (M/V = 48")	57
Figure 3.12	Flange Stresses For Hole 6, Beam C (M/V = 24")	58
Figure 3.13	Shear Stresses At Hole Centreline For Hole 5, Beam C	59
Figure 3.14	Shear Stresses At Hole Centreline For Hole 6, Beam C	60
Figure 4.1	Details Of Test Beams	68
Figure 4.2	Schemetic Diagram Showing Experimental Set Up	69
Figure 5.1	Component Regions Of Interaction Diagrams	76
Figure 5.2	Interaction Diagram For $2R/d = 0.20$	77
Figure 5.3	Interaction Diagram For $2R/d = 0.25$	78
Figure 5.4	Interaction Diagram For $2R/d = 0.30$	79
Figure 5.5	Interaction Diagram For $2R/d = 0.35$	80
Figure 5.6	Interaction Diagram For $2R/d = 0.40$	81
Figure 5.7	Interaction Diagram For $2R/d = 0.45$	82
Figure 5.8	Interaction Diagram For $2R/d = 0.50$	83
Figure 5.9	Interaction Diagram For $2R/d = 0.55$	84

Figure 5.10	Interaction Diagram For $2R/d = 0.60$	85
Figure 5.11	Interaction Diagram For $2R/d = 0.65$	86
Figure 5.12	Interaction Diagram For $2R/d = 0.70$	87
Figure 5.13	Interaction Diagram For $2R/d = 0.75$	88
Figure 5.14	Proportion Of Shear Force Carried In Top Tee-Section	89
Figure 5.15	Example Beam And Interaction Diagram	90
Figure I.1	Free Body Diagram For Shear Division	98
Figure I.2	Typical Vertical Tee-Section	99
Figure III.1	Curved Beam Method	110
Figure VIII.1	Hole Edge Stresses For Hole 1, Beam A ( $M/V = 48"$ )	144
Figure VIII.2	Hole Edge Stresses For Hole 2, Beam A ( $M/V = 48"$ )	145
Figure VIII.3	Shear Stresses At Hole Centreline For Hole 1, Beam A	146
Figure VIII.4	Shear Stresses At Hole Centreline For Hole 3, Beam B	147
Figure VIII.5	Shear Stresses At Hole Centreline For Hole 4, Beam B	148
Figure VIII.6	Comparison Of Results Obtained In Ref. 10	149
Figure VIII.7	Flange Stresses For Hole 1, Beam A	150
Figure VIII.8	Flange Stresses For Hole 2, Beam A ( $M/V = 48"$ )	151
Figure VIII.9	Flange Stresses For Hole 3, Beam B ( $M/V = 24"$ )	152

Figure VIII.10 Flange Stresses For Hole 4, Beam B

(M/V = 48")

153

Figure VIII.11 Flange Stresses For Hole 4, Beam B

(M/V = 24")

154

## FOREWORD

Three of the chapters presented in this thesis are written in the form of papers, two of which were published in journals and the third will be submitted for publication on a later date. Other materials not included in these papers are described and discussed in other chapters.

Chapter 1 provides a full introduction on the subject.

Chapter 2 with Appendix I which deals with unreinforced holes was published as a paper in the Proceedings of the American Society of Civil Engineers under the title of "Stresses in Beams with Circular Eccentric Web Holes". (Ref. 6)

Chapter 3 which deals with circular reinforced holes is written in the form of a paper to be submitted for publication in a journal.

Chapter 4 describes the experimental set up and testing procedure.

Chapter 5 which provides design aids for the design of unreinforced holes was published as a paper in the Proceedings of the American Society of Civil Engineers under the title of "Design Aids for Beams with Circular Eccentric Web Holes". (Ref. 16)

Chapter 6 is the Summary and Conclusions.

Appendix VIII contains additional experimental results which supplement those given in Chapter 2. The results given in this Appendix were not included in the paper reproduced as Chapter 2 for reason of conciseness.

## ACKNOWLEDGEMENT

This research project was jointly supported by the National Research Council under Grant A-3366, and by the Canadian Steel Industries Construction Council, under Project No. 695.

Acknowledgement is also made to Dominion Bridge Company Ltd., Montreal, who provided financial support for the writer through a Dominion Bridge Fellowship award.

- The writer also wishes to express his appreciation
- to his research director, Prof. R.G. Redwood, for his unceasing patience, keen interest and guidance during the course of this project;
  - to the technical staff of the Structural Laboratory of Department of Civil Engineering and his fellow student Mr. T.S. Chu for their help in performing some of the experiments;
  - to Mr. J.L. deStein of deStein & Associates for allowing the writer to take time off during his employment with the firm to write part of the thesis;
  - to Mr. L.J. Vroomen of the DATAC Center, McGill University, for his technical assistance in writing the Assembler part of the computer program used in the experiment;
  - to his fellow students and friends, whose names are too

numerous to mention, for their valuable suggestions;  
- to his dear wife for her care and encouragement during the  
course of his study.

## NOTATION

- A - area of gross beam section;
- $A_T$  - area of vertical top sections;
- $A_f$  - area of one flange;
- $A_w$  - area of unperforated web (=dw);
- $A_\phi$  - area of inclined sections defined by angle  $\phi$ ;
- b - width of flange;
- $b_n$  - actual projecting width of reinforcement flange;
- $b'_n$  - effective projecting width of reinforcement flange;
- $\bar{C}_\phi$  - distance from the hole edge to the centroid of the vertical top sections;
- $c_\phi$  - distance from the hole edge to the centroid of inclined sections;
- d - overall depth of beam;
- E - Young's Modulus;
- e - eccentricity with respect to the mid-depth of beam;
- $F_b$  - allowable bending stress;
- $F_v$  - allowable shear stress;
- $F_y$  - yield stress of steel;
- G - shear modulus;
- I - moment of inertia of gross beam section;
- $I_B$  - moment of inertia of the vertical bottom sections;
- $I_T$  - moment of inertia of the vertical top sections;
- $I_\phi$  - moment of inertia of the inclined sections;
- K - stress concentration factor;

- $k_B$  - shear stress parameter for vertical bottom sections;  
 $k_T$  - shear stress parameter for vertical top sections;  
 $M$  - moment at hole centreline;  
 $M_{all}$  - allowable bending moment based on  $F_b$  and the gross section of the beam;  
 $M_\phi$  - resulting moment at inclined sections;  
 $M_B^1$  - bending moment at bottom sections (high moment edge of hole);  
 $M_B^2$  - bending moment at bottom sections (low moment edge of hole);  
 $M_T^1$  - bending moment at top sections (high moment edge of hole);  
 $M_T^2$  - bending moment at top sections (low moment edge of hole);  
 $N$  - normal force at hole centreline;  
 $N_\phi$  - resulting normal force at inclined sections;  
 $Q_B$  - first moment of area about the centroid of bottom vertical sections;  
 $Q_T$  - first moment of area about the centroid of top vertical sections;  


---

 $R$  - hole radius;  
 $r$  - distance from hole centre to the centre of reinforcement flange;  
 $t_f$  - flange thickness;  
 $t_r$  - thickness of reinforcement flange;  
 $u_1$  - distance of flange from the neutral axis of inclined tee-sections (Figure 2.2);

- $u_2$  - distance of the web-flange interface from the neutral axis of inclined tee-sections (Figure 2.2);
- $V$  - shear force at hole centreline;
- $V_B$  - shear force at the bottom section;
- $V_T$  - shear force at the top section;
- $V_{all}$  - allowable shear force based on  $F_v$  and the gross section of the web;
- $w$  - web thickness;
- $Z$  - property of area;
  
- $\alpha$  - a ratio (obtained from Bleich's solution);
- $\beta$  - angle measured from the horizontal through the hole centre;
- $\Gamma$  - ratio of maximum nominal shear stress to  $\tau$ ;
- $\phi, \theta$  - angle measured from the vertical through the hole centre;
- $\sigma$  - nominal bending stress at outside fibre of the beam based on gross section;
- $\sigma_b$  - bending stress at hole edge;
- $\sigma_t$  - tangential stress at hole edge;
- $\tau$  - nominal average shear stress based on gross web area;
- $\tau_{B,max}$  - maximum shear stress of vertical bottom sections;
- $\tau_{T,max}$  - maximum shear stress of vertical top sections;
- $\xi_T$  - length of web of any vertical top tee-section (Figure I.2);
- $\xi_T^0$  - length of web of vertical top section at hole ends (Figure I.2).

CHAPTER 1

INTRODUCTION

## CHAPTER 1

### INTRODUCTION

#### 1.1 General

Distribution of mechanical services such as air-conditioning, heating and water supplies becomes an integral part in the planning of present day buildings. These mechanical systems are usually distributed vertically, from floor to floor through openings on the floor slabs provided by the architects, and then distributed horizontally on each floor. For floor systems supported by open web steel joists, these systems pass through the open web of the joists. However, in the past, when beam-girder floor systems were required to support heavy live loads and when no information was available regarding web holes in beams, these systems were usually located beneath the structural floor, that is, below the beams and girders. This results in the increase of floor to floor height and consequently the overall height of the building. With the high cost of construction material, and the extra costs in heating and air-conditioning due to the increased volume of the building, this becomes an expensive practice. Therefore more frequently, architects and engineers are specifying that access openings be provided in beams and girders for the passage of service ducts.

Castellated beams provide one possible solution. However, since only a few openings are usually required along the length of the beam and many different beam sections may be involved, the high cost of fabricating these beams generally restricts their uses at least in North America. The other solution is to cut holes in the webs of structural beam sections in locations where access openings are required. They may be rectangular or circular in shape depending on their usage.

At present, a designer is permitted, according to CSA Standard S16-1969, to locate openings in the webs of beams without performing any analysis based on the net section of the beam provided that these openings satisfy a certain number of requirements. These are: (1) the beam is simply supported and is designed to carry uniform loading, (2) the beam section is symmetrical, (3) the openings are located within the middle third of the depth and middle half of the span of the beam, and (4) the spacing between the centres of two adjacent holes should be a minimum of two and a half times the diameter of the larger opening. However, the above requirements are very restrictive. Therefore, in the past few years, a number of methods of analysis and design have been suggested for beams containing circular or rectangular holes. These are reviewed in the next section.

## 1.2 Previous Work

Heller et al<sup>11,12</sup> first attempted to investigate the stresses around a rectangular hole with round corners in a plate subjected to bending, shear and axial load using methods based upon the theory of elasticity. This work is based on the assumption that the size of hole is small compared to the plate itself, and that the edge of the opening is remote from the applied load. Solutions were obtained using the complex variable method of Muskhelishvili. Explicit expressions were given for the hole edge stresses as a function of mapping coefficients and applied loading. Although the analysis are based on a rectangular hole with round corners, the solution is also valid for circular holes provided the appropriate mapping coefficients are used. Solutions for holes which are eccentric with the centreline of the plate are also given in the appendix of Ref. 12.

Bower<sup>1</sup> also used the theory of elasticity method to develop an analytical method to predict the elastic stresses around circular holes for wide-flange beams subjected to uniform loads. Stresses were considered not just at the hole edge but throughout the web. The applicability of this analysis depends on the shear-to-moment ratio as well as the hole diameter-to-beam depth ratio. The author concluded that the analysis would be deficient for holes with diameter-to-depth

ratio bigger than 0.5, and for high shear-to-moment ratios. A series of tests on W16×36 beams were carried out to substantiate the above theory.

A method of analysis using the Vierendeel truss analogy was proposed by Bower<sup>2</sup> for rectangular holes located at the mid-depth of the beam. This method assumes that a point of counter-flexure exists at the mid-length of the tee-section of the beam above and below the hole. At this point, the tee-section is subjected to a shear force  $V_T$  or  $V_B$  which is equal to half of the applied shear at the hole centreline (Figure 1.1). The stresses at the hole centreline are calculated using the flexural formula based on the moment of inertia of the net section of the beam. Stresses at other points of the tee-section can then be obtained by superimposing these stresses with that due to local bending caused by the shear force at the hole centreline. This analysis has been found to be satisfactory in analysing rectangular holes.

The Vierendeel method has been extended by Cooper and Snell<sup>9</sup> to analyse mid-depth rectangular holes reinforced by horizontal bars. Satisfactory results were obtained for bending stresses for both one sided and two sided reinforcement cases.

Elastic analysis using the finite element method has

been investigated extensively at McGill University by Redwood et al.<sup>7, 15</sup>. This applies only to circular holes since local yielding at corners of rectangular holes makes fully elastic analysis unrealistic. Adjacent circular holes with different spacing between them, and single large holes with different types of reinforcements were analysed by plane stress analysis using constant strain triangular elements. The results obtained were compared with experimental and theory of elasticity results.

Analysis of rectangular holes using plastic design method was investigated independently by Bower and Redwood<sup>4, 8, 13, 14</sup>. Although two different approaches were followed, they led to similar results. The theories are primarily based on a failure mechanism consisting of four plastic hinges at the corners of the hole. The results are given in the form of moment-shear interaction diagrams. Each beam and each hole configuration requires a curve and any combination of moment and shear represented by a point on the concave side of this curve is a safe loading. Because of the lengthy numerical computation involved in obtaining these curves, an approximate solution has been suggested by Redwood<sup>13</sup>. By assuming the flange thickness of beam is small compared with the beam and hole depth, the result can be simplified and expressed non-dimensionally. Thus one interaction diagram is required

for geometrically similar beams instead of the series of diagrams originally required.

The plastic design method can also be used to analyse circular holes<sup>13</sup>. In this case, the locations of plastic hinges are not clearly known, and therefore many locations must be tried. The solutions obtained for these locations are then plotted on the same interaction diagram and the minimum envelope produced represents the appropriate curve to be used in design. Redwood in Ref. 14 suggested that, for practical purposes, a circular hole can be represented and analysed as a rectangular hole of length and height equal to 0.9 and 1.80 of the radius respectively (Figure 1.2). This simplified procedure proves to be satisfactory provided that a vertical and horizontal cut-off are used to account for the under-estimation of bending and shear capacities at the centreline of the hole.

It was Frost<sup>10</sup> who first attempted to analyse rectangular holes located eccentrically with respect to the mid-depth of the beam. Unlike mid-depth holes, the shear force at the hole centreline is not divided equally between the top and bottom tee-sections (Figure 1.1). By assuming that the slopes and deflections at the ends of the top and bottom sections are equal, a relationship exists between the shear forces carried by the top and bottom sections. After these forces are

identified, the Vierendeel method can then be used to obtain the normal stresses. Four W16×40 beams containing circular eccentric holes were also tested by Frost<sup>10</sup>, however, hole edge stresses were measured at only a few locations. Some of these results are used for comparison in this thesis.

### 1.3 Scope

The objective of the work described in this thesis was:

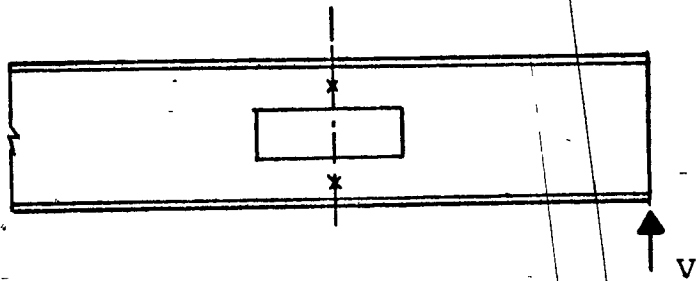
- (1) to investigate the behaviour of circular web holes, both mid-depth and eccentric, in wide flange beams;
- (2) to develop an approximate method of analysis based on simplified theories such that elastic stresses can be obtained easily and efficiently;
- (3) to carry out experimental work to verify the theories;
- (4) to provide design aids for designers and engineers.

Although the plastic design method may be preferred as a method in analysing beams with web holes, analysis based on allowable stress design method (elastic design method) may be necessary in some cases, such as for non-compact beam sections and for repeated loading cases because of fatigue consideration. For rectangular holes, local yielding occurs at the corners of the holes due to stress concentrations even under working loads. Because of this well defined locations of plastic hinges and

failure mechanism, the plastic design method is a more rational method to use in the design of rectangular holes. Such is not the case for circular holes. The stress concentration produced by circular holes are much lower than those produced at the corners of rectangular holes. The stresses in all regions of the beam may well remain elastic under working loads, hence, elastic analysis is appropriate.

The theory of elasticity method has proven to be a satisfactory method of analysis for circular holes providing they are of small diameters. Although the finite element method may be applied to analyse holes of larger diameters, the amount of computer time, the cost and the involvement in the preparation of data generally makes its use not feasible under normal design situations. Therefore it is the intent of this thesis to formulate methods of analysis for both large and small holes based on some simplified theories.

Much of the research done to date has been concerned with mid-depth holes. However, situations may arise in which holes need be located eccentric with respect to the mid-depth of the beam; therefore, analysis of eccentric holes is of considerable importance. Although some research has been done for eccentric rectangular holes, information concerning eccentric circular holes is still lacking, and special attention is therefore paid to these.



\* POINT OF COUNTER-FLEXURE

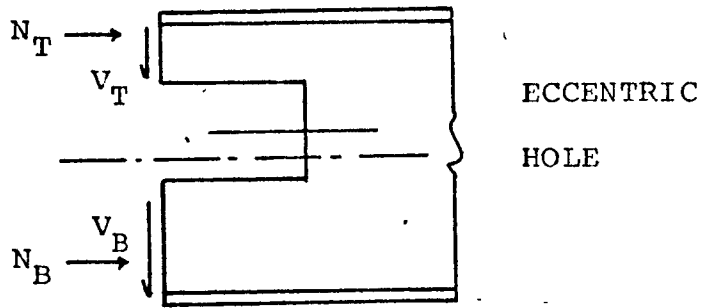
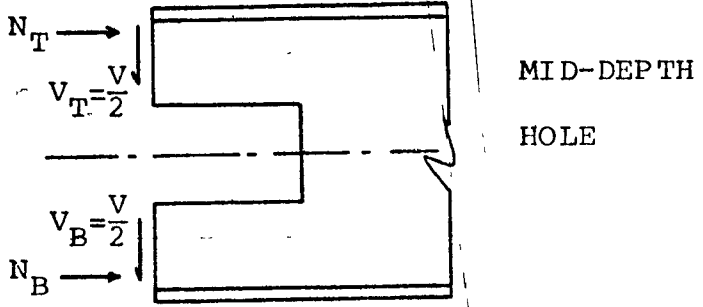


Figure 1.1 Vierendeel Method

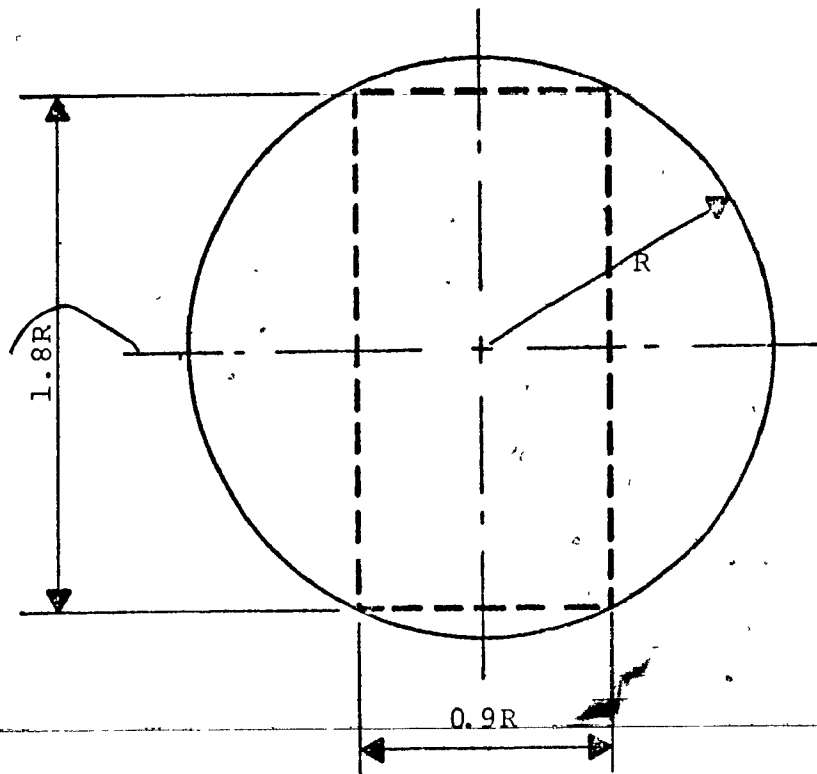


Figure 1.2 Equivalent Rectangular Hole

CHAPTER 2

UNREINFORCED HOLES

7

CHAPTER 2

UNREINFORCED HOLES

2.1 Introduction

The stress analysis of beams containing web holes has received considerable attention because of the frequency of occurrence of such holes in building construction. While plastic design methods may be preferred because of their rationality, and because their application to rectangular holes has been explored extensively, the allowable stress approach to design may be necessary in some cases. In particular, holes in noncompact sections require elastic analysis, and the treatment of circular holes by plastic design methods is currently less satisfactory than rectangular holes.<sup>20</sup> The stress concentrations produced by circular holes are much lower than those produced near the corners of rectangular holes, and whereas the latter will normally produce local yielding under working loads, the former may be low enough that stresses under working loads can be kept within permissible limits.

Much of the previous work directed to the analysis of webs with circular holes has been restricted to mid-depth holes. It is probable that designers are more frequently concerned with the case of eccentric holes than with mid-depth

holes, since service ducts or piping may well be located at different levels between floors to facilitate any crossing which may be necessary. Analysis of eccentric holes is therefore of considerable importance.

The avoidance of fabricating reinforcement is desirable on the basis of cost, and it is, therefore, of some importance to determine the stress levels around unreinforced holes. While some specifications<sup>19</sup> permit unreinforced circular holes subject to certain size and location limitations, without the need for analysis these are, of necessity, quite restrictive. In this paper, more general conditions are considered, so that any practical sized circular web hole can be investigated in terms of the maximum stresses it produces. Attention is restricted to stress analysis and it is assumed that buckling does not occur. The buckling of web and flanges near holes is the subject of a current investigation.

Much previous analytical work concerning such holes has made use of the theory of elasticity in analysing the web as a large plate containing a small hole<sup>1,12</sup> and in addition, emphasis has been placed on mid-depth holes, although an outline of an analytical procedure for eccentric holes has been given in Ref. 12. The accuracy of the theory of elasticity solution has been investigated by Bower<sup>1,2</sup> and

it is clear that the method is seriously deficient under some circumstances, in particular for large holes and under high shear-to-moment ratios, both of which frequently arise in practice. Alternative approaches, for mid-depth holes, have been proposed in which parts of the beam around the hole have been treated-as frame members and analysed by elementary beam theory<sup>17</sup> with the inclusion of stress concentration factors to account for the curved edge.

The two approaches: (1) Theory of elasticity; and (2) curved beam analysis, are compared herein for mid-depth holes, and the conditions under which each is most appropriate are determined. The approximate approach is then extended to deal with eccentric holes by considering the division of shear between the parts of the beam above and below the hole. Experiments on large mid-depth holes and eccentric holes are described and results compared with the analytical solutions. Previous experimental results, obtained elsewhere<sup>10</sup> are also used for comparison, and it is shown that the analytical methods can be used to predict the stress levels in the web and flanges with adequate accuracy for design purposes.

## 2.2 Analysis

The two approaches are outlined in the following for mid-depth holes and eccentric holes. The relevant method

to use is considered in a subsequent section, in the light of experimental results.

### 2.2.1 Mid-Depth Holes

#### 2.2.1.1 Theory of Elasticity Solution

This theory is outlined in Refs. 1 and 12. A useful explicit relationship for the tangential normal stress on the edge of a hole is given by Eq. 6 in Ref. 12. For the specific case of a circular hole, this reduces to

$$\frac{\sigma_t}{F_b} = \frac{M}{M_{all}} \left(\frac{2R}{d}\right) (\sin \beta - \sin 3\beta) + 4 \left(\frac{M}{M_{all}}\right) \left(\frac{\tau}{\sigma}\right) \Gamma \sin 2\beta \quad (2-1)$$

in which  $\sigma_t$  = the tangential normal stress on the hole edge;  $F_b$  = the allowable bending stress;  $M$  = the applied moment at the hole centreline;  $M_{all}$  = the allowable bending moment based on  $F_b$  and the gross section of the beam;  $R$  = the hole radius;  $d$  = the overall beam depth;  $\beta$  = the angle measured from the horizontal through the hole centre;  $\tau$  = the nominal average shear stress based on the gross web area;  $\sigma$  = the nominal bending stress at the outside fibre of the beam, again based on gross section; and  $\Gamma$  = the ratio of the maximum nominal shear stress to  $\tau$ . Explicit relationships for stresses in

other locations are not available. Equation 2-1 is valid for small value of hole diameter to beam depth ratio, except that if the shear-to-moment ratio is low, holes with diameter equal to or somewhat larger than one-half the hole depth may be analysed with satisfactory results. For larger holes, especially if the shear-to-moment ratio is not low, the following analysis is proposed.

#### 2.2.1.2 Curved Beam Analysis ✓

In this analysis parts of the beam near the hole are treated as individual structural members, and analysed accordingly by well-established methods. The resultant forces acting on a cross-section of the beam through the centre of the hole, as shown in Figure 2.1, are first estimated. Symmetry requires that half of the total shear force be carried above the hole, and the magnitude and line of action of the normal force,  $N$ , can be approximated by application of the simple flexure formula. This can be based on the moment applied at the centreline of the hole, and the properties of the net section at that location. Stresses are then calculated for several sections radiating from the hole centre, as indicated. The normal force acting through the centroid of such a section and the moments,  $N_{\phi}$  and  $M_{\phi}$ , are then used to calculate the stresses.

The stresses due to bending may be calculated on

the assumption that the section defined by the angle,  $\phi$ , is the cross-section of a curved beam with centre of curvature at the centre of the hole. Then using the Winkler-Bach curved beam formula<sup>18</sup> the bending stress at the edge of the hole is

$$\sigma_b = \frac{M_\phi}{A_\phi (R + c_\phi)} \left(1 - \frac{c_\phi}{ZR}\right) \quad (2-2)$$

$$\text{in which } Z = -\frac{1}{A_\phi} \int_{\text{area}} \frac{y}{(R + c_\phi) + y} dA_\phi \quad (2-3)$$

in which  $A_\phi$  = the area of the inclined tee-section defined by the angle,  $\phi$ ;  $c_\phi$  = the distance from the hole edge to the centroid of the inclined tee; and  $y$  = a coordinate measured from the centroid of the inclined tee-section.

The integration of Equation 2-3 may be performed numerically, or alternatively explicit formulae are given for a number of different section shapes in Ref. 18. In particular, for a tee-section as shown in Figure 2.2

$$Z = -1 + \frac{R + c_\phi}{A_\phi} \{ b \ln(R + c_\phi + u_1) + (w - b) \ln(R + c_\phi + u_2) - w \ln(R) \} \quad (2-4)$$

It is convenient to calculate a stress concentration factor,  $K$ , for the hole edge stress based on Equation 2-2.

Thus

$$K = \frac{\frac{M_{\phi}}{A_{\phi}(R + c_{\phi})} \left(1 - \frac{c_{\phi}}{ZR}\right)}{\frac{-M_{\phi} c_{\phi}}{I_{\phi}}} \quad (2-5)$$

in which  $I_{\phi}$  = the moment of inertia of the inclined tee-section about its centroid.

The stress caused by  $N_{\phi}$  must be added to the bending component and it has been found sufficiently accurate to apply the same stress concentration factor,  $K$ , to the normal axial stress value as derived by consideration of the bending stresses<sup>5</sup>. Thus the tangential stress at the hole edge becomes

$$\sigma_t = K \left( \frac{N_{\phi}}{A_{\phi}} + \frac{M_{\phi} c_{\phi}}{I_{\phi}} \right) \quad (2-6)$$

This calculation is repeated for various values of  $\phi$  until a maximum value of  $\sigma_t$  is reached. This process can be carried out to a maximum,  $\phi$ , of about  $45^{\circ}$ , and it has been found that for practical hole and beam geometries, the maximum

always occurs with  $\phi < 45^\circ$ .

## 2.2.2 Eccentric Holes

### 2.2.2.1 Theory of Elasticity Solution

The theory is outlined in Ref. 12, and the following explicit relationship for the hole edge stress for circular holes may be derived:

$$\begin{aligned} \frac{\sigma_t}{F_b} = & \frac{M}{M_{all}} \left(\frac{2R}{d}\right) (\sin\beta - \sin 3\beta) + 4 \left(\frac{M}{M_{all}}\right) \left(\frac{\tau}{\sigma}\right) \Gamma \sin 2\beta \\ & + 2 \left(\frac{M}{M_{all}}\right) \left(\frac{e}{d}\right) (1 - 2\cos 2\beta) \\ & - \frac{1}{2} \left(\frac{V}{V_{all}}\right) \left(\frac{F_v}{F_b}\right) \left(\frac{e}{d}\right) \left(\frac{A_w}{A_f}\right) \left(\frac{A_f d^2}{I}\right) \left(\frac{2R}{d}\right) \\ & \cdot \{\cos\beta - 3\cos 3\beta + 4 \left(\frac{e}{d}\right) \left(\frac{d}{2R}\right) \sin 2\beta\} \end{aligned} \quad (2-7)$$

in which  $e$  = the eccentricity measured as the distance from the centre of the hole to the beam centreline;  $V$  = the total shear;  $V_{all}$  = the allowable shear;  $F_v$  = the allowable shear stress;  $A_w$  = the gross web area (=  $dw$ );  $A_f$  = the area of one flange; and  $I$  = the moment of inertia of gross beam section.

### 2.2.2.2 Curved Beam Solution

This method follows the identical procedure as for the mid-depth hole; the only difference is that the shear force is no longer distributed equally above and below the hole. In order to calculate the division of shear, the sections of beam above and below the hole are treated separately, and conditions of slope and deflection compatibility between their ends are employed.

Equilibrium requires that the sum of shear forces in the top and bottom sections must be equal to the total shear force at hole centreline,  $V$ , i.e.

$$V_T + V_B = V \quad (2-8)$$

in which  $V_T$  and  $V_B$  = the shear forces in the top and bottom sections, respectively. From slope and deflection compatibility, i.e., equality of the changes in slope and deflection of the top and bottom sections over the length of the hole, the following shear force ratio is obtained:

$$\frac{V_T}{V_B} = \frac{\frac{R^2}{E} \int_0^{\pi/2} \frac{\sin^2 \theta \cos \theta d\theta}{I_B} + \frac{1}{G} \int_0^{\pi/2} k_B \cos \theta d\theta}{\frac{R^2}{E} \int_0^{\pi/2} \frac{\sin^2 \theta \cos \theta d\theta}{I_T} + \frac{1}{G} \int_0^{\pi/2} k_T \cos \theta d\theta}$$

(2-9)

in which  $E$  = Young's Modulus;  $I_T, I_B$  = the moment of inertia of top and bottom sections, respectively, about their centroids;  $\theta$  = an angle measured from the centre of the hole from its vertical centreline;  $G$  = shear modulus; and  $k_T, k_B$  = shear stress parameters for the top and bottom sections, respectively, as defined in full in Appendix I, which also gives a detailed analysis of the derivation of Equation 2-9.

In order to verify the previous theories, and to determine which is the more appropriate to use in a given case, some experiments were performed, and are described in the next section.

### 2.3 Test Program and Results

Two beams each containing two holes were tested to determine elastic stress distributions and deflections. Details of the beams, holes, and test arrangements are shown in Figure 2.3. The two holes in beam A were chosen to be large enough that the theory of elasticity solution would almost certainly be inadequate for their analysis, and the results, therefore, represent a test of the curved beam method of analysis. The smaller holes of beam B were chosen in an attempt to explore the limitations in application of the two analytical approaches. All holes were tested under two different shear-to-moment ratios, since the adequacy of the analytical approaches is known to be very dependent on this ratio.

The holes were machined with a fly cutter, and thus, had clean, notch-free edges. While in practice most holes would be flame-cut, the resulting stress raisers would in fact be ignored by the designer, unless fatigue was a consideration. It was, therefore, preferred to eliminate the effects of a rough edge and so provide a clearer picture of the relevance of the analyses. The webs and flanges of the beams in the vicinity of each hole were strain-gauged, and gauge locations are shown in Figure 2.4.

The beams were simply supported at each end, and because of the low magnitudes of load, no lateral support was provided. Load was applied by means of an Amsler hydraulic jack and readings of gauges and deflections recorded at a minimum of five increments of load. A maximum load of 13 kips (57.9 kN) was applied to beam A, and 21 kips (93.5 kN) to beam B, and no nonlinearity was observed in any of the readings. The beams were tested with the holes in the positions shown in Figure 2.3, and then with the reversed position with the holes eccentric below the mid-depth. Much of the data was automatically recorded and stored on disk for later analysis.

Tangential normal stresses around the hole edge are shown in Figures 2.5 to 2.8. For ease of comparison, all results are presented for a shear force of 10 kips. Also plotted are solutions given by the theory of elasticity and by the curved beam method; for the latter, stresses are plotted only for sector  $\pm 45^\circ$  from

the vertical centreline of the hole, because of the limitation of the method. Stresses around the large holes of beam A are shown in Figures 2.5 and 2.6 for  $M/V = 24$  in. (0.588 m). In both cases, the theory of elasticity solution is quite inadequate and the curved beam solution accurately predicts the measured stresses. Similar results were also obtained for these holes under a  $M/V$  ratio of 48 in. (1.176 m). Results for hole 3 of beam B are shown in Figure 2.7 for the two  $M/V$  ratios. Under the lower  $M/V$  ratio, the two analyses give very close results and both predict the measured stresses well. At the higher  $M/V$  ratio, the theory of elasticity solution provides a good estimate of the measured stresses while the accuracy of the curved beam results is diminished. Similar conclusions can be drawn from the results for hole 4, shown in Figure 2.8. These results are consistent with the known dependence of both methods on the  $M/V$  ratio.

Shear stresses were measured by rosette gauges placed on the hole centreline. Experimental results are shown for one case in Figure 2.9 and are compared with the theoretical stress distributions based on the shear force values given by Equations 2-8 and 2-9, with the distribution according to standard elastic theory. Satisfactory agreement was also found in all other cases.

Longitudinal normal stresses were measured on the

centreline of the flanges at various positions over the length of the hole. Typical values are shown in Figures 2.10 and 2.11, and are compared with values obtained in the following two ways: (1) Flexural stresses calculated from the applied bending moment and based on the gross (i.e., unperforated) beam section modulus; and (2) values of flange stresses obtained from the curved beam analysis. The latter were calculated on planes  $\pm 45^\circ$  from the hole centreline, and it can be expected that the accuracy will diminish as the angle increases. The results generally do not show great deviations from the nominal stress values, except in cases where the hole is very large or the eccentricity is large. In either case, it can be expected that the maximum hole edge stress will be large, and might in any case govern. The curved beam estimates of the longitudinal flange stresses generally indicate the stress distributions and predict the maximum values quite well although the location is generally not predicted accurately.

Four W16x40 beams of A36 steel containing eccentric circular holes were tested by Frost<sup>10</sup>. The holes were of 6.4-in. (162.6 mm) diameter, and eccentricities were 1.0 in. (25.4 mm) and 2.0 in. (50.8 mm). Stresses were measured on three cross-sections of the beam corresponding to the centreline and the two ends of the hole. However, strains were not recorded at the edges of the holes other than at these sections.

Thus, only the stresses at the hole centreline can be compared with the theories herein. The stresses were plotted similarly to those shown in Figure 2.9, and showed equally good agreement.

#### 2.4 Conclusions

For the experimental cases presented herein, it has been shown that, depending upon the hole size and the  $M/V$  ratio, either the curved beam method or the theory of elasticity method gives a satisfactory solution for the maximum hole edge stress. The appropriate solution is always the one predicting the greater stress magnitude. It is, therefore, apparent that for a given case, if both solutions are obtained, the larger stress predicted may be taken as the more accurate; however, it has not been demonstrated that such a result will be sufficiently accurate for all practical values of  $M/V$  and  $2R/d$ .

A study of the accuracy of the two methods predicting the maximum hole edge stress for mid-depth holes has been presented in Ref. 5. For a number of reported results of experiments and finite element analyses of mid-depth holes, the maximum stresses predicted by the two analyses have been compared, and nondimensionalised stresses plotted against a nondimensional parameter,  $M/Vd$ , representing the moment-to-shear ratio. Results for the smallest hole ( $2R/d = 0.434$ ) and the largest one ( $2R/d = 0.758$ ) are shown in Figure 2.12. These

and other results showed that taking the largest of the two stresses could result in unsafe prediction of the actual stress, with a maximum underestimate of about 14%. This however applies only over a limited range of  $M/Vd$  ratios, and only to small holes, for which stress levels elsewhere in the beam may well be critical. Thus, for most purposes, the largest value of stress given by the two methods may be considered sufficiently accurate. While insufficient results for eccentric holes are available to carry out a similar extensive test of the theories, it is reasonable, on the basis of the results presented herein, to assume that the conclusions arrived at for mid-depth holes hold equally for eccentric holes.

The results reported herein provide a basis for the estimation of stress levels around unreinforced eccentric circular holes, on the assumption that local buckling does not occur. The appropriate methods for given hole and beam sizes and loadings have been identified. Design aids based on these results will be presented in a subsequent paper.

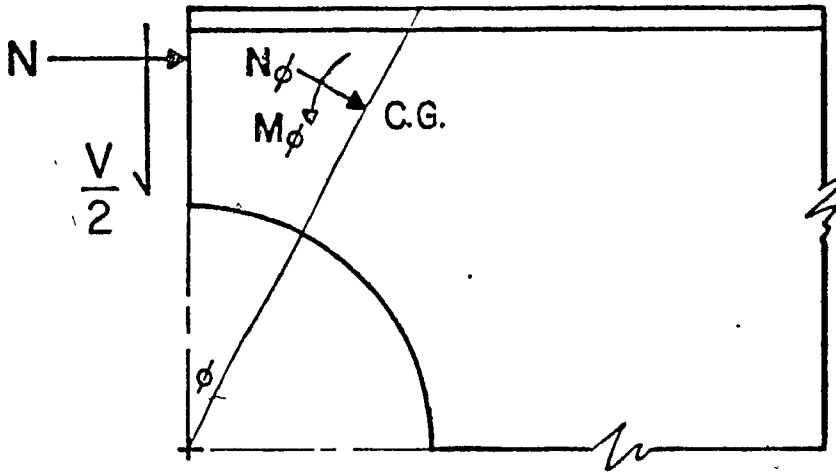
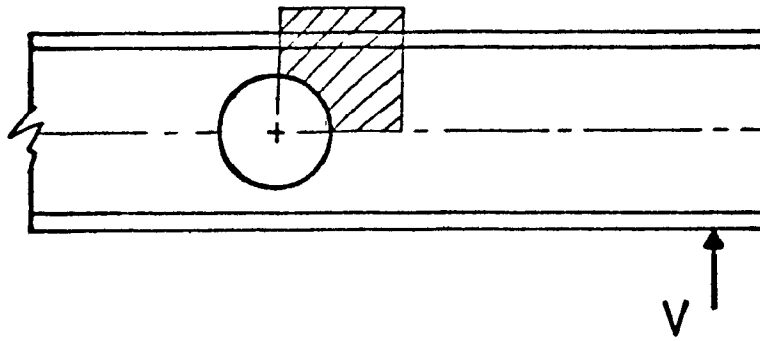


Figure 2.1 Curved Beam Idealisation

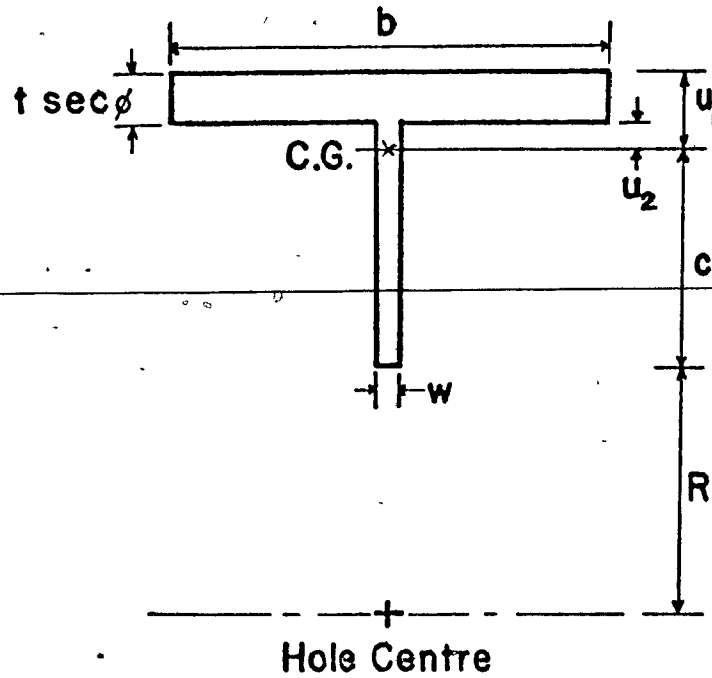
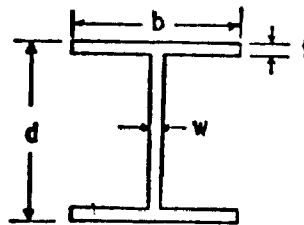
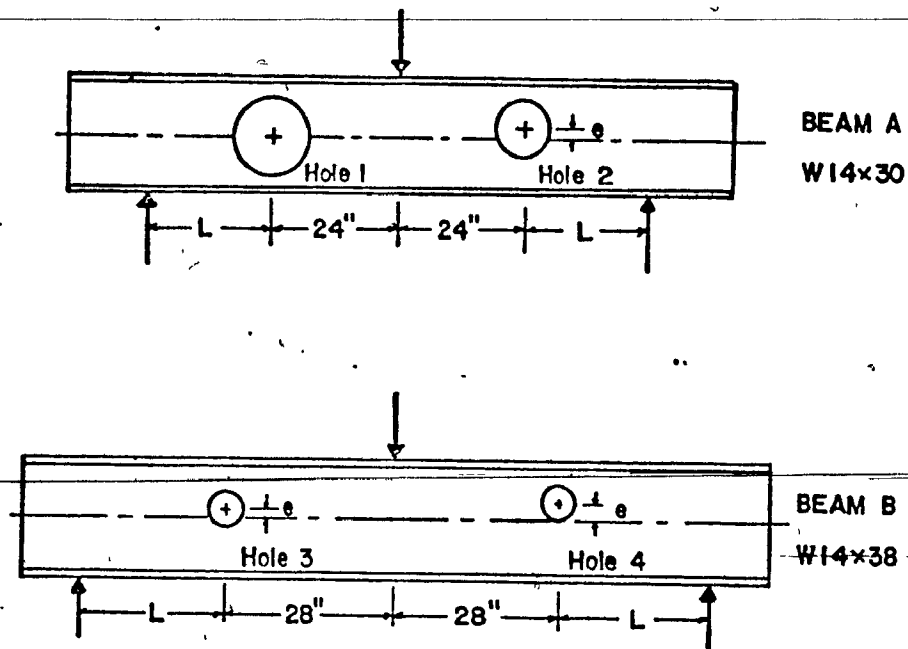
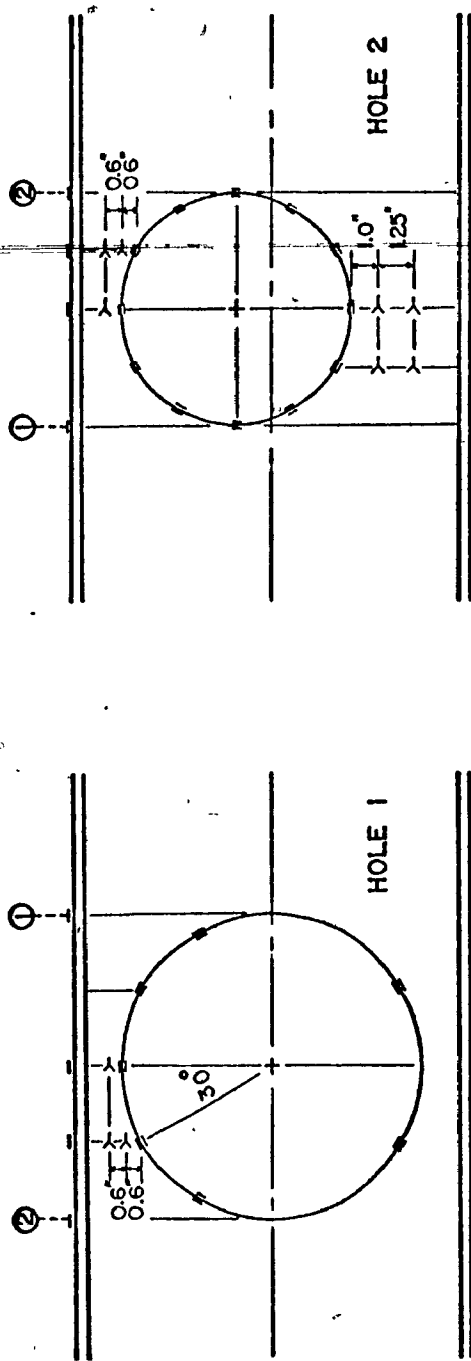


Figure 2.2 Typical Inclined Tee-Section



Beam	d	b	t	w	Hole	Dia. (2R) (in.)	e (in.)	$\frac{2R}{d}$	$\frac{e}{d}$	L (in.)	
										Test 1	Test 2
A	14.0	6.75	.38	.27	1	10.5	0	.750	0	48	24
					2	8.0	1.25	.571	.089	48	24
B	14.2	6.75	.51	.32	3	5.0	1.00	.352	.070	48	24
					4	5.0	2.50	.352	.176	48	24

Figure 2.3 Details Of Test Beams



① HIGH MOMENT EDGE  
 ② LOW MOMENT EDGE

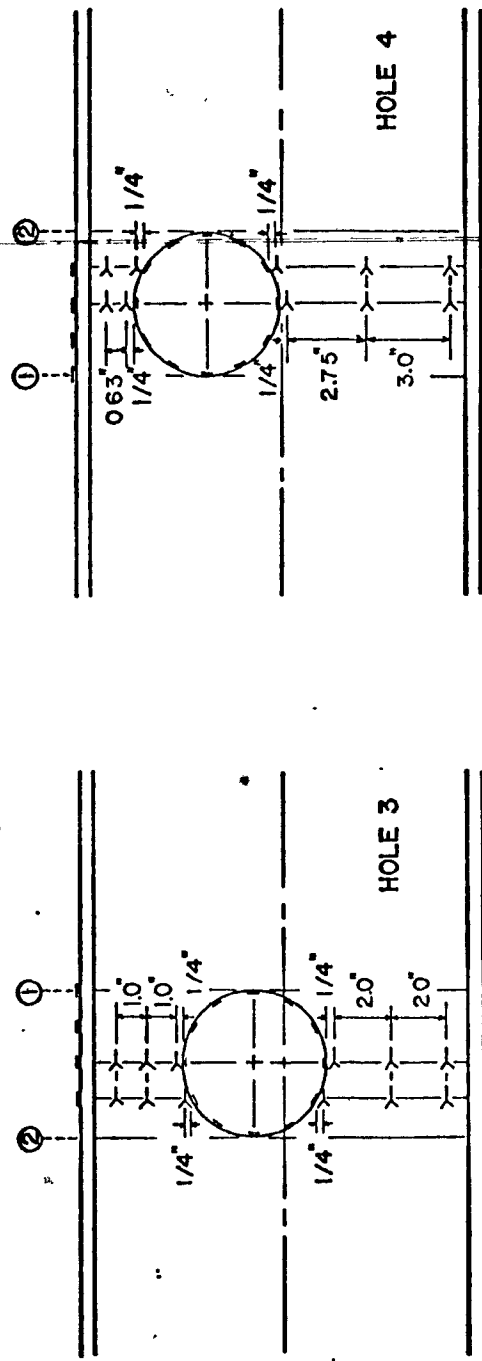


Figure 2.4 Instrumentation Of Beams

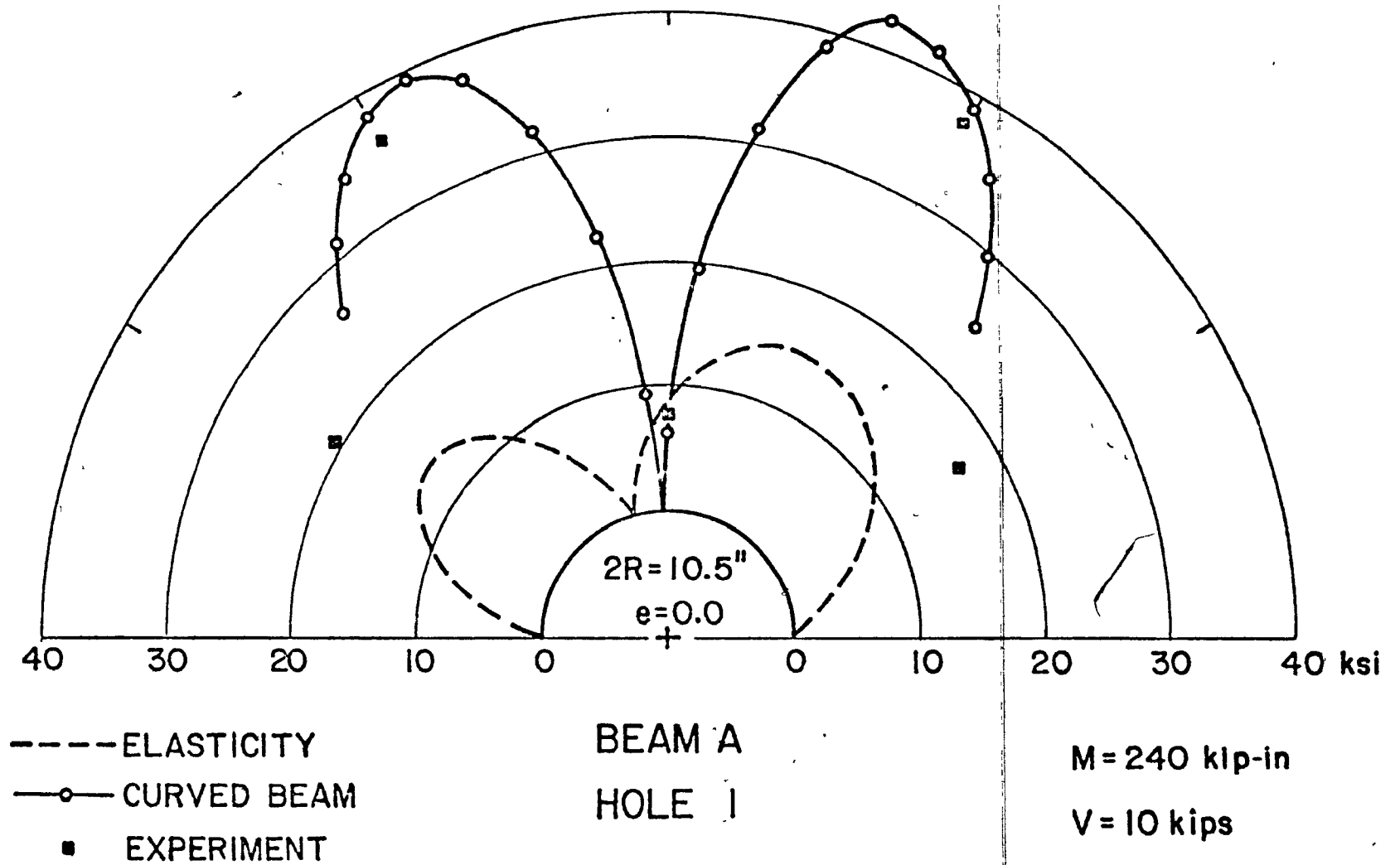
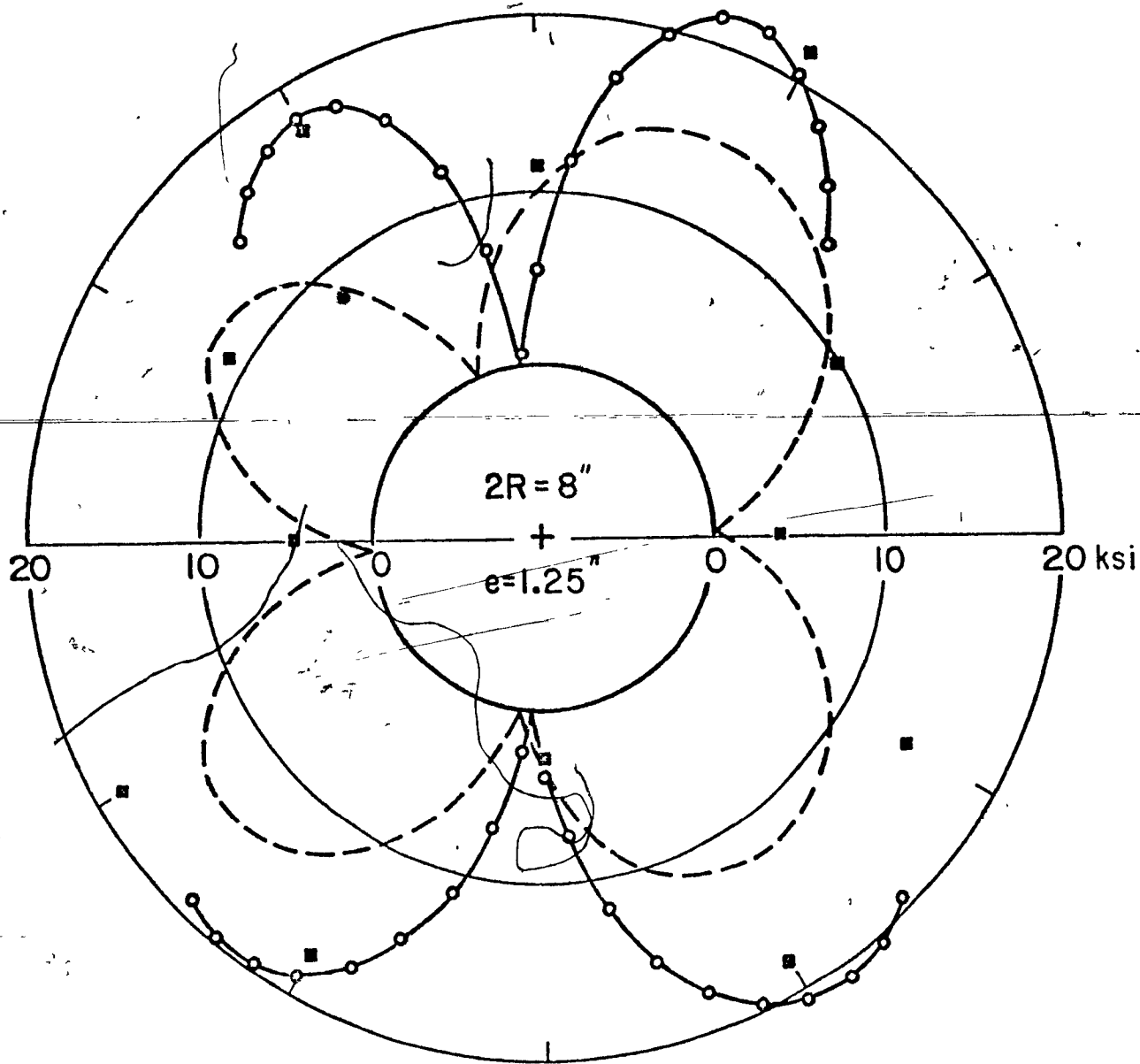
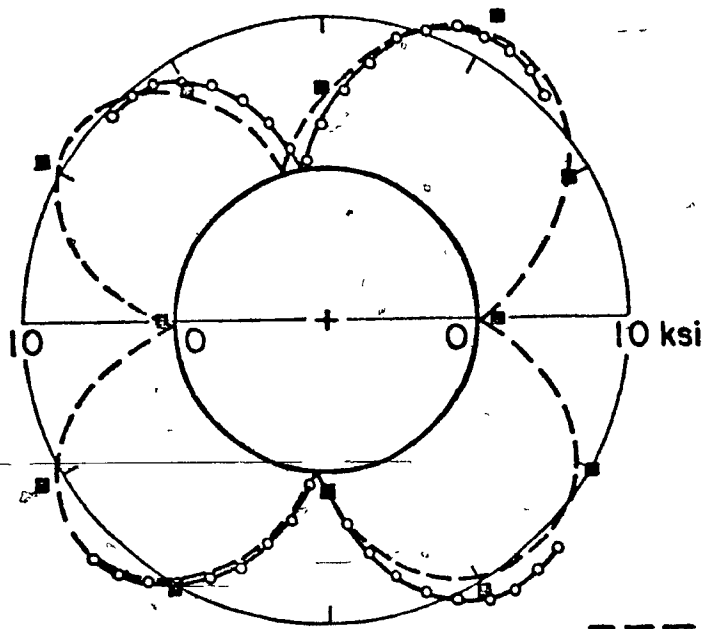


Figure 2.5 Hole Edge Stresses For Hole 1, Beam A



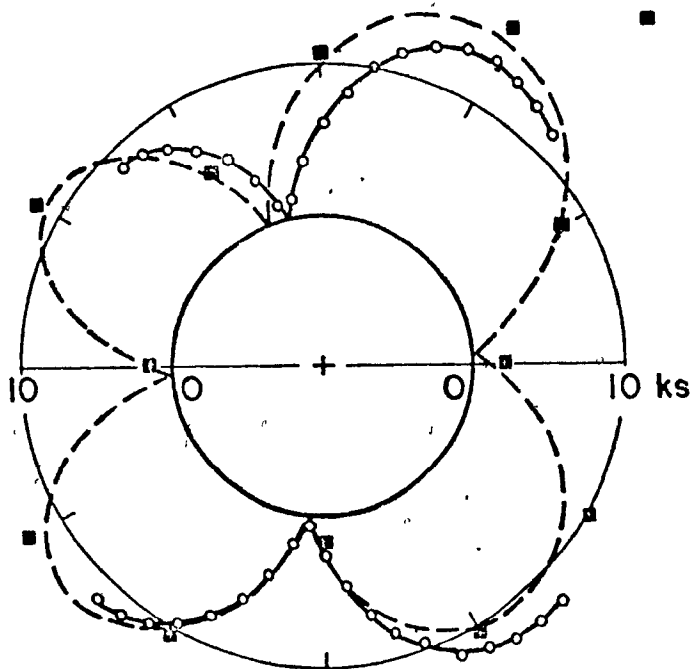
- |     |             |        |              |
|-----|-------------|--------|--------------|
| --- | ELASTICITY  | BEAM A | M=240 kip-in |
| —○— | CURVED BEAM | HOLE 2 | V=10 kips    |
| ■   | EXPERIMENT  |        |              |

Figure 2.6 Hole Edge Stresses For Hole 2, Beam A



$M = 240 \text{ kip-in}$   
 $V = 10 \text{ kips}$

----- ELASTICITY  
 —○— CURVED BEAM  
 ■ EXPERIMENT

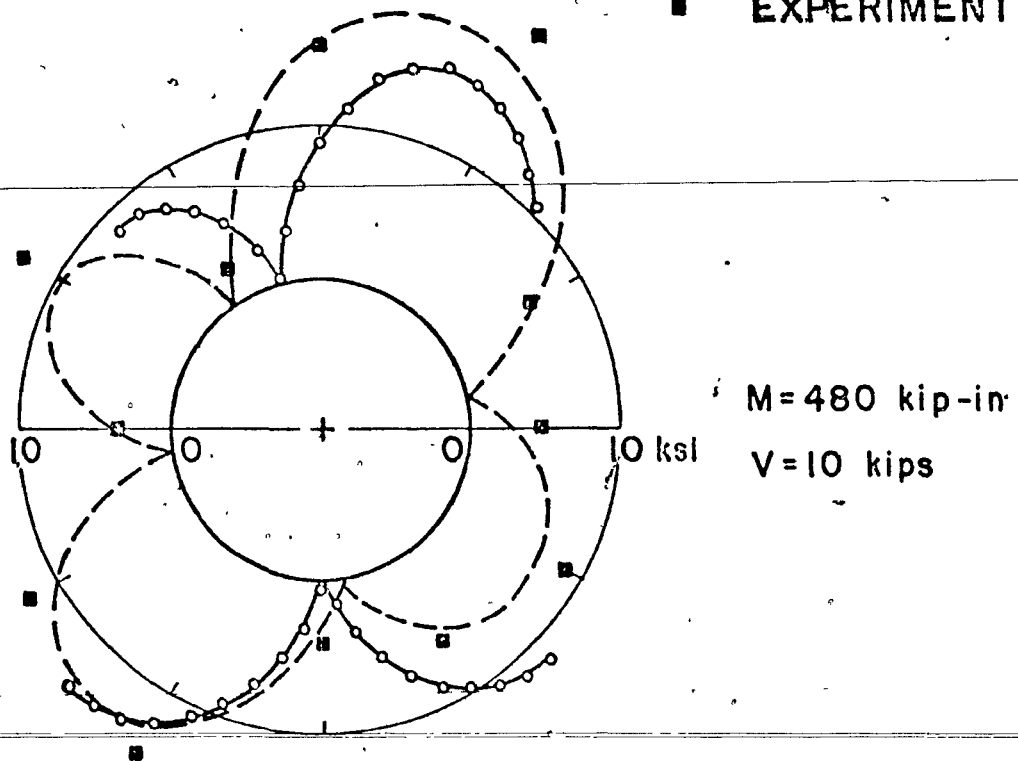
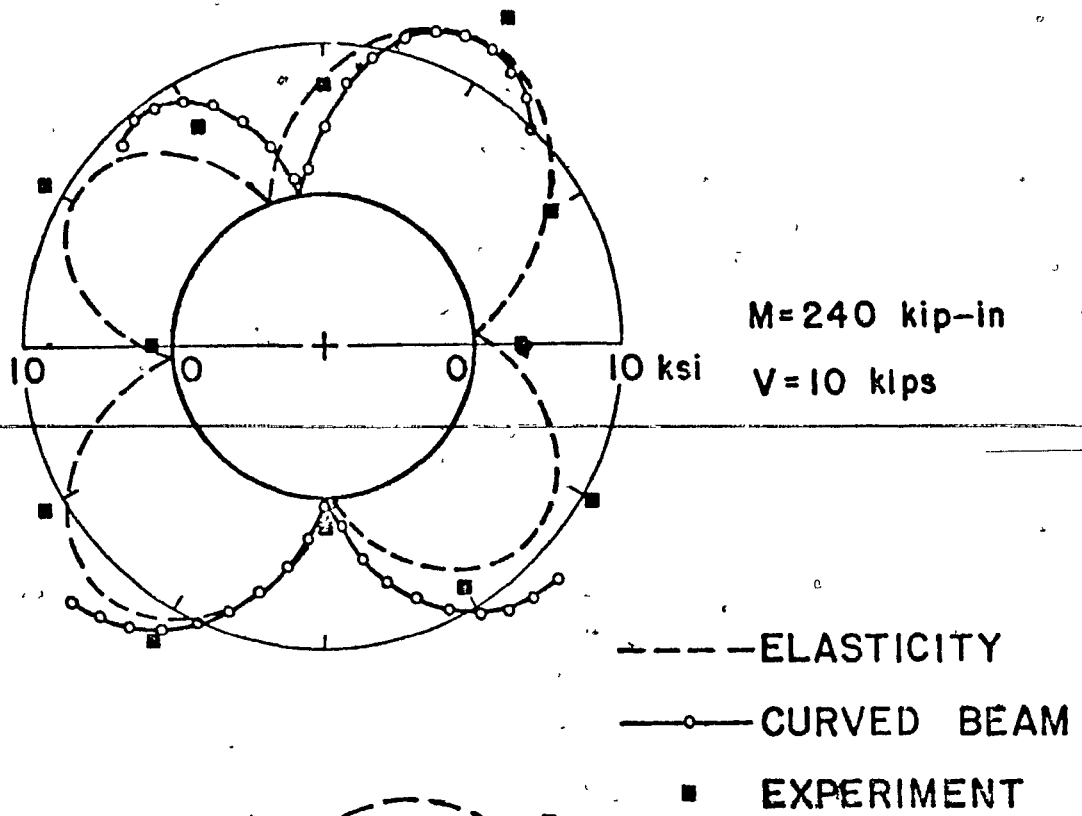


$M = 480 \text{ kip-in}$   
 $V = 10 \text{ kips}$

BEAM B  
 HOLE 3

$2R = 5''$   
 $e = 1.0''$

Figure 2.7 Hole Edge Stresses For Hole 3, Beam B



BEAM B  
HOLE 4

$2R=5''$   
 $e=2.5''$

Figure 2.8 Hole Edge Stresses For Hole 4, Beam B

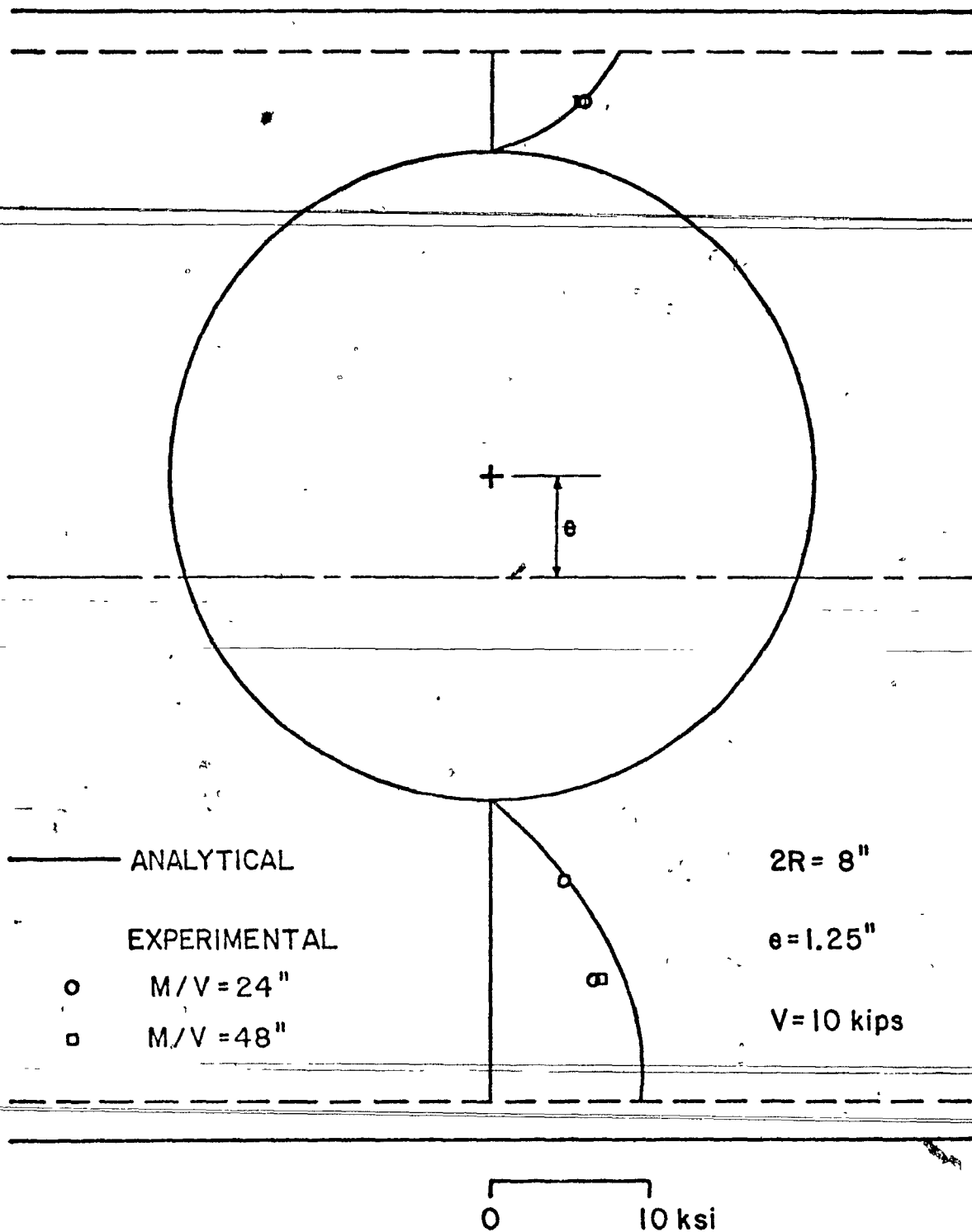


Figure 2.9 Shear Stresses At Hole Centreline  
For Hole 3, Beam B

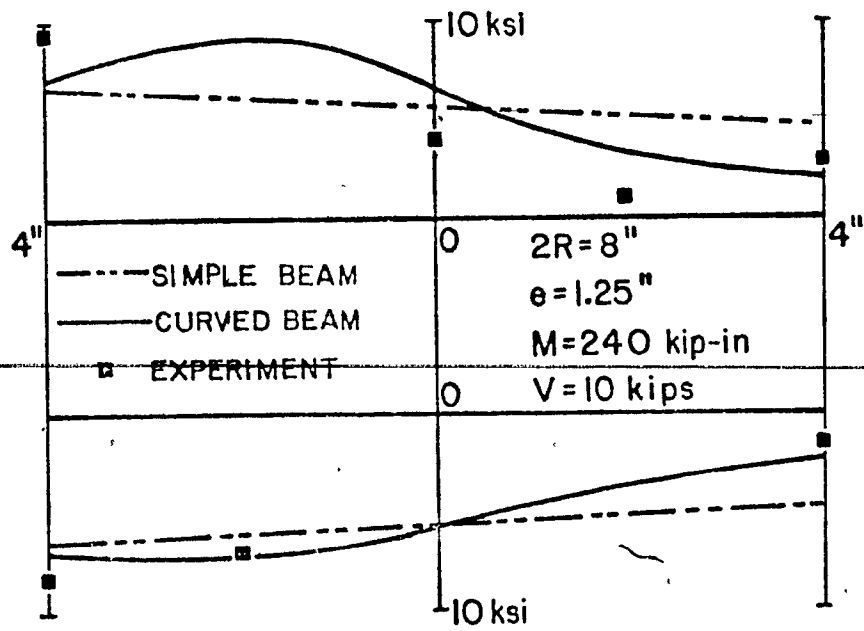


Figure 2.10 Flange Stresses For Hole 2, Beam A

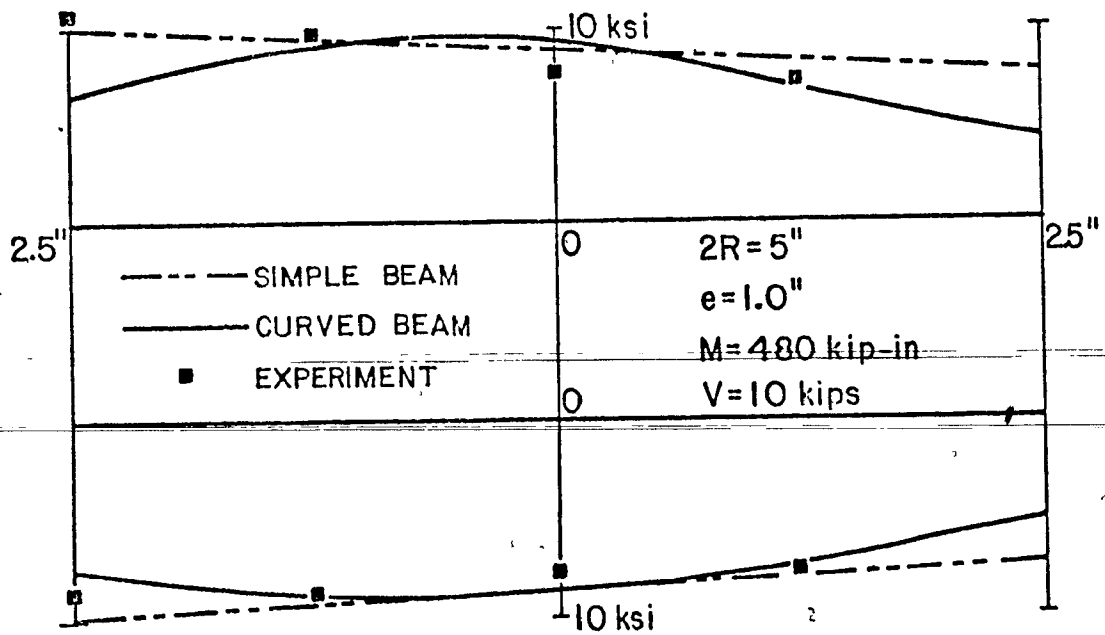


Figure 2.11 Flange Stresses For Hole 3, Beam B

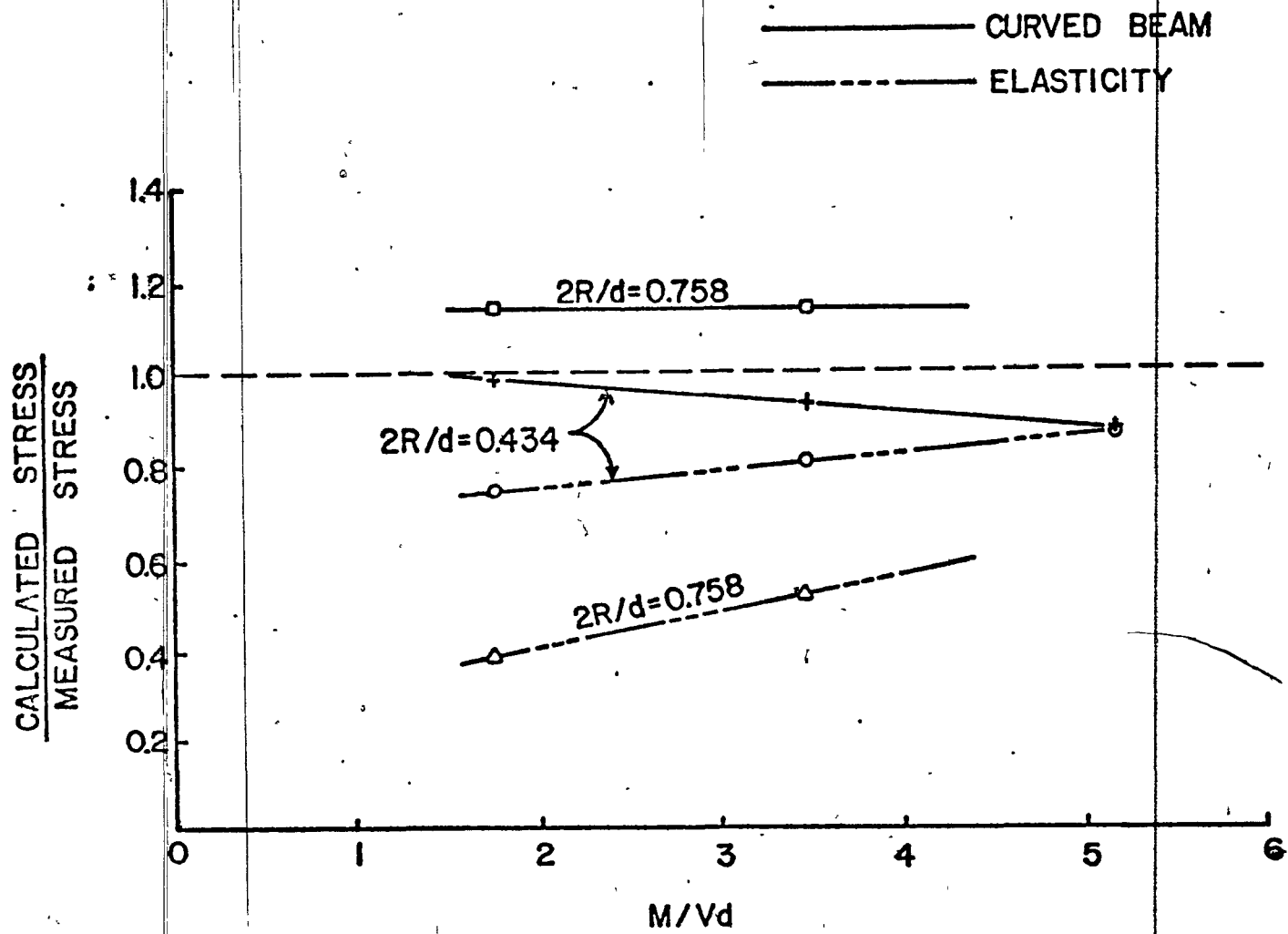
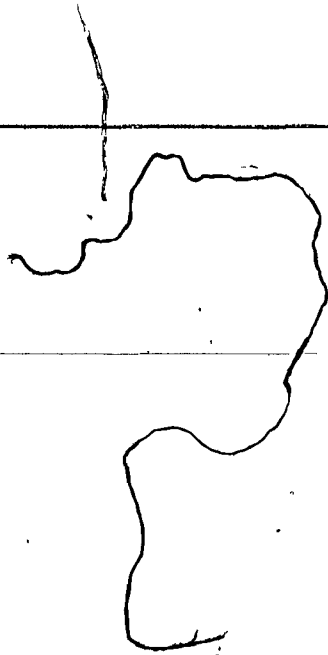


Figure 2.12 Comparison Of Analytical Methods

CHAPTER 3

REINFORCED HOLES



## CHAPTER 3

### REINFORCED HOLES

#### 3.1 Introduction

The need for web holes in beams and girders for the passage of utility ducts and pipes has been discussed widely in the literature, and various methods of analysis and design have been suggested. Unreinforced holes in general are preferred in order to minimise fabrication costs, however, in many cases, the stresses in the beam caused by the presence of the hole will be so high that reinforcement is required. For circular holes, the reinforcement can be in the form of plates welded horizontally to the web near the hole or circular rings welded to the edge of the hole. It has been shown elsewhere<sup>7</sup> that horizontal plates are not effective in reducing the hole edge stresses around circular holes except under pure bending conditions, and it is concluded that the circular type of reinforcement is definitely superior if the design is based on allowable stresses.

In previously reported work<sup>6</sup>, satisfactory methods of analysis of stresses for beams with unreinforced circular holes were proposed. Two theories were suggested as being appropriate: (1) theory of elasticity solution and (2) curved beam analysis. The first theory is based on the analysis of

the web as a large plate containing a small hole. The second theory assumes that a portion of the web and flange can be treated as a section of a curved beam and this is then analysed using the Winkler-Bach curved beam formula. The appropriate theory to use is dependent upon the size of the hole and the relative magnitudes of moment and shear, and the larger the hole diameter (measured as a fraction of the beam depth, for example) and the smaller the moment-to-shear ratio, the more appropriate it is to use the curved beam analysis.

In this paper, the curved beam analysis is applied to the case of a circular web hole reinforced by means of a circumferential plate as illustrated in Figure 3.1. A solution of the equations of the theory of elasticity has not been attempted because of the limited range of practical sizes for which it is applicable in the unreinforced case, and the expectation that the range would be as limited for reinforced holes. However, holes which might be expected to lie within this range of sizes are investigated experimentally.

## 3.2 Analysis

### 3.2.1 Mid-Depth Holes

The analysis is basically identical to that discussed in Ref. 6. The normal force  $N_\phi$  and moment  $M_\phi$  for a section defined by angle  $\phi$ , as shown in Figure 3.1, is first determined

and then used to calculate the bending stresses at the edge of the hole using the Winkler-Bach curved beam formula;

$$\sigma_b = \frac{M_\phi}{A_\phi (R + c_\phi)} \left(1 - \frac{c_\phi}{ZR}\right) \quad (3-1)$$

$$\text{in which } Z = - \frac{1}{A_\phi} \int_{\text{area}} \frac{y}{(R + c_\phi) + y} dA_\phi \quad (3-2)$$

in which  $A_\phi$  = area of the inclined section defined by the angle,  $\phi$ ;  $c_\phi$  = the distance from the hole edge to the centroid of the inclined section; and  $y$  = a coordinate measured from the centroid of the inclined section.

This is repeated for various values of the angle  $\phi$  from  $0^\circ$  to  $\pm 45^\circ$ . It is generally not possible to obtain meaningful solution for  $\phi > 45^\circ$ , but in all cases computed, maximum normal stresses in the reinforcement were found to occur when  $\phi < 45^\circ$ .

For unreinforced holes, the tangential stresses at the edge of the hole is assumed to be uniformly distributed across the thickness of the web. However, for curved reinforcement at this location, the assumption of uniform stresses is not correct. The primary bending causes the outer portion of the reinforcement to deflect radially, inward or outward depending upon whether it is tensile or compressive. Referring to Figure 3.2 and considering element strips AB and

CD, axial forces due to the primary bending are applied at the ends of the strip AB. In the case of tensile forces, since the forces are nonconcurrent and the fact that the strip AB is curved, a resultant force will act towards the centre of the hole, thus causing the deflection of strip CD which is perpendicular to AB. This deflection increases from a zero value at the junction of the reinforcement with the web to a maximum value at the free edges (Figure 3.2). Also, this deflection will result in a change in the circumferential strain resulting from the primary bending. Thus the circumferential stress at the free edges will be lower than that at the junction with the web. An approximate solution given by Bleich<sup>18</sup> for the case of a curved beam section can be utilised here. The projecting width on each side of the reinforcement flange is assumed to be reduced such that the stresses may be assumed to be uniform across the width of the flange. If the magnitude of this uniform stress distribution is taken to be equal to the maximum stress at the junction of the web, the effective projecting width of the reinforcement flange is given by,

$$b'_n = \alpha b_n \quad (3-3)$$

in which  $b'_n$  = the effective (reduced) projecting width of the reinforcement flange;  $b_n$  = the actual projecting width of the reinforcement flange; and  $\alpha$  = a ratio obtained from Bleich's

solution. The ratio  $\alpha$  is a function of  $b_n^2/rt_r$  where  $t_r$  is the thickness of reinforcement flange and  $r$  is the radius of curvature to the centre of the reinforcement flange. Tabulated values of  $\alpha$  for different values of  $b_n^2/rt_r$  are presented in Ref. 18. These values may be represented by a fitted polynomial, and a suitable relationship was found to be,

$$\alpha = 1.093 - 0.514 \left( \frac{b_n^2}{rt_r} \right) + 0.128 \left( \frac{b_n^2}{rt_r} \right)^2 - 0.0112 \left( \frac{b_n^2}{rt_r} \right)^3 \quad (3-4)$$

It is usually more convenient to express Equations 3-3 and 3-4 in terms of the actual total width of reinforcement,  $b_r$ , and not the projecting width,  $b_n$ , in which case,

$$b_n = \frac{b_r - w}{2} \quad (3-5)$$

### 3.2.2 Eccentric Holes

As in the case of unreinforced holes, the only difference in the analysis from that of mid-depth holes is the fact that the shear force across the hole centreline will no longer be distributed evenly between the top and bottom sections. The shear forces  $V_T$  and  $V_B$ , carried by the beam above and below the hole respectively, can be obtained by solving simultaneously Equations 8 and 9 in Ref. 10 (Equations 2-8 and 2-9 in Chapter 2).

These equations are reproduced herein,

$$V_T + V_B = V \quad (3-6)$$

$$\frac{V_T}{V_B} = \frac{\frac{R^2}{E} \int_0^{\pi/2} \frac{\sin^2 \theta \cos \theta d\theta}{I_B} + \frac{1}{G} \int_0^{\pi/2} k_B \cos \theta d\theta}{\frac{R^2}{E} \int_0^{\pi/2} \frac{\sin^2 \theta \cos \theta d\theta}{I_T} + \frac{1}{G} \int_0^{\pi/2} k_T \cos \theta d\theta} \quad (3-7)$$

However, the moments of inertia  $I_T$  and  $I_B$  and the shear parameters  $k_T$  and  $k_B$  are calculated based on the reduced section.

### 3.3 Test Program and Results

A beam containing two eccentric holes of equal diameters was tested to verify the above theory. Reinforcement in the form of circular rings was welded to the web of the beam at the edge of the holes. The circular rings were of the same thickness, 1/4 inch (6.4 mm), but of different width, and were cut from 5 inch (127 mm) outside diameter pipe. The wider reinforcement was used for the hole with larger eccentricity where higher hole edge stresses were expected, and the narrower width was used for the hole with a lesser eccentricity. Details of beam, holes and reinforcement are shown in Figure 3.3.

The flange and web in the vicinity of the hole were

instrumented with strain gauges, and the locations of these are shown in Figure 3.4. The beam was simply supported and was loaded by a single concentrated load applied by an Amsler hydraulic jack. No lateral support was provided because of the low magnitude of applied loads. Strain readings and deflections were recorded for loadings from 2 kips (8.9 kN) to 30 kips (133.5 kN) in seven increments of 4 kips (17.8 kN), and readings were automatically recorded and stored on tape for later analysis. Two tests corresponding to two moment-to-shear ratios of 24 inches (0.588 m) and 48 inches (1.176 m) were performed. The beam was tested with the holes in the position shown in Figure 3.3, and then in the reversed position with hole centres below the mid-depth of the beam. This leads to two sets of corresponding readings for each strain gauge, one set being of opposite sign to the other. The averaged stresses for these two positions (obtained with the appropriate sign change) are given herein, and the values given correspond to the position of the holes above the mid-depth of the beam, as shown in Figure 3.3.

The experimental tangential normal stresses around the hole edges are shown in Figures 3.5 to 3.8. These stresses were calculated from strain gauges located at the centre of the reinforcement, i.e. in the plane of the web, and thus correspond to the stresses assumed to be uniform over the

effective width of the reinforcement. Also plotted are the stresses obtained by the curved beam analysis. Stresses for the hole with a large eccentricity are shown in Figures 3.5 and 3.6 for M/V ratios of 24 inches (0.588 m) and 48 inches (1.176 m). Good agreement between the stresses are observed in both cases, in the zones where high stresses are predicted, i.e. in the low moment side of the hole for the upper part of the beam and in the high moment side of the hole for the lower part of the beam. Results for the hole with a smaller eccentricity are shown in Figures 3.7 and 3.8. They show similar agreement to results for the case of the hole with a larger eccentricity.

Longitudinal normal stresses were measured over the length of the hole on both flanges along the centreline of the beam and results are plotted in Figures 3.9 to 3.12 for both holes and both M/V ratios. Also plotted are flange stresses obtained from the flexural formula applied to the gross beam section, that is, ignoring the presence of hole and reinforcement. For the smaller eccentricity considered, Figures 3.9 and 3.10, it is clear that flange stresses are not significantly affected by the presence of the reinforced hole. For the larger eccentricity, Figures 3.11 and 3.12, the stresses in the flange closest to the hole are influenced by the hole to the extent that the flexural formula underestimates the measured flange stress at the high moment end by 23%, and

overestimates it at the low moment end by about 30%. It is relevant to note that the highest flange stresses measured are lower than the predicted maximum hole edge stresses. This is so for both moment-to-shear ratios tested.

Shear stresses on the centreline of the holes were measured by rosette gauges and are shown in Figures 3.13 and 3.14. Also plotted are the shear stresses calculated according to the standard shear formula using the shear forces  $V_T$  and  $V_B$  obtained from Equations 8 and 9 in Ref. 10. For the hole with a smaller eccentricity, quite close agreement was found for both the top and bottom sections; for the other hole, agreement is not as close. From these results it appears that the shear force predicted for the larger section (in this case below the hole) is overestimated when the eccentricity is large, and in the smaller section it would be correspondingly underestimated. However, the error is not unacceptably large since this shear is also used to calculate the normal stresses in the reinforcement, and the agreement between theory and experimental measurement of these stresses is satisfactory.

#### 3.4 Conclusions

The purpose of this study was to formulate an analysis to predict the maximum hole edge stresses for eccentric circular web holes reinforced by circular rings. The

curved beam analysis which was used in analysing unreinforced holes as described in Ref 10 is modified and employed here. Due to secondary bending of the curved reinforcement flange, a modified cross-section was used in calculating the stresses.

Based on the results obtained from the experimental program and the agreement between the measured stresses and the theoretically predicted stresses, it can be concluded that the curved beam analysis is a suitable method for use in design of circular reinforcement for the type of holes considered.

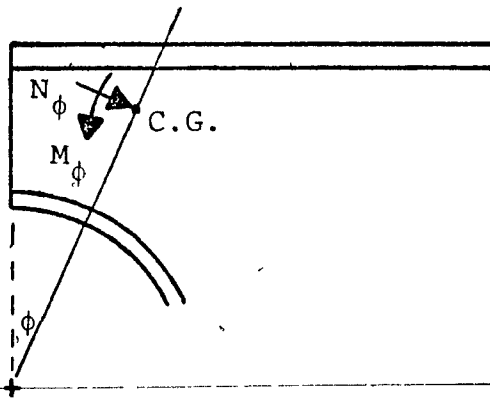
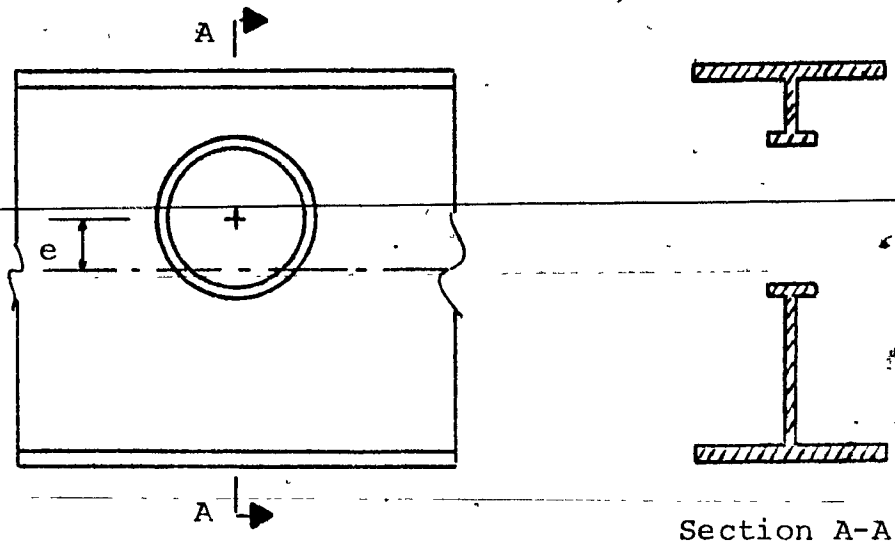


Figure 3.1 Curved Beam Idealisation

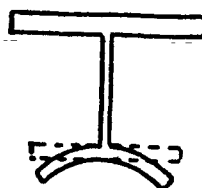
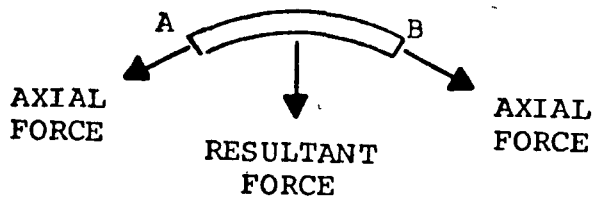
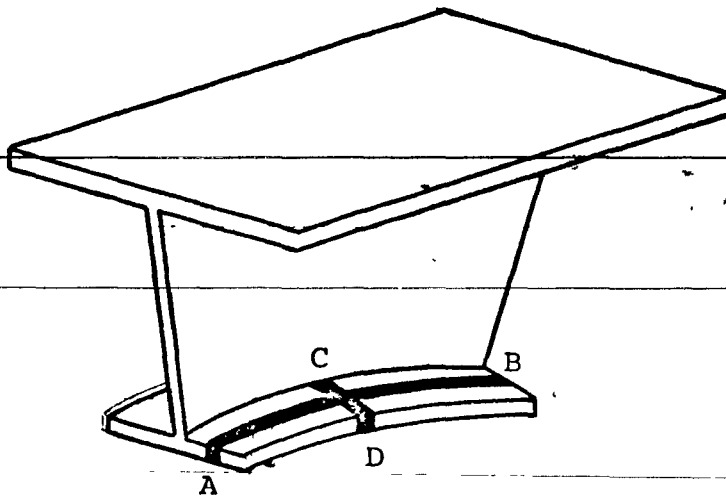
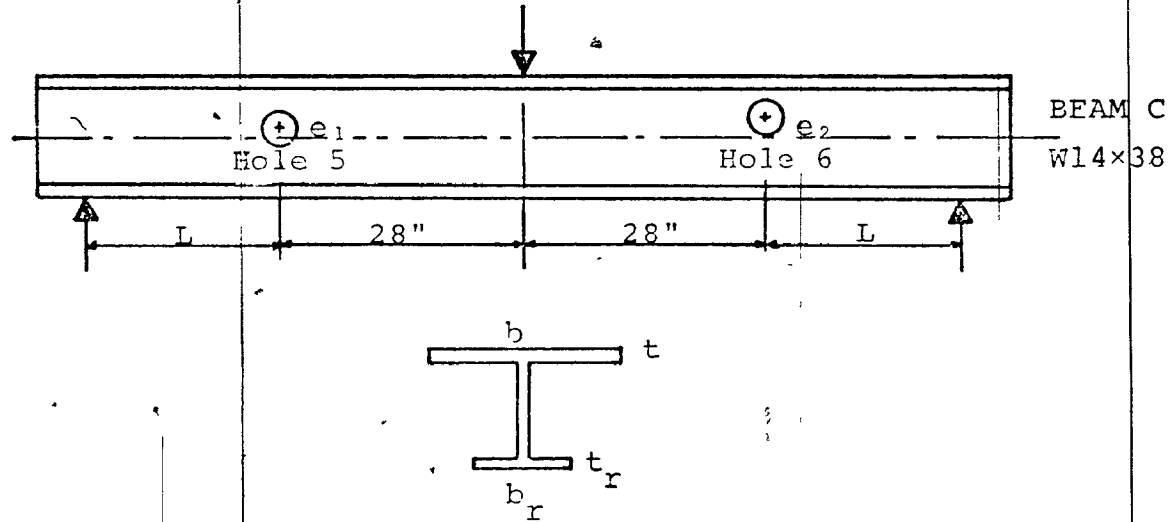


Figure 3.2 Deflection Of Curved Reinforcement Flange



Beam	d	b	t	w	Hole	2R	e	b <sub>r</sub>	t <sub>r</sub>	L (in.)	
										Test 1	Test 2
C	14.2"	6.75"	0.51"	0.32"	5	4.5"	1.0"	2.1"	0.25"	48	24
					6	4.5"	2.5"	3.5"	0.25"	48	24

Figure 3.3 Details Of Test Beam

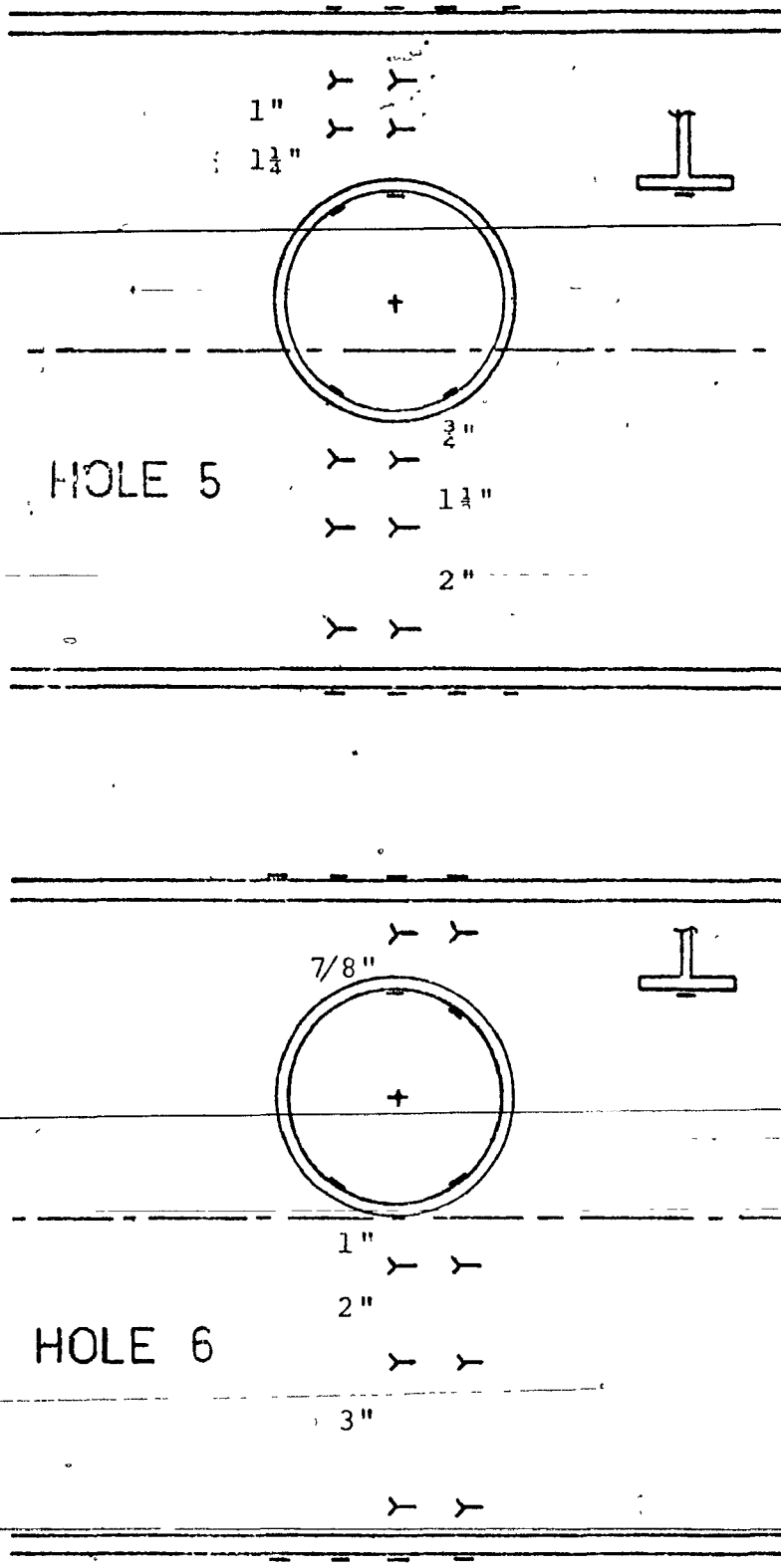
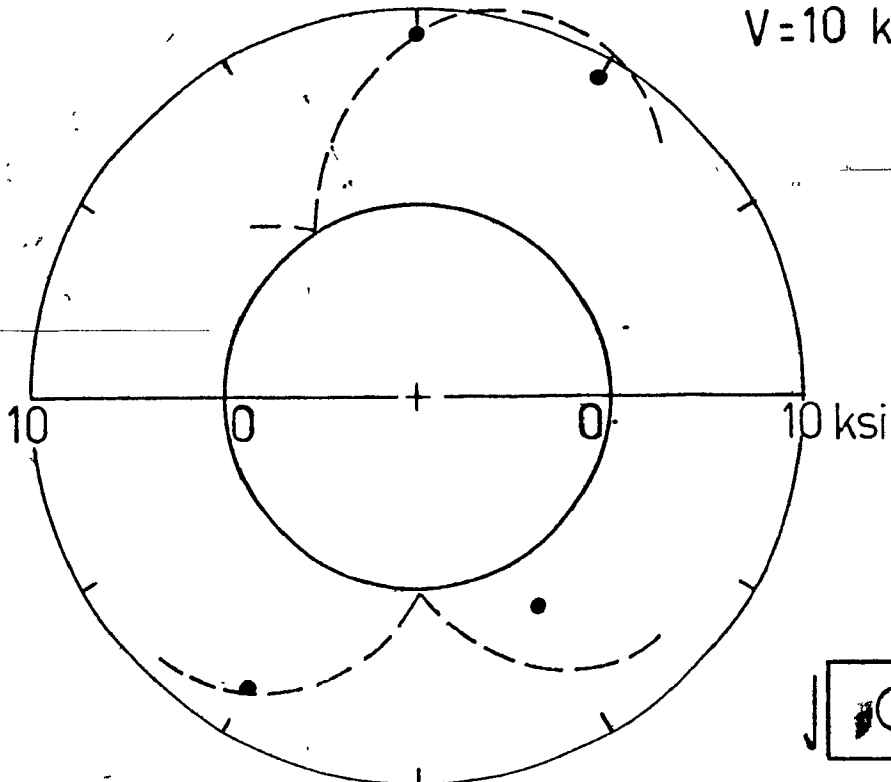


Figure 3.4 Instrumentation Of Beam

M=480 k-in  
V=10 kips



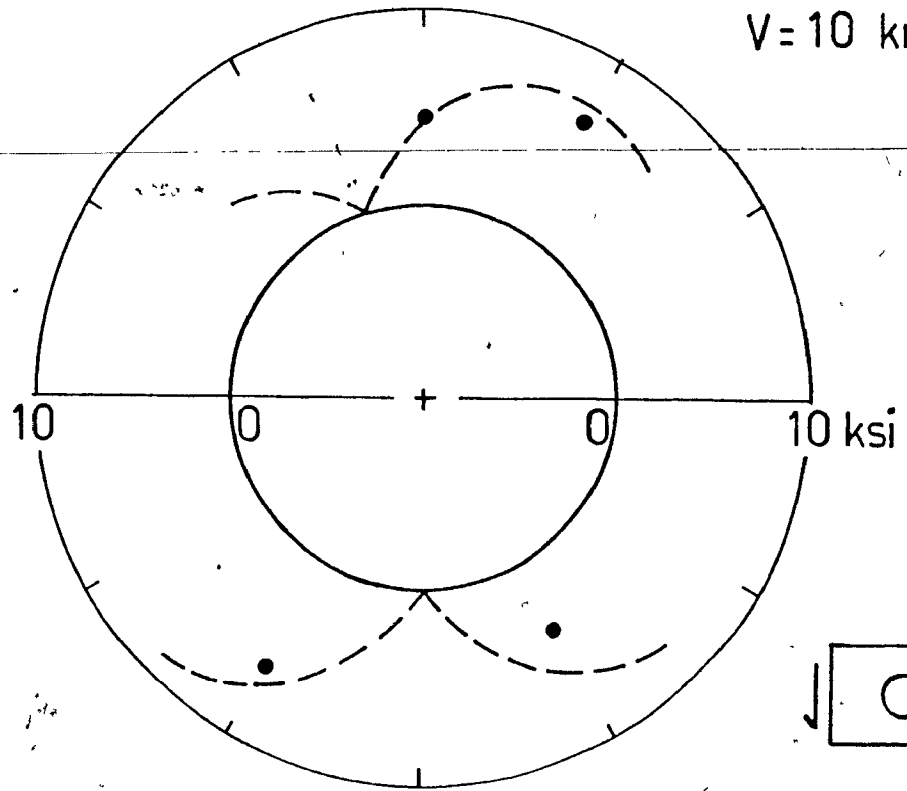
BEAM C  
HOLE 6

$2R=4.5''$   $b_r=3.5''$   
 $e=2.5''$   $t_r=0.25''$

• EXPERIMENT  
--- CURVED BEAM

Figure 3.5 Hole Edge Stresses For Hole 6, Beam C  
(M/V = 48")

M=240 k-in  
V=10 kips



BEAM C

$2R = 4.5''$

$b_r = 3.5''$

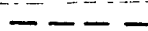
HOLE 6

$e = 2.5''$

$t_r = 0.25''$



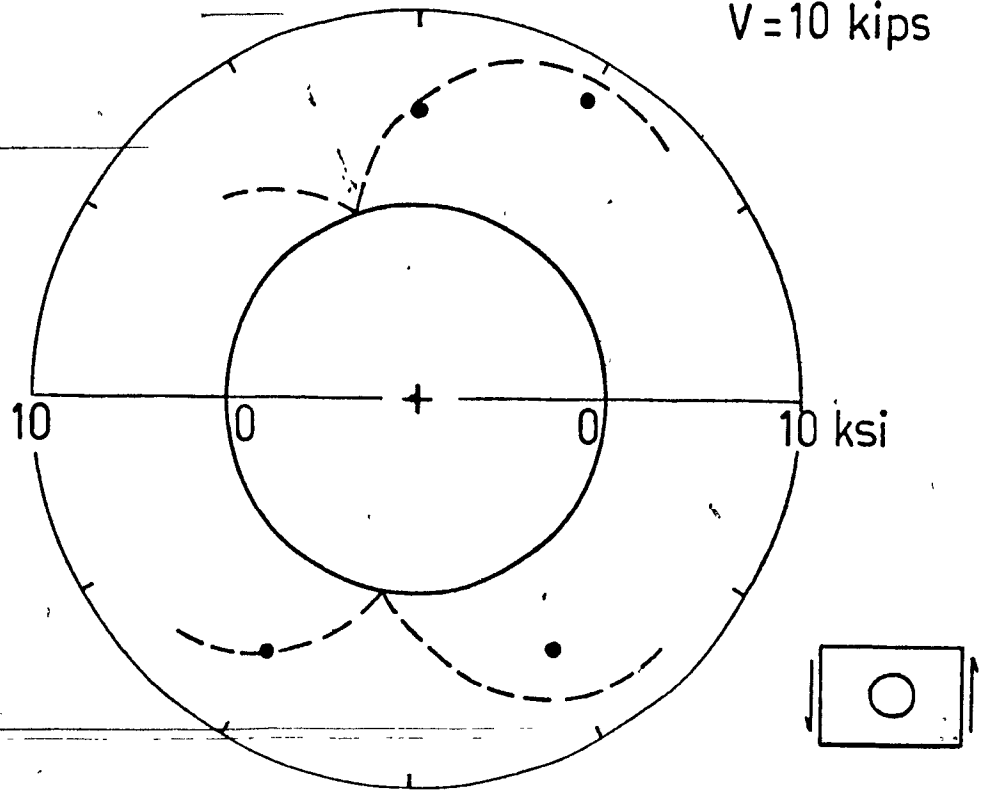
EXPERIMENT



CURVED BEAM

Figure 3.6 Hole Edge Stresses For Hole 6, Beam C  
( $M/V = 24''$ )

$M=480$  k-in  
 $V=10$  kips



BEAM C  
HOLE 5

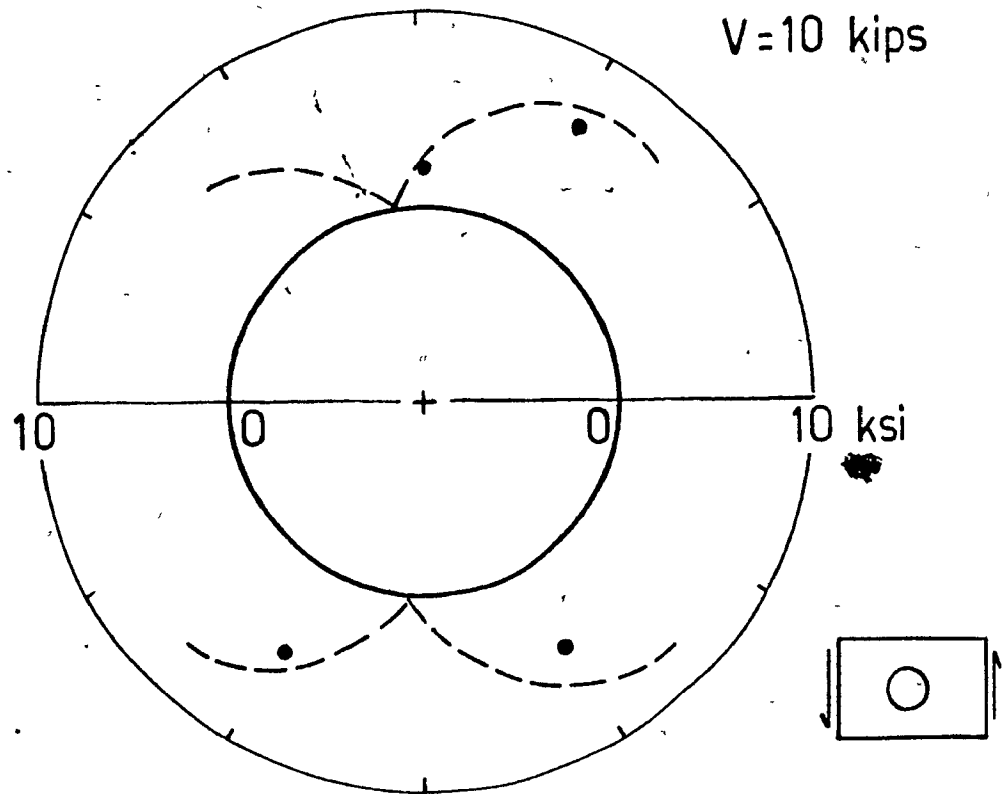
$2R=4.5''$   
 $e=1.0''$

$b_r=2.1''$   
 $t_r=0.25''$

• EXPERIMENT  
--- CURVED BEAM

Figure 3.7 Hole Edge Stresses For Hole 5, Beam C  
( $M/V = 48''$ )

M=240 k-in  
V=10 kips



BEAM C  
HOLE 5

$2R=4.5$   
 $e=1.0$

$b_f=2.1$   
 $t_f=0.25$

• EXPERIMENT  
--- CURVED BEAM

Figure 3.8 Hole Edge Stresses For Hole 5, Beam C  
(M/V = 24")

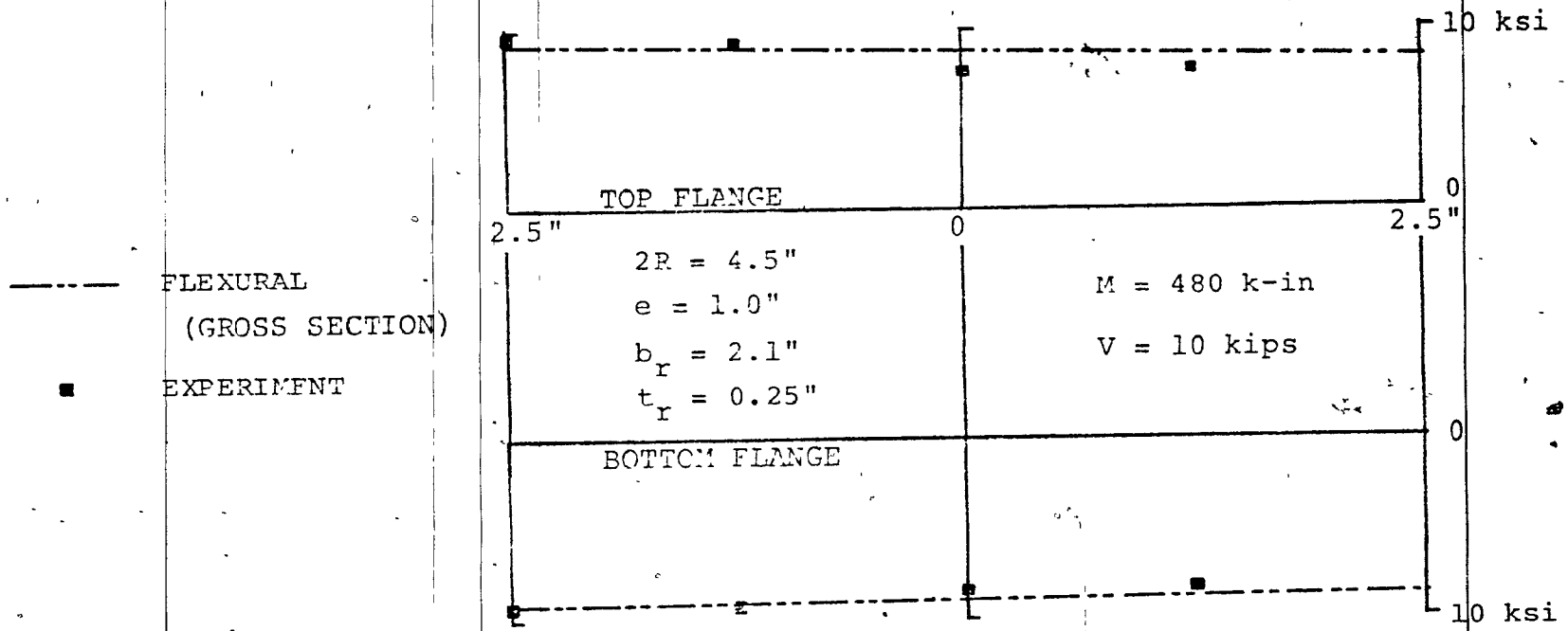


Figure 3.9 Flange Stresses For Hole 5, Beam C  
( $M/V = 48"$ )

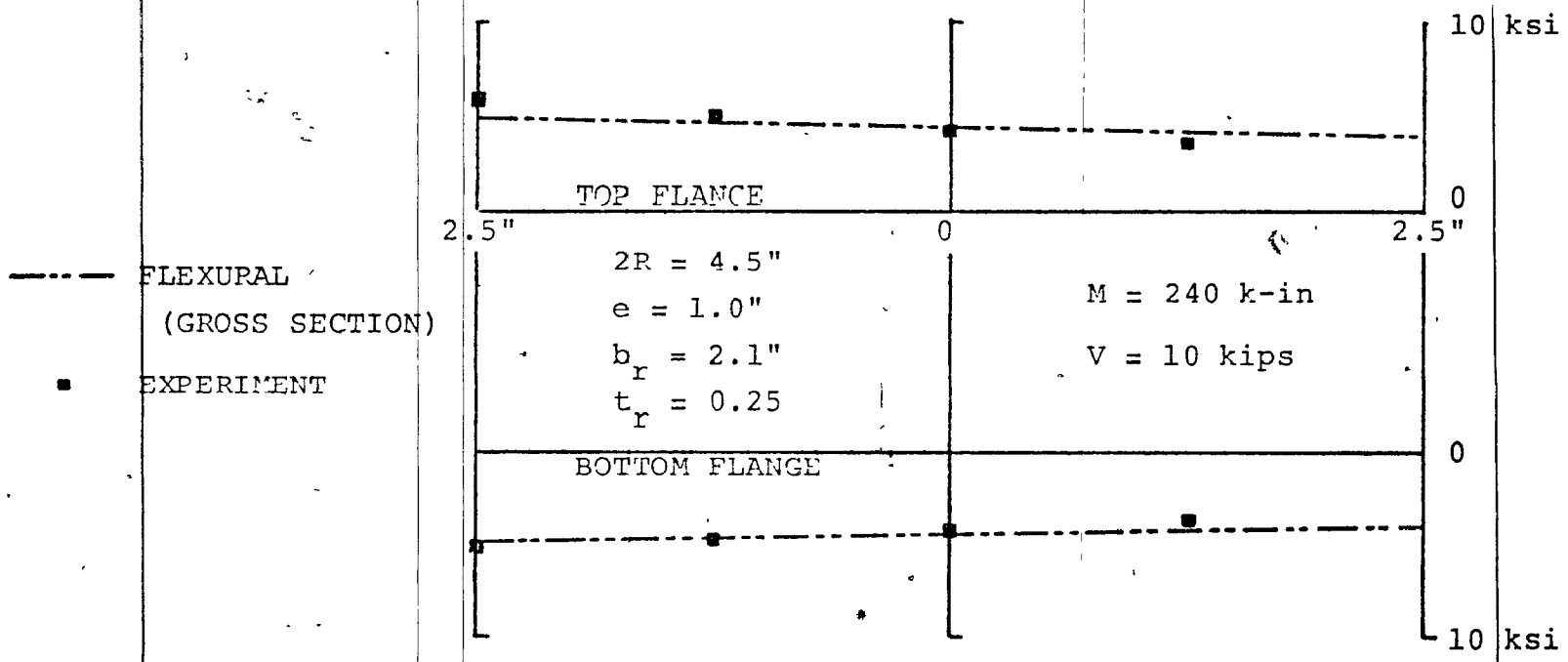


Figure 3.10 Flange Stresses For Hole 5, Beam C  
( $M/V = 24''$ )

- - - - FLEXURAL  
 (GROSS SECTION)  
 ■ EXPERIMENT

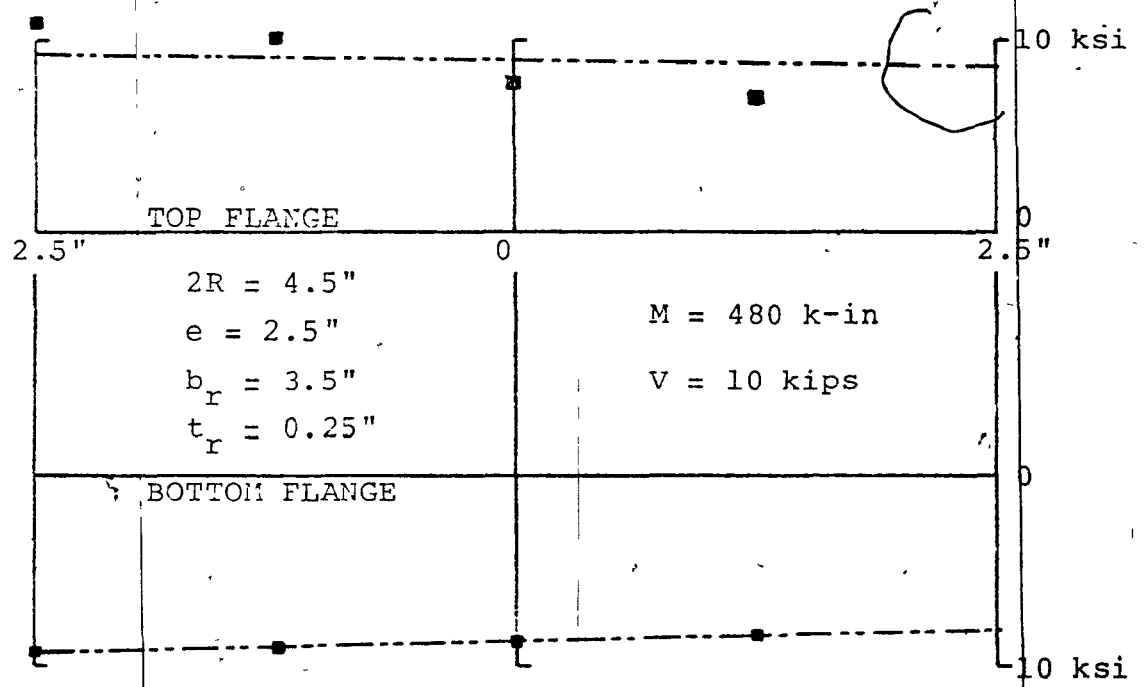


Figure 3.11 Flange Stresses For Hole 6, Beam C  
 ( $M/V = 48"$ )

- - - - FLEXURAL  
 (GROSS SECTION)  
 ■ EXPERIMENT

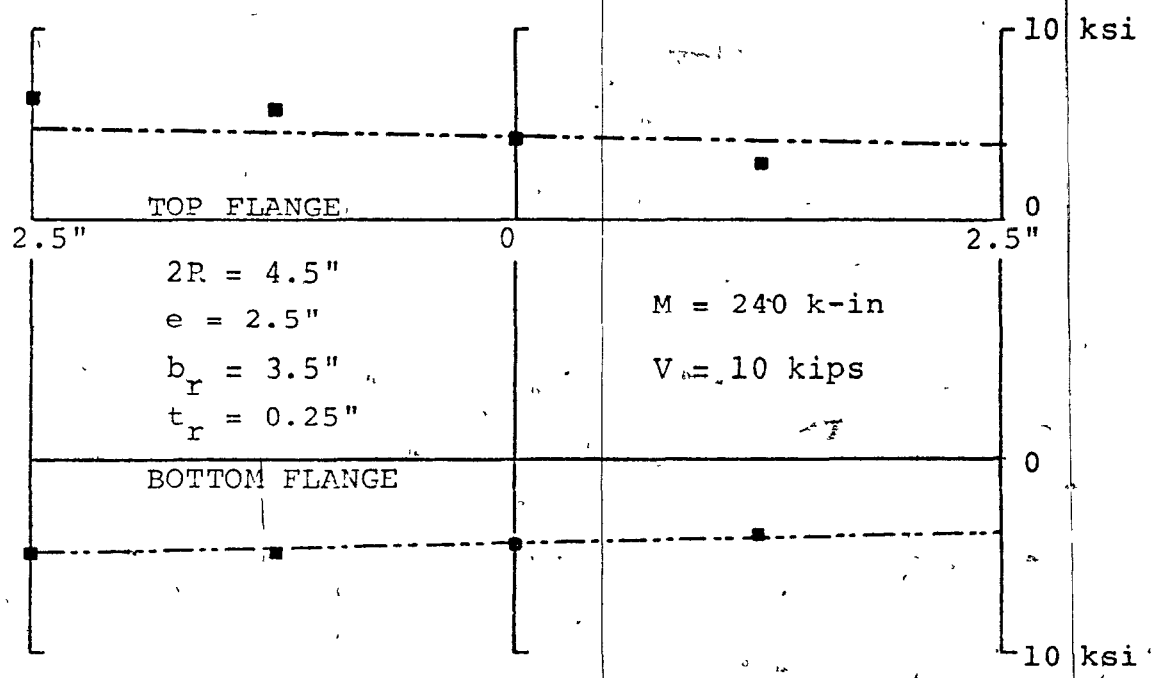


Figure 3.12 Flange Stresses For Hole 6, Beam C  
 ( $M/V = 24"$ )

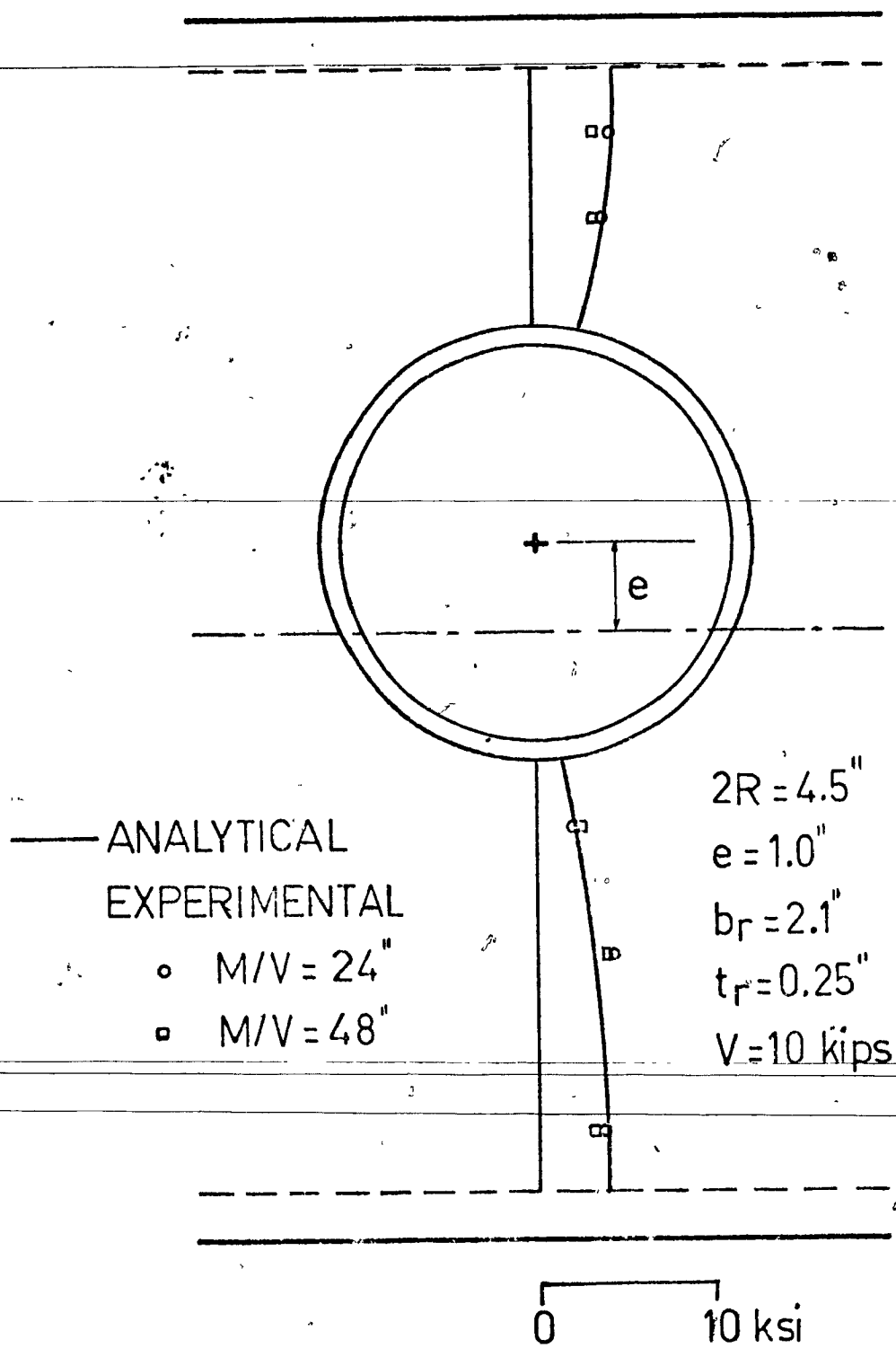


Figure 3.13 Shear Stresses At Hole Centreline  
For Hole 5, Beam C

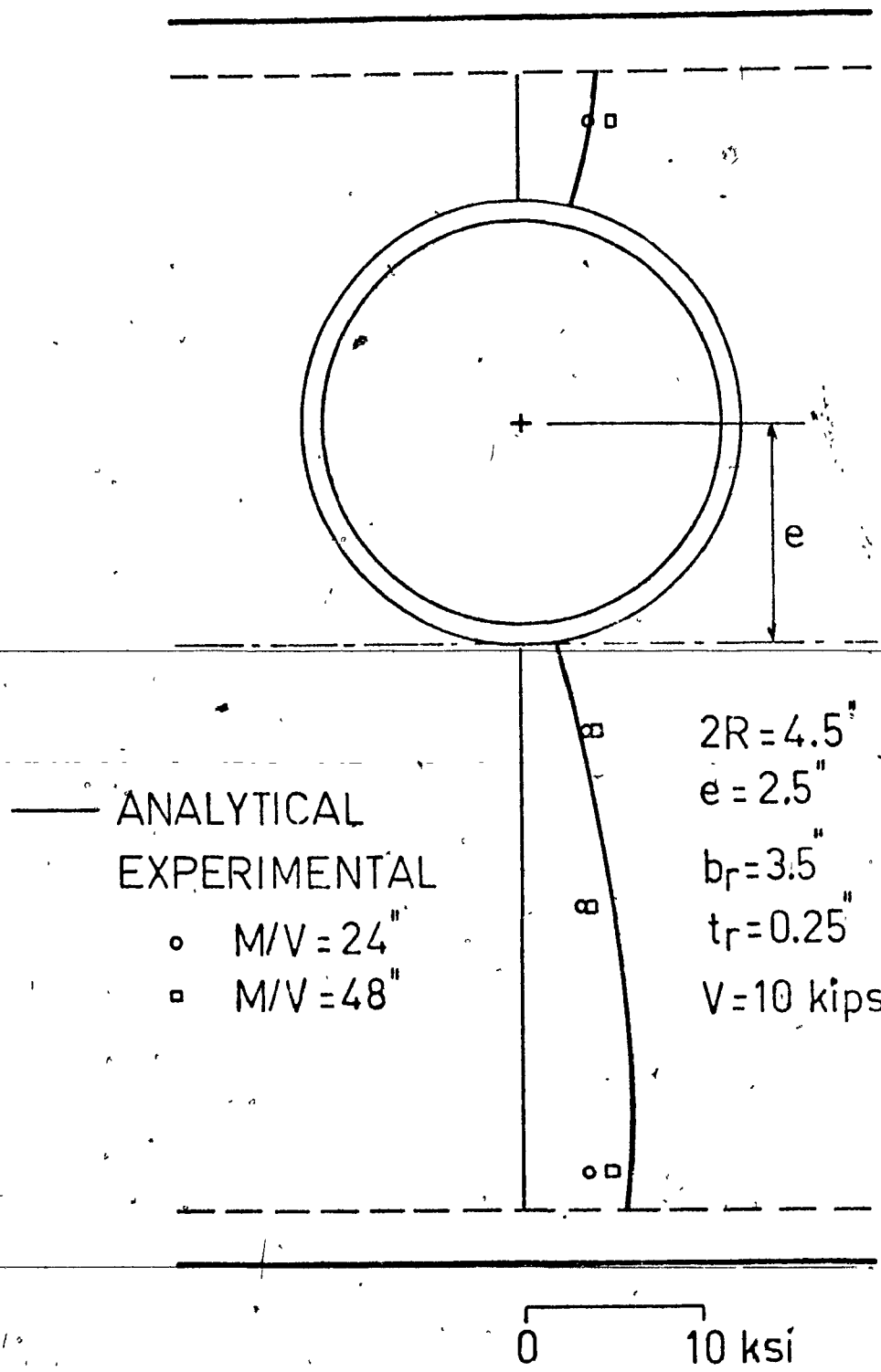


Figure 3.14 Shear Stresses At Hole Centreline  
For Hole 6, Beam C

CHAPTER 4

EXPERIMENTAL PROGRAM

## CHAPTER 4

### EXPERIMENTAL PROGRAM

While analytical methods are proposed for the analysis of circular holes in the previous chapters, it is essential that some experimental data be obtained to check their applicability. In this chapter, the test procedures used are described.

#### 4.1 Test Specimens

Two wide-flange beams with web holes were tested. Beam A, a W14×30 beam was 12 feet 2 inches (3.71 m) long and contained two large circular holes of diameters  $10\frac{1}{2}$  inches (266.7 mm) and 8 inches (203.2 mm). These two holes were chosen large enough that the theory of elasticity method would not be adequate for their analysis and the results, therefore, represent a test of the curved beam method. The larger hole was centred at the mid-depth of the beam whereas the smaller hole was 1 inch (25.4 mm) eccentric to the mid-depth. These two holes were centred 48 inches (1.219 m) apart which was more than sufficient to ensure that the presence of one hole would not affect the stress distribution around the other (Figure 2.3). Beam B, a W14×38 beam was 15 feet (4.572 m) in length and contained two eccentric circular holes of equal diameters, 5 inches (127 mm). This hole diameter was chosen to explore the limitation in application of the two theories. They were centred 56 inches

inches (1.422 m) apart (Figure 2.3). After Beam B was tested, circular reinforcements in the form of circular rings cut from a 5 inch outside diameter pipe were fitted into the holes of Beam B and welded to both sides of the web with 3/16 continuous fillet welds. For identification purpose, Beam B after the addition of circular reinforcement is denoted as Beam C. Due to the low magnitude of loads applied during the testing, no stiffeners were welded to either beam. The surface of the beams was slightly polished with an electric sander to get rid of the rust and mill scale in locations where strain gauges were to be attached. The hole diameters, locations of holes and sizes of reinforcement are summarized in Figure 4.1.

All of the holes were machine-cut with a fly cutter mounted on a drilling machine. The radius of the fly cutter could be extended to account for different hole sizes.

During the process of cutting, a small crack near the 10½ inch diameter hole on Beam A was discovered. This was later filled with weld material. However, it was apparent that the crack was a fabricating defect and was not caused by the cutting process.

#### 4.2 Instrumentation

The webs, flanges and reinforcements of both beams were instrumented with electric resistance strain gauges

manufactured by Tokyo Sokki Kenkyujo Co., Japan. Two types of these gauges were used, PL-5, uniaxial gauges and PR-5, 45 degree rosette gauges. Adhesive type CN, a quick setting adhesive made by the same manufacturer was used to mount the gauges on the surface of the beam. A waterproofing coating was applied to all gauges after they have been mounted on the beam to protect them from atmospheric humidity. The gauge locations for both beams are shown in Figure 2.4 and Figure 3.2 in Chapters 2 and 3 respectively. Loadings for all tests were supplied by a 220 kip capacity Amsler hydraulic jack. The beams were tested simply supported with a concentrated load at mid-span and no lateral support was provided because of the low magnitude of applied loads.

Two positions of the beam were tested, first with the holes in the position shown in Figures 2.3 and 3.3 and then in the reversed position with the hole centres below the mid-depth.

#### 4.3 Testing Procedure

Two different methods of recording strains were employed during the experimental programs. Strains obtained from tests performed on Beam A were recorded by a multi-channel automatic Budd Strain Recorder with the results printed out on a printer. A more refined, computerized procedure was used in

recording the strain readings for tests performed on Beams B and C. A multi-channel strain recorder manufactured by B & F Instrument Inc. and a computer system were used in recording the strains. The computer system used was the GEPAC System (manufactured by General Electric) of the DATAC Centre, operated by the Department of Mechanical Engineering, McGill University. A conversational program was designed and stored in the computer which would give a step by step instruction to the operator during the performance of the tests. The strain recorder was linked to the computer through a connecting terminal mounted in the laboratory. A tele-typewriter connected to the Bell Telephone system was used to send instructions and input data to the computer. A schematic diagram showing the essential parts in the test set up is given in Figure 4.2.

Before the start of each test, the strain recorder with the gauges connected to it was first calibrated according to the gauge factors specified by the manufacturer. The computer was then activated for testing by dialing an on-line number through the Bell Telephone system. The computer would first scan through all the channels of the strain recorder and print out the number of those channels that were not properly connected, e.g. loose connections and void channels. This would be fixed and a recheck done by the computer. When this

was completed, a load of 2 kips was gradually applied to the beam to get the initial reading on the gauges. The Amsler loading machine was then switched to constant-loading mode which would keep the applied load constant at the prescribed level. Under an instruction given by a type-in message, the computer would again scan through all the channels, record the readings and store them on the disk. A set of the recorded readings was also printed out by the teletype as a precaution measure in case the records on disk were destroyed. After all these readings had been recorded, the beam was loaded by the next increment and the above procedure was repeated.

An account of the details of test beams, strain gauge locations and load increments is discussed in detail in Chapters 2 and 3. The conversational program and some of the computer printouts are given in Appendix V.

#### 4.4 Analysis of Data

After each individual test, the data stored on disk was transferred onto a magnetic tape. When all the tests were finished, the data stored on the tape were analysed using two computer programs; the first program, Program 1, calculated the differences in strain between each load increment and the second program, Program 2, analysed the strain readings using linear regression techniques. Before fitting the regression

line on any set of readings, the confidence intervals of each individual reading was first established. If any point was outside this interval, it would be discarded when fitting the regression line. A confidence limit of 90% was used on all of the readings. The computer would print out the slopes, i.e. strain per unit load and the intercepts of the regression line of all the gauges and the number of points used in the fitting of the lines. It was observed that only a few points were discarded in the entire experiment.

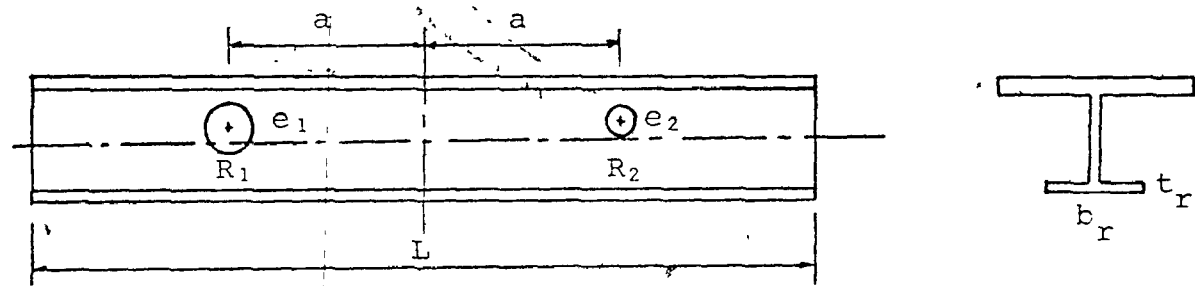
For linear gauges, the stresses were obtained by multiplying the slopes by the modulus of elasticity,  $E$ , which is equal to 29,600,000 psi. As for the rosettes, the principle strains were first calculated based on the strain readings from the three gauges and the stresses were obtained using the biaxial stress-strain relationship. A shear modulus value of 11,400,000 psi and Poisson's ratio of 0.3 were used in the analysis.

The two computer programs mentioned above are given in Appendix V.

#### 4.5 Experimental Results

Experimental stresses around the hole edges and the beam flanges are plotted and compared with theoretical stresses, and in most cases, they show good agreement. Also plotted are

the shear stresses at hole centrelines for eccentric holes, so as to compare the shear stress distributions based on unequal shear forces in the top and bottom sections determined by the method shown in Chapters 2 and 3. Comparisons of results for unreinforced holes and reinforced holes are given in Chapters 2 and 3 respectively. Supplementary results for the unreinforced hole are given in Appendix VIII.



Beam	Beam Size	L	a	$R_1$	$R_2$	$e_1$	$e_2$	$b_{r1}$	$b_{r2}$	$t_{r1}$	$t_{r2}$
A	W14×30	12'-2"	2'-0"	10.5"	8.0"	0	1.25"	-	-	-	-
B	W14×38	15'-0"	2'-4"	5.0"	5.0"	1.0"	2.5"	-	-	-	-
C	W14×38	15'-0"	2'-4"	4.5"	4.5"	1.0"	2.5"	2.1"	3.5"	0.25"	0.25"

Figure 4.1 Details of Test Beams

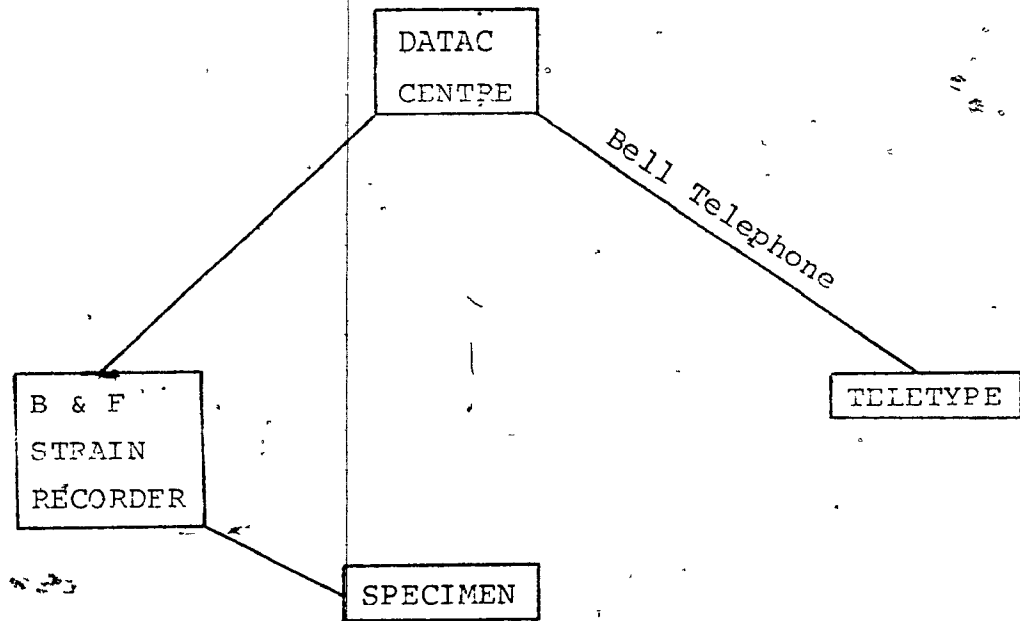


Figure 4.2 Schematic Diagram Showing Experimental Set Up

CHAPTER 5

DESIGN OF UNREINFORCED HOLES

## CHAPTER 5

### DESIGN OF UNREINFORCED HOLES

#### 5.1 Derivation of Design Aids

Previous work has been concerned with the identification of suitable methods of analysis for stresses in beams in the region of circular unreinforced holes<sup>6</sup>. A satisfactory solution for design purposes can be obtained either by a solution based on the theory of elasticity or by one based on simplifying assumptions in which parts of the beam around hole are treated by curved beam theory. The appropriate method depends upon the eccentricity of the hole centre from the mid-depth of the beam, the moment-to-shear ratio, and the diameter of the hole relative to the beam depth. These two methods have been outlined in Ref. 6, and the purpose herein is to provide design aids, based on these methods, which can be used in allowable stress design. The aids relate to I-beams symmetric about the neutral axis.

The design aids take the form of interaction curves relating the shear force,  $V$ , and moment  $M$  which, acting together, will just cause the maximum normal stress in the region of the hole to reach the allowable value. Thus, values of  $M$  and  $V$  which just cause the maximum stress to reach  $F_b$ , the allowable normal stress in bending, are represented by

points on the curve, and points on the concave side of the boundary represent lower values of the maximum stress. Points outside the curve represent unsafe load combinations. Shear and moment have been nondimensionalised by dividing by  $V_{all}$  and  $M_{all}$ , respectively, these being the allowable values of shear and moment, based on the nominal gross beam section. It has been assumed that  $F_v = 2F_b/3$ , in which  $F_v$  = the allowable shear stress. In addition, it has been assumed that  $t/d = 0.05$  and  $A_w/A_f = 2.0$ , in which  $t$  = the flange thickness;  $d$  = the overall beam depth;  $A_w$  = the area of the unperforated web; and  $A_f$  = the area of one flange. The results are not sensitive to these ratios, and the assumed values both lead to slightly conservative results. It has been assumed throughout that parts of the beam around the hole remain stable, and therefore are not subject to local buckling at stress levels lower than those predicted.

An interaction diagram consisting of four regions is shown in Figure 5.1; one part of the curve corresponds to the case when flange stresses govern, and the other three to hole edge stresses, and a typical interaction diagram will contain two or more of these regions. Of the latter three, the theory of elasticity solution may govern at the higher moment-to-shear ratios, and the other two are derived from the simplified curved beam analysis. Flange stresses are based on the curved beam analysis, which has been shown to adequately predict the

maximum stress in the flange over the length of the hole. These flange stresses govern in only a few cases; these correspond to small holes with small or zero eccentricity under low shear forces.

Figures 5.2 to 5.13 provide design aids for most practical situations, and account for the effects of the hole on normal stresses in both flange and web. The interaction diagrams may be used if the hole is centred either above the neutral axis or below it. They also apply to both positive and negative values of the shear force and bending moment. In all cases therefore, the diagrams should be entered with the absolute values of  $e$ ,  $V$  and  $M$ . If a situation arises in which  $F_v$  is not  $2/3$  of  $F_b$ , then the same interaction diagrams may be used, but the abscissa is taken as a measure of  $1.5(V/V_{all})$ . ( $F_v/F_b$ ). In the case of compact sections in which  $F_b$  is normally taken as  $0.66 F_y$  (based upon the ability of the beam to attain its plastic moment) it would not be appropriate to use the value  $0.66 F_y$  in the elastic design procedure proposed herein. It would be satisfactory to take  $F_b = 0.60 F_y$  when considering stresses around the hole, and if the web slenderness was such that  $F_v = 0.40 F_y$ , the diagrams could then be used directly.

Another check which a designer must make concerns the maximum shear stress. As an aid to this, Figure 5.14 gives

the division of shear force above and below the hole. Because these values are dependent upon  $A_w/A_f$ , although not very sensitively, results are given for  $A_w/A_f = 0.75$  and  $2.0$ , and intermediate values may be obtained by interpolation. This may be used to calculate the shear stresses in the top and bottom tee-sections on the hole centreline.

### 5.2 Example

Given the beam dimensions and loading shown in Figure 5.15, it is required to check the adequacy of the beam if a hole with a 9-in. (230-mm) diameter and eccentricity 2 in. (51 mm) is placed 6 feet (1.8 m) from the left-hand support. The beam is laterally supported along the span and has a yield stress of 50 ksi (340 MN/m<sup>2</sup>).

Taking the allowable stresses as,

$$F_b = 0.60 F_y = 30 \text{ ksi (210 MN/m}^2\text{) and}$$

$$F_v = 0.40 F_y = 20 \text{ ksi (140 MN/m}^2\text{),}$$

the maximum bending moment at mid-span =  $\frac{40 \times 20 \times 12}{4} = 2400 \text{ kip-in.}$   
(271 kN-m);

$$\text{the maximum bending stress} = \frac{2400 \times 18}{2 \times 802} = 26.93 \text{ ksi (185.7 MN/m}^2\text{)}$$

<  $F_b$ , therefore, O.K.

the hole diameter to beam-depth ratio  $(2R/d) = 9/18 = 0.5$ ; and

the eccentricity to beam-depth ratio  $(e/d) = 2/18 = 0.11$ .

The moment at the hole centreline,  $M = 20 \times 6 \times 12 = 1440 \text{ kip-in.}$   
(163 kN-m).

The shear at the hole centreline,  $V = 20$  kips (89 kN).

The allowable moment,  $M_{all} = \frac{30 \times 2 \times 802}{18} = 2673.3$  kip-in. (302.2 kN-m).

The allowable shear,  $V_{all} = 20 \times 18 \times 0.358 = 128.8$  kips (573 kN).

Thus

$$\frac{M}{M_{all}} = \frac{1440}{2673.3} = 0.54$$

$$\frac{V}{V_{all}} = \frac{20}{128.8} = 0.16$$

This point is plotted in Figure 5.15 and is found to be in the safe region.

#### 5.2.1 Shear Stress at Hole Centreline

Interpolating from Figure 5.14,  $V_T = 0.26V = 5.2$  kips (23 kN) and  $V_B = 0.74V = 14.8$  kips (65.9 kN). The locations of the neutral axis for the top and bottom tee-sections are given in Figure 5.15.

The moment of inertia of the top tee-section,  $I_T = 1.26$  in<sup>4</sup> (52.5 cm<sup>4</sup>) and the moment of inertia of the bottom tee-section,  $I_B = 21.32$  in<sup>4</sup> (888 cm<sup>4</sup>). Maximum shear stress in top tee is

$$\frac{V_T Q_T}{I_T w} = \frac{5.2 \times 1.93 (2.041 - 1.93/2)}{1.26}$$

$$= 8.57 \text{ ksi (59.1 MN/m}^2) < F_v \text{ Therefore O.K.}$$

Maximum shear stress in bottom tee is

$$\frac{V_B Q_B}{I_B^w} = \frac{14.8 \times (5.137)^2}{21.32 \times 2}$$

$$= 9.16 \text{ ksi (63.2 MN/m}^2\text{)} < F_v \text{ Therefore O.K.}$$

Thus, the stresses at the hole are within allowable limits.

### 5.3 Conclusions

The design aids presented herein can be used in allowable stress design of beams with eccentric or mid-depth circular holes, without reinforcement. They are based upon normal and shear stresses, and do not include consideration of local buckling. The curves are given for hole diameter-to-beam depth ratios of 0.20 to 0.75, and for eccentricities of the hole centre from mid-depth of up to 0.25 of the beam depth. In all cases where the hole diameter is larger than 0.3 of the beam depth, eccentricity is limited to less than 0.25 of the beam depth because of the proximity of the hole edge to the flange.

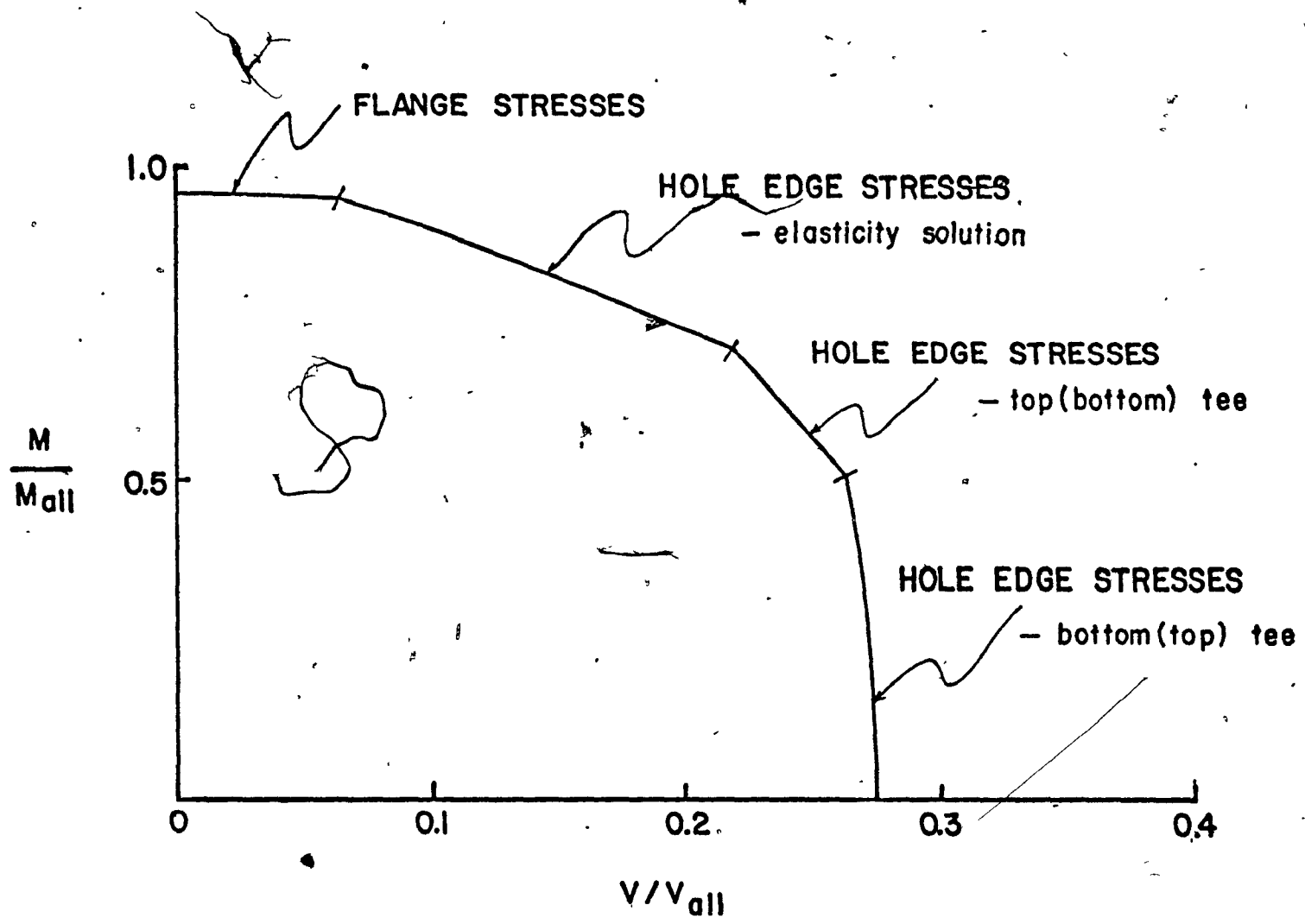


Figure 5.1 Component Regions Of Interaction Diagrams

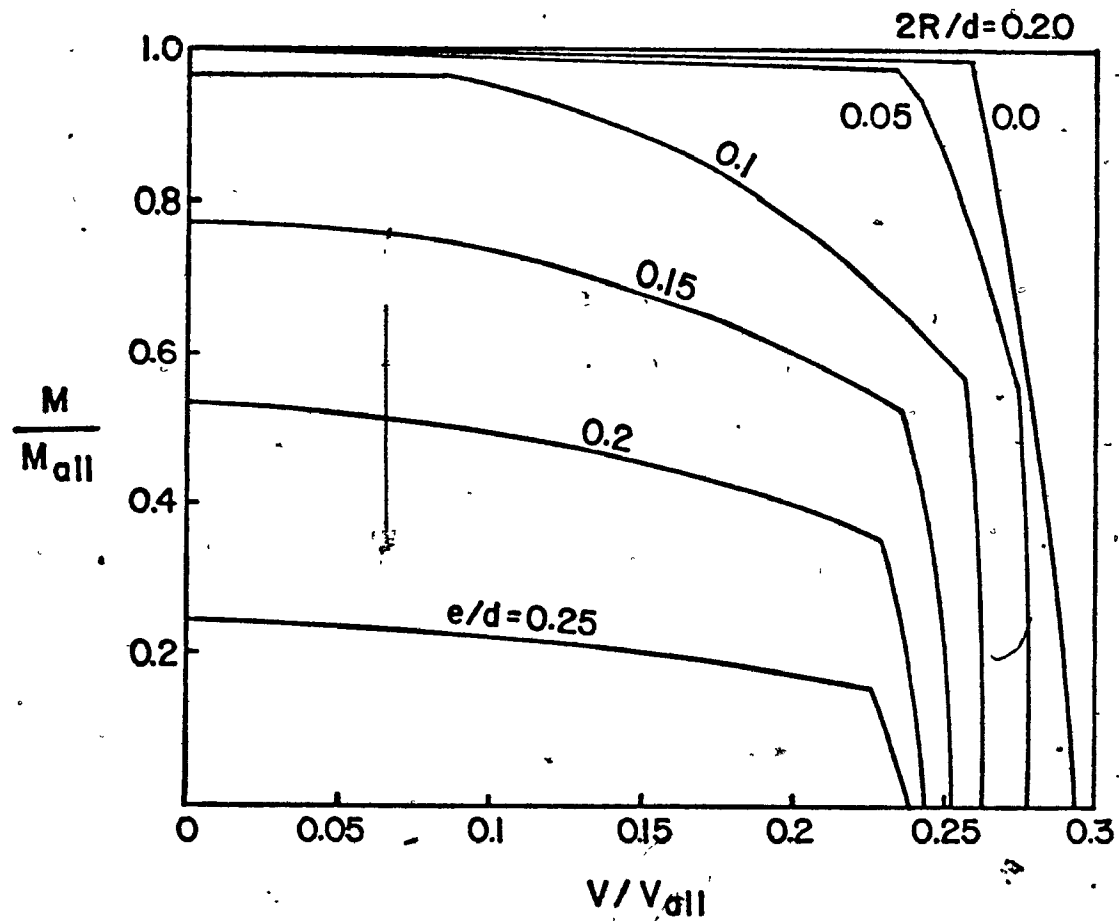


Figure 5.2 Interaction Diagram For 2R/d = 0.20

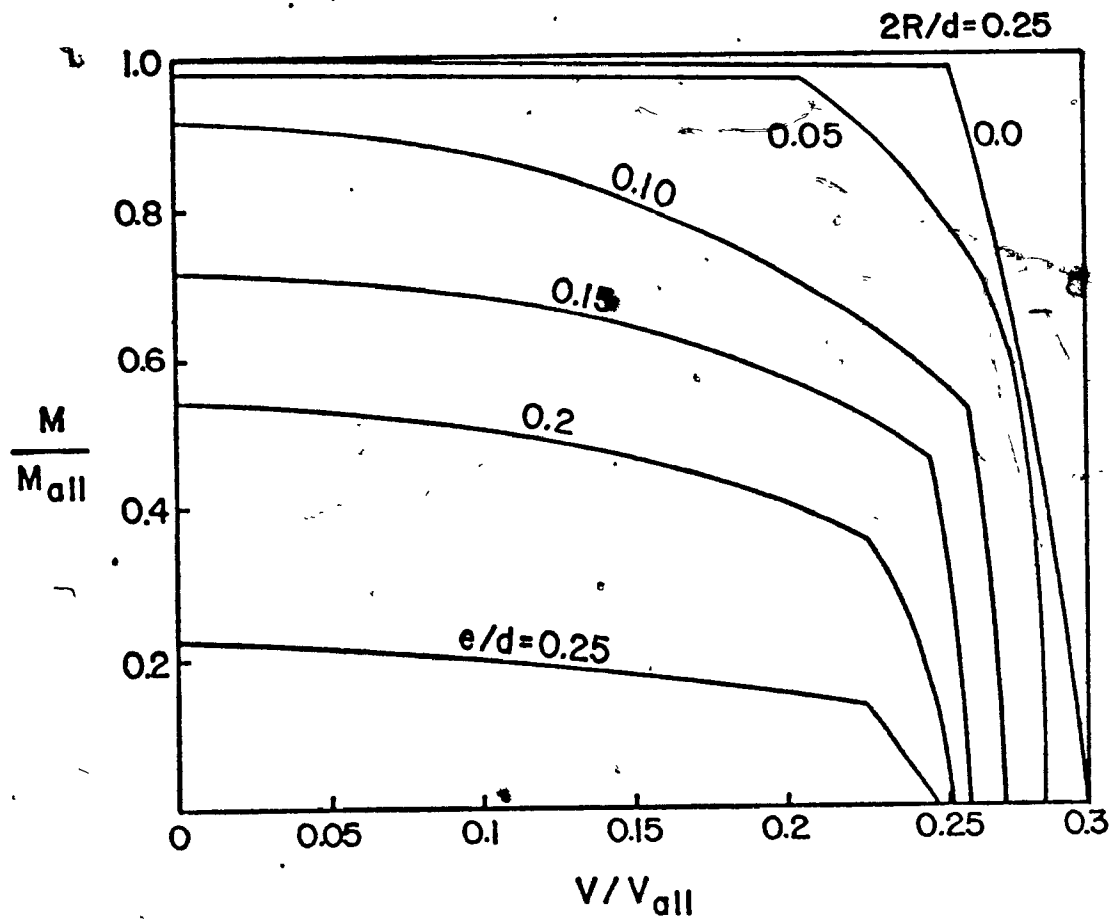


Figure 5.3 Interaction Diagram For  $2R/d = 0.25$

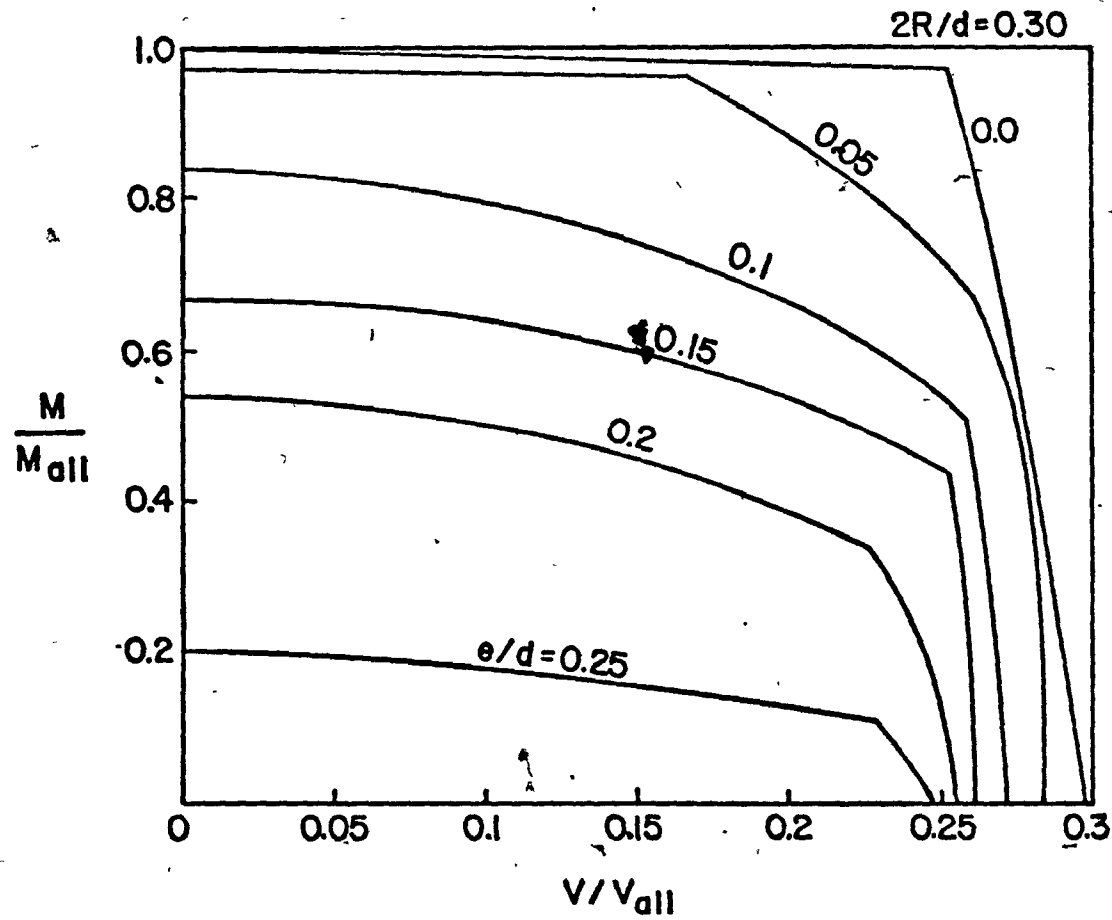


Figure 5.4 Interaction Diagram For  $2R/d = 0.30$

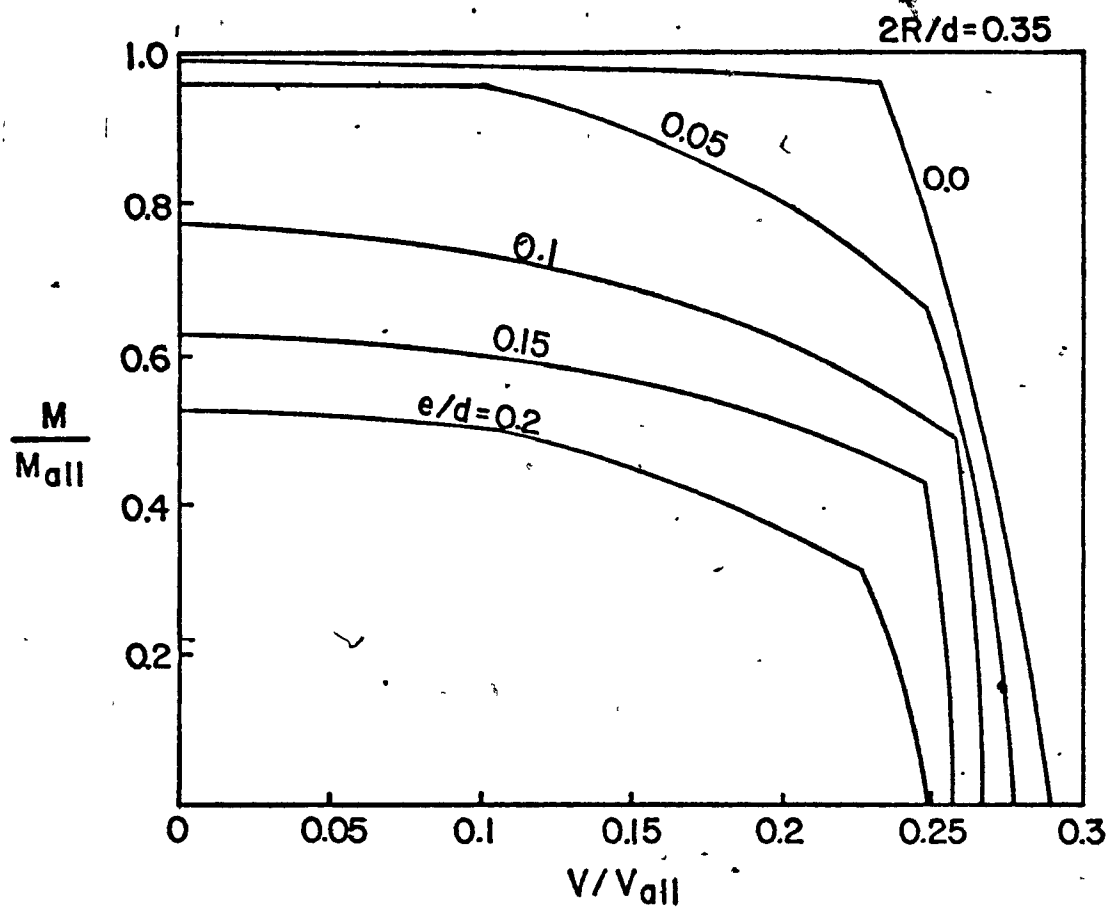


Figure 5.5 Interaction Diagram For  $2R/d = 0.35$

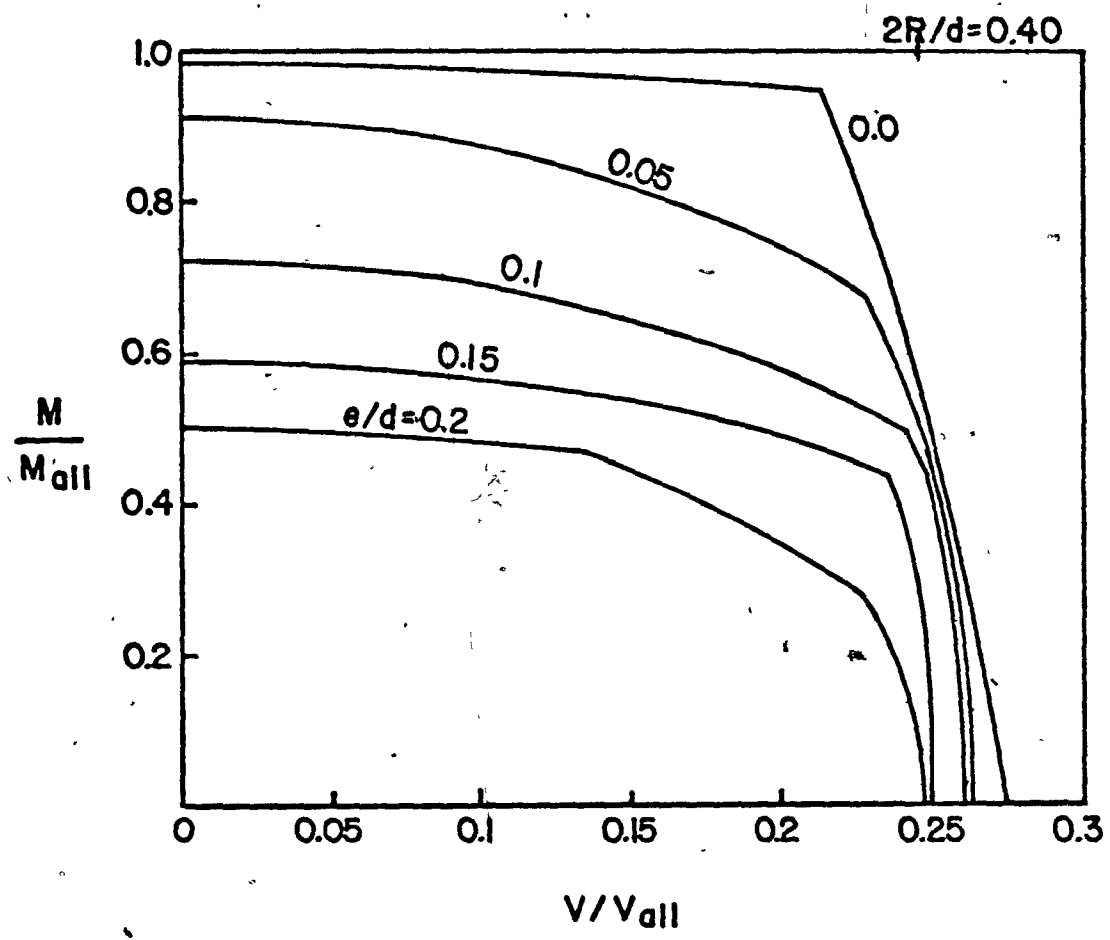


Figure 5.6 Interaction Diagram For 2R/d = 0.40

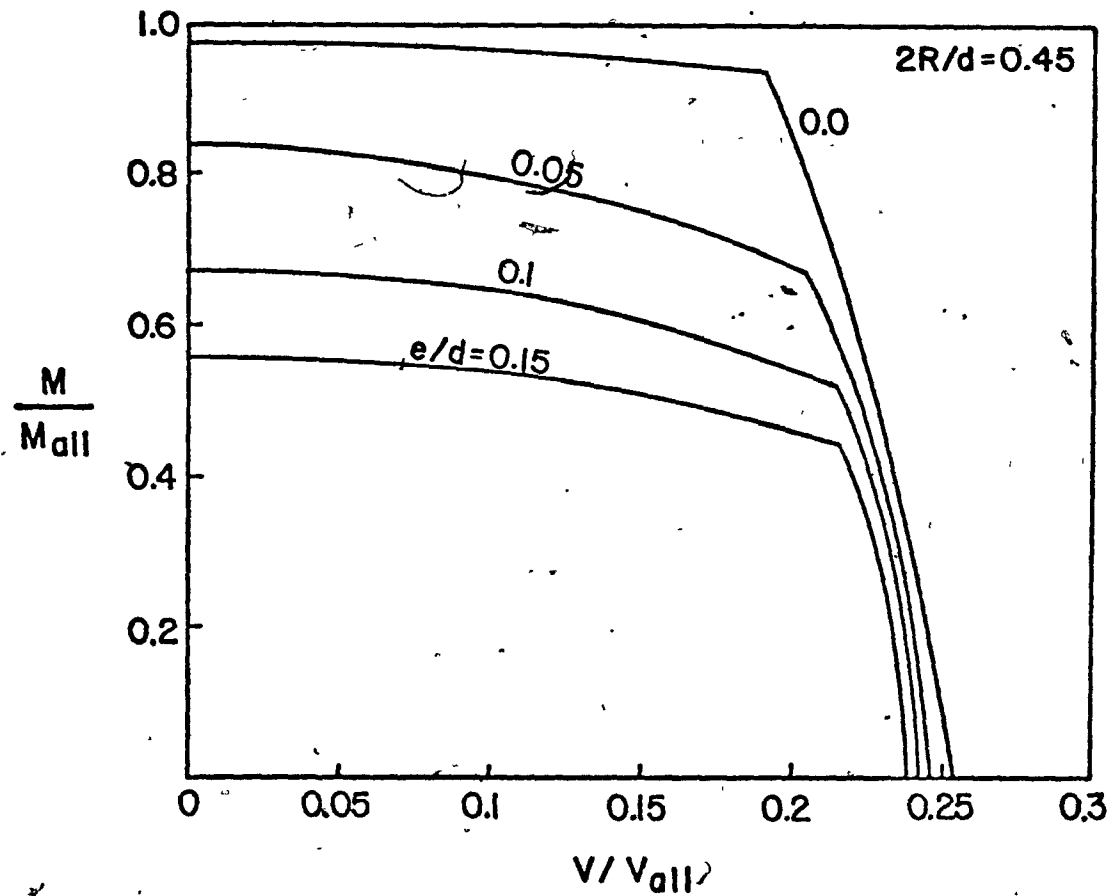


Figure 5.7 Interaction Diagram For  $2R/d = 0.45$

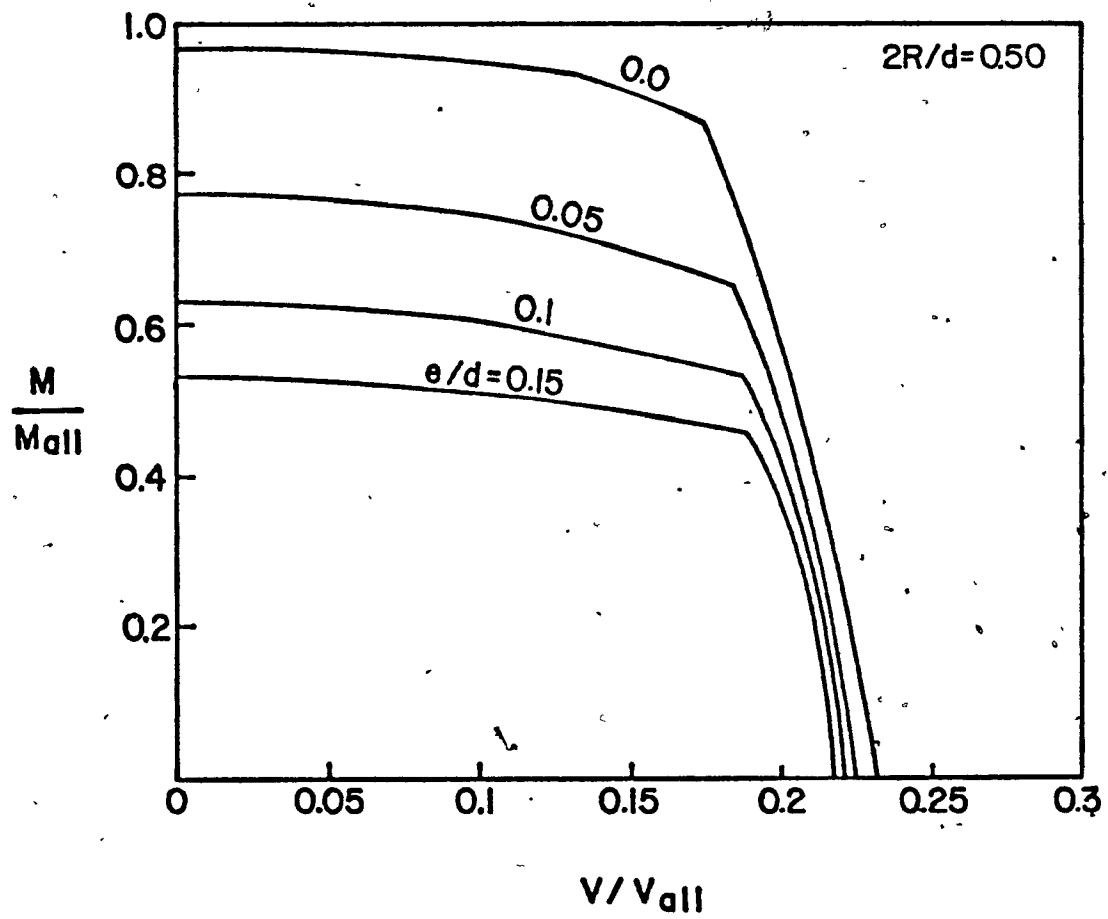


Figure 5.8 Interaction Diagram For  $2R/d = 0.50$

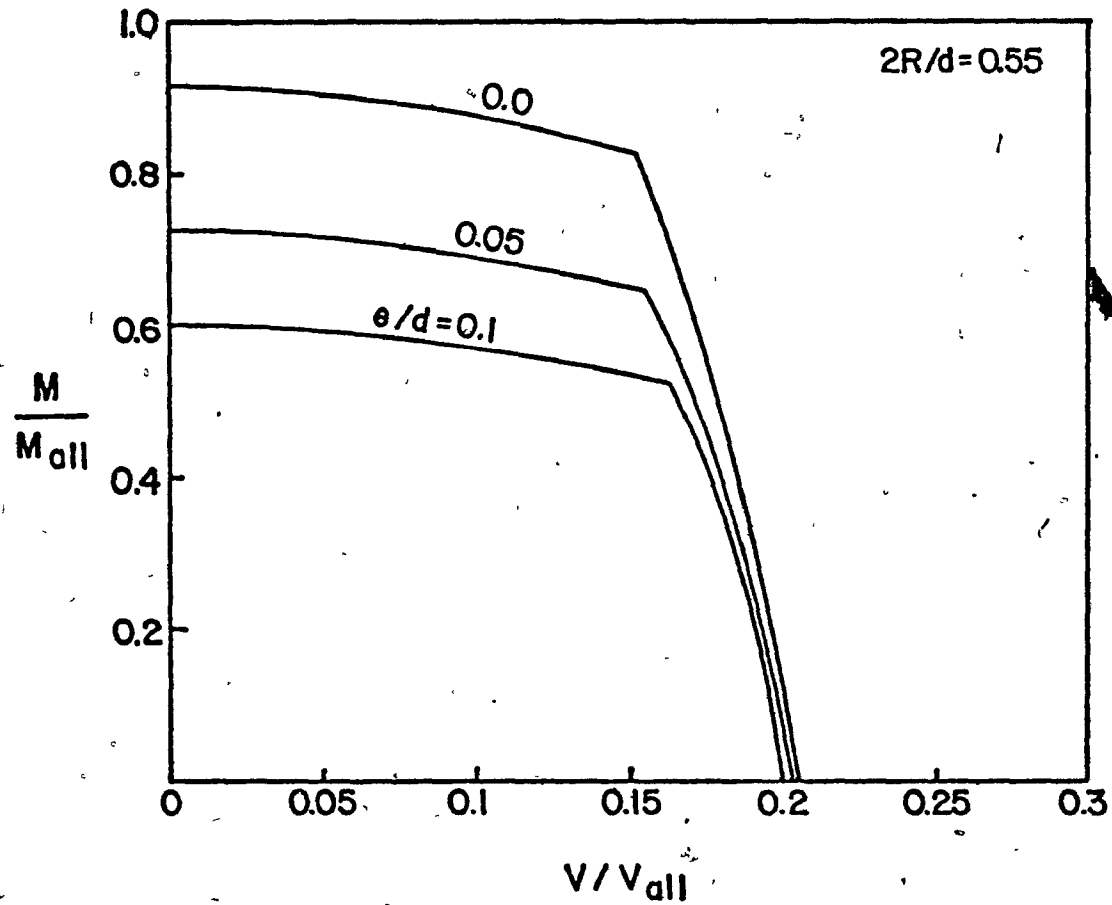


Figure 5.9 Interaction Diagram For 2R/d = 0.55

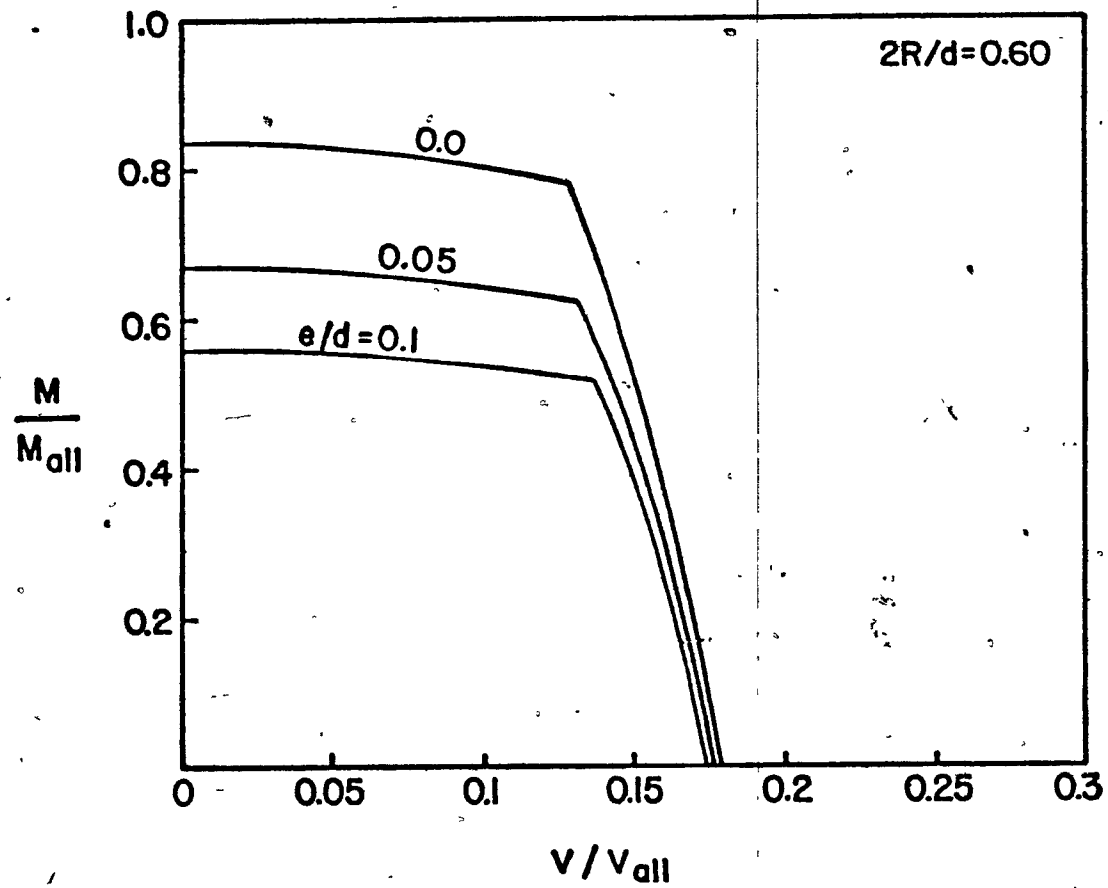


Figure 5.10 Interaction Diagram For 2R/d = 0.60

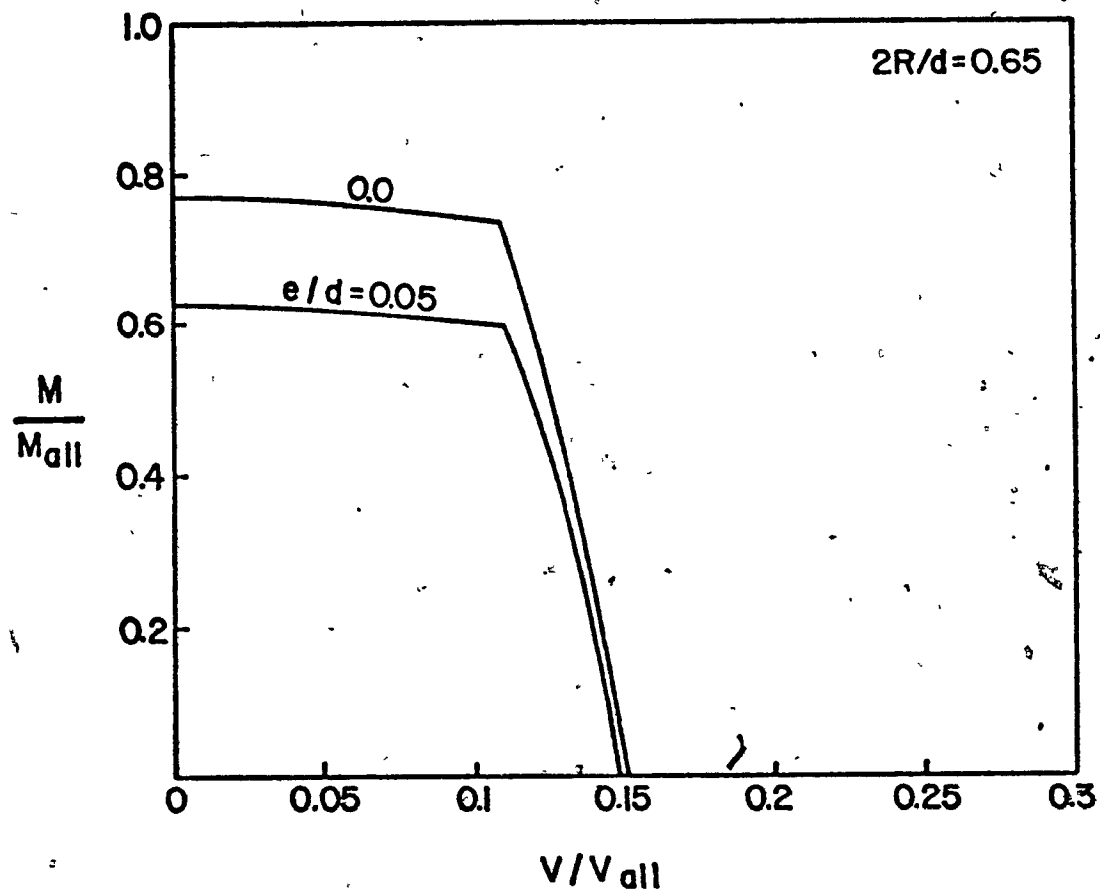


Figure 5.11 Interaction Diagram For 2R/d = 0.65

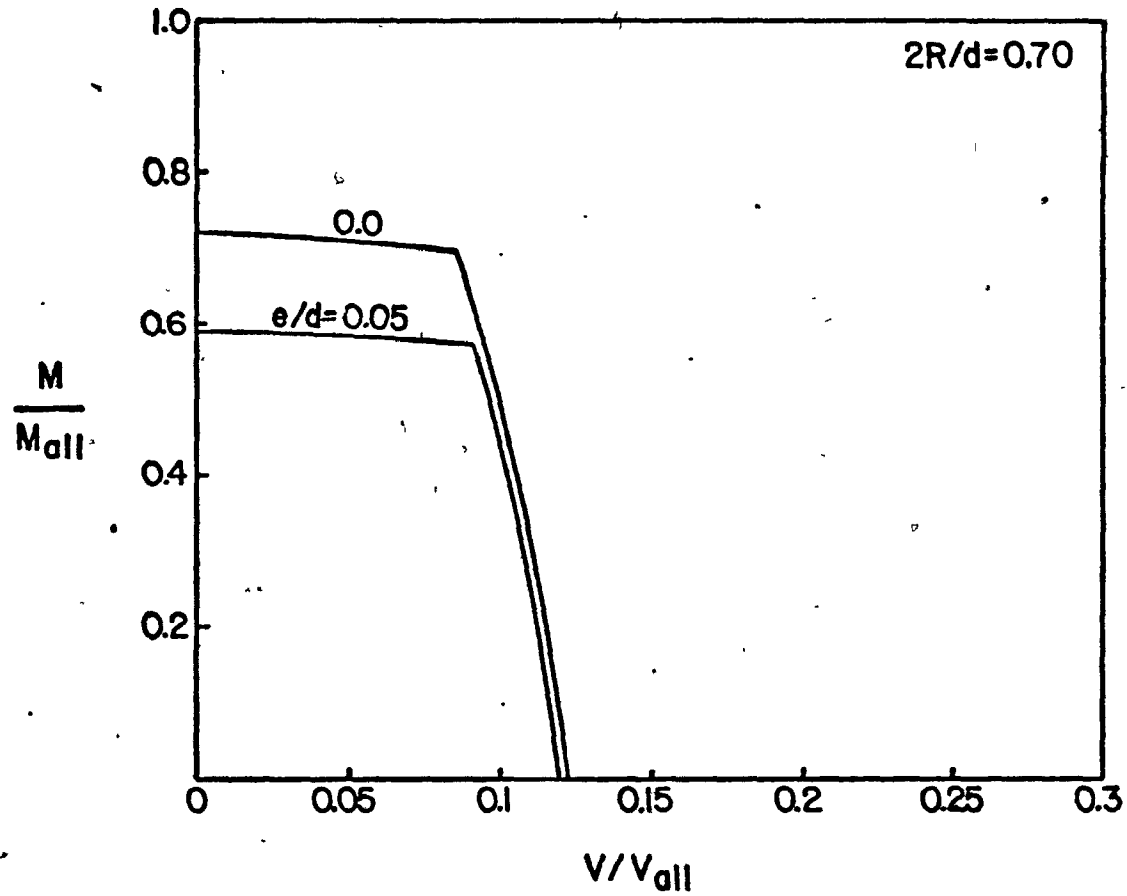


Figure 5.12 Interaction Diagram For 2R/d = 0.70

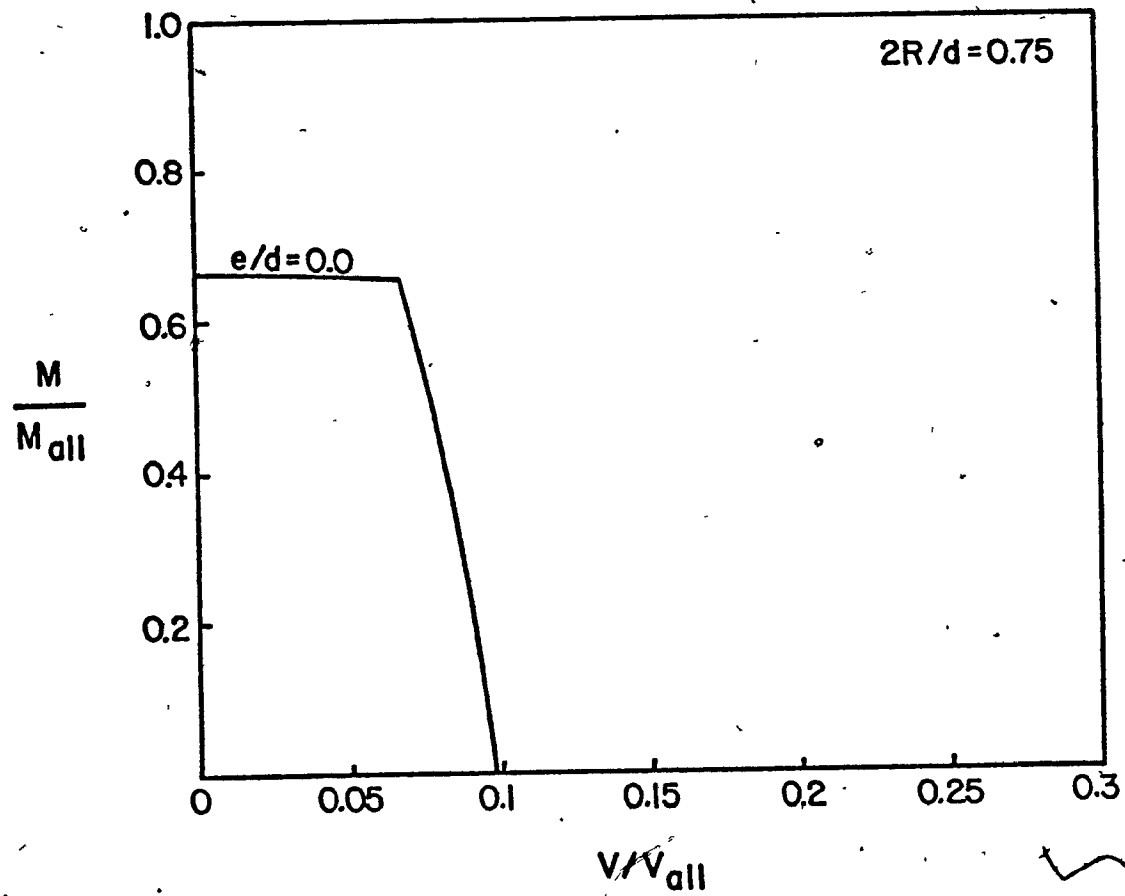


Figure 5.13 Interaction Diagram For  $2R/d = 0.75$

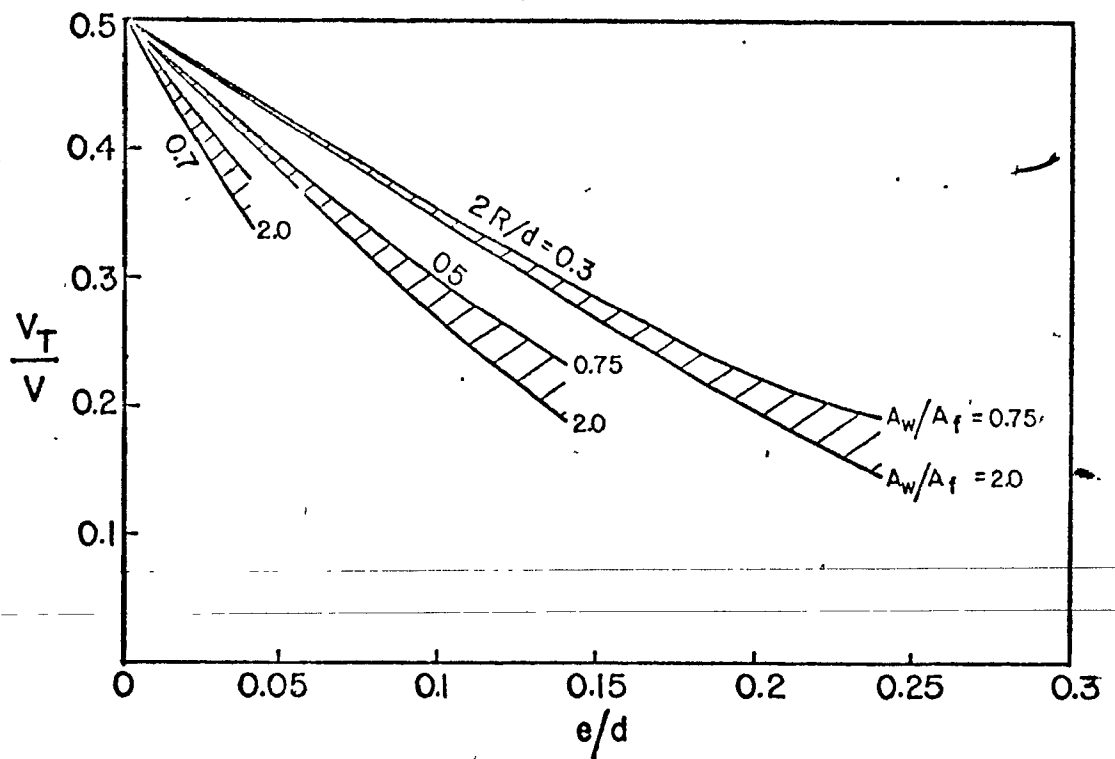
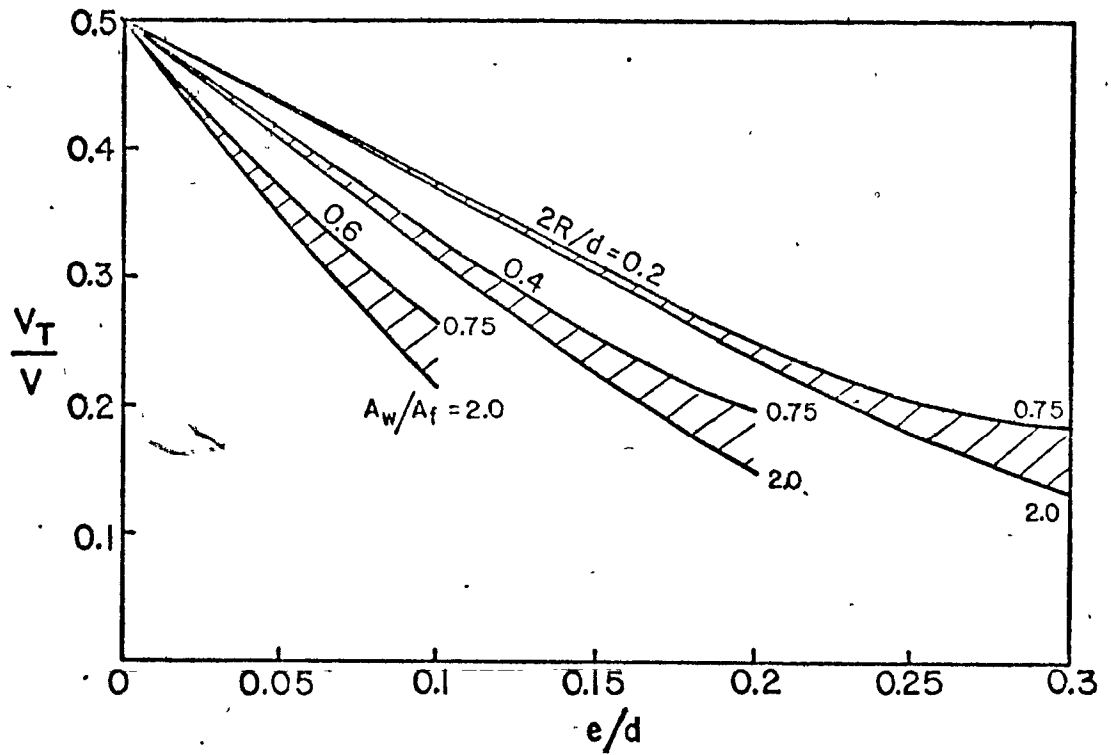
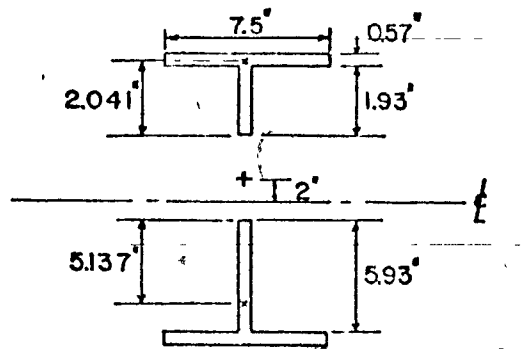
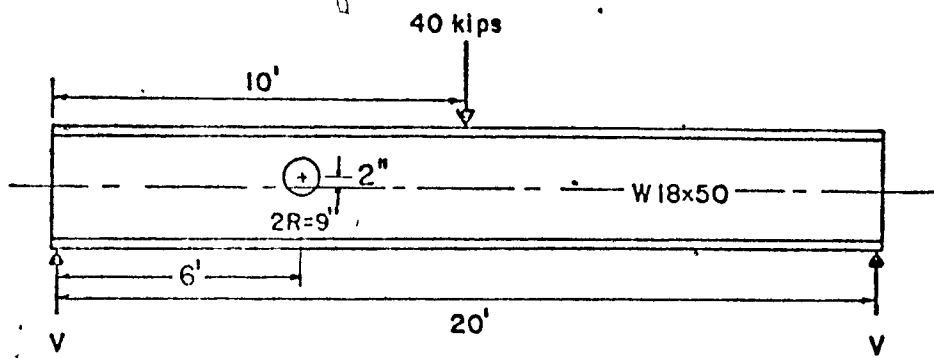


Figure 5.14 Proportion Of Shear Force Carried In Top Tee-Section



SECTION AT l-l

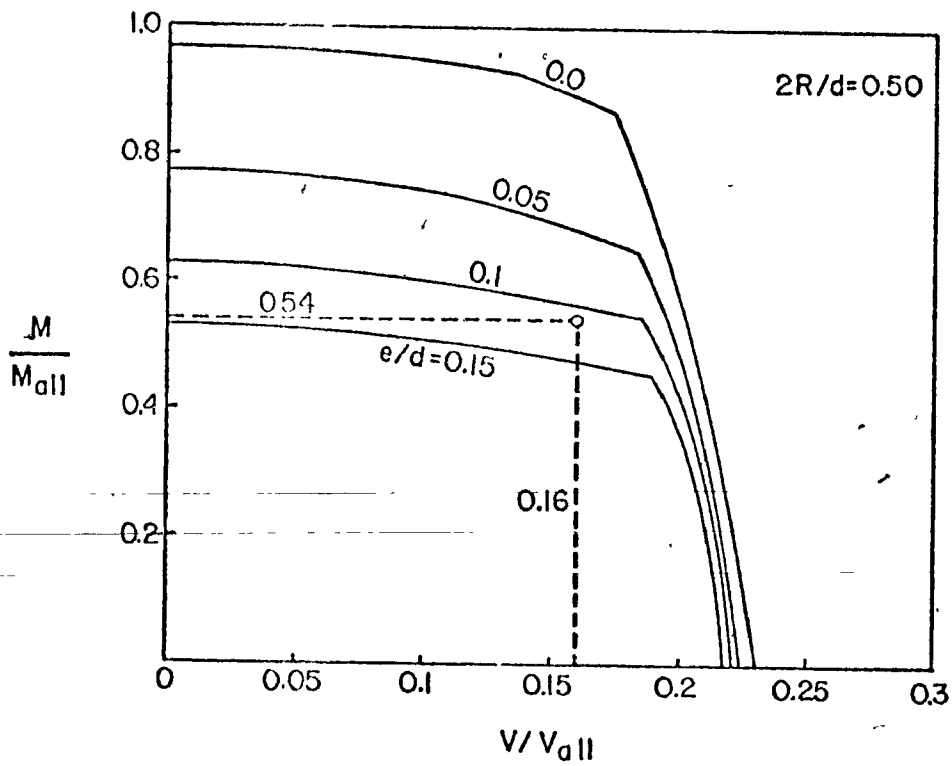


Figure 5.15 Example Beam And Interaction Diagram

CHAPTER 6

SUMMARY AND CONCLUSIONS

## CHAPTER 6

### SUMMARY AND CONCLUSIONS

This thesis provides an analytical method to determine the stresses at the edge of the circular hole on the web of a beam. Both eccentric and mid-depth holes are considered. Sections of the beam around the hole were analysed as curved beam sections using the Winkler-Bach curved beam formula. Stresses were calculated only for a region of  $\pm 45^\circ$  with the vertical centreline of the hole. Any stresses obtained for sections outside this region were deemed to be inaccurate because of the severe inclination of the sections.

Experimental work was carried out to verify the above theory, and the experimental stresses and those calculated using the curved beam method were compared with the theory of elasticity method. It was observed that for large holes and for low  $M/V$  ratios, the theory of elasticity method was inadequate and gave stresses much lower than that of the experiment, whereas the curved beam method accurately predicted the stresses. For smaller holes, both methods gave close results and predicted the measured stresses well for small  $M/V$  ratios, however, for higher  $M/V$  ratios, the accuracy of the curved beam method diminished.

The curved beam method was extended to analyse

circularly reinforced holes. Due to secondary bending of the reinforcement flange, modified curved beam sections were used. Experiments were also performed. Good agreement between the calculated and the experimental stresses were observed.

Interaction curves were produced as aids for the design of unreinforced holes. Any loading represented by a point on the concave side of these curves is a safe loading and a point on the curve itself indicates that the stresses at either the hole edge or the flange, is equal to the allowable bending stress. A design example is also provided.

An attempt to produce design aids for reinforced holes was not successful. In place of this, a short computer program is provided in Appendix VII which can be used for the rapid analysis of such holes.

Conclusions are presented at the end of each chapter.

9

APPENDIX I

SHEAR FORCE DIVISION

APPENDIX I

SHEAR FORCE DIVISION

The division of shear force,  $V$ , between the unequal top and bottom sections across the web hole can be determined by assuming that the deflections and slopes of the top and bottom sections are equal <sup>10</sup>. Using the Moment Area Method, the deflections and change in slopes of the high moment end of the hole with respect to the low moment end, or vice versa, can be calculated. The free-body diagram, the bending moment diagram, and the  $M/EI$  diagram for a typical top section are given in Figure I.1.

I.1 Deflections and Slopes

With the coordinate system indicated in Figure I.1, the deflections and slopes due to bending and shear for the top and bottom sections are given as follows:

	<u>Deflection</u>	<u>Slope</u>
Bending (top section)	$\int_0^{2R} \frac{M_T^1 x}{EI_T} dx$ $-\int_0^{2R} \frac{V_T x^2}{EI_T} dx$	$\int_0^{2R} \frac{M_T^1}{EI_T} dx$ $-\int_0^{2R} \frac{V_T x}{EI_T} dx$
Shear (top section)	$-\int_0^{2R} \frac{\tau_{T,max}}{G} dx$	$-\int_0^{2R} \frac{d\tau_{T,max}}{G} dx$

Bending (bottom section)

$$2R \frac{M_B^1 x}{EI_B} dx$$

$$- \int_0^{2R} \frac{V_B x^2}{EI_B} dx$$

$$\int_0^{2R} \frac{M_B^1}{EI_B} dx$$

$$- \int_0^{2R} \frac{V_B x}{EI_B} dx$$

Shear (bottom section)

$$- \int_0^{2R} \frac{\tau_{B,max}}{G} dx$$

$$- \int_0^{2R} \frac{d\tau_{B,max}}{G}$$

### I.2 Sectional Properties

It is convenient to express the sectional properties, area and moment of inertia, in polar coordinates  $(r, \theta)$  rather than the cartesian coordinates  $(x, y)$ . With reference to Figure I.2, the transformation equations are:

$$x = R(\sin \theta + 1) \quad (I-1)$$

and  $y = R \cos \theta \quad (I-2)$

From Figure I.2, it can be shown that for any section n-n,

$$\xi_T^0 = d/2 - t - e,$$

$$\xi_T = \xi_T^0 - R \cos \theta,$$

$$A_T = bt + w \xi_T,$$

$$\bar{C}_T = \{bt(\xi_T + t/2) + w \xi_T^2/2\} / A_T,$$

and 
$$I_T = \frac{bt^3}{12} + bt(\xi_T + \frac{t}{2} - \bar{C}_T)^2 + \frac{w \xi_T^3}{12} + w \xi_T (\bar{C}_T - \frac{\xi_T}{2})^2$$

in which  $t$  = flange thickness;  $A_T$  = sectional area;  $b$  = flange width;  $w$  = web thickness;  $\bar{C}_T$  = the distance of the neutral axis from the hole edge; and  $I_T$  = the moment of inertia of the section.

For the location of the maximum shear stress, and its magnitude,  $\tau_{T,max}$ , two cases need to be considered, i.e., when the neutral axis lies in the web and in the flange.

When the neutral axis lies on the web,

$$\tau_{T,max} = \frac{V_T \bar{C}_T^2}{2I_T} \quad (I-3)$$

and when the neutral axis lies on the flange,

$$\tau_{T,max} = \frac{V_T (\bar{C}_T - \xi_T/2)}{I_T} \quad (I-4)$$

In general,  $\tau_{T,max}$  can be expressed as,

$$\tau_{T,max} = k_T V_T \quad (I-5)$$

in which  $k_T$  can be obtained from either Equations I-3 or I-4.

### I.3 Equating Deflections and Slopes

By equating the deflections and slopes of the top and bottom sections, the following equations are obtained:

$$\int_0^{2R} \frac{M_T^1 x}{EI_T} dx - \int_0^{2R} \frac{V_T x^2}{EI_T} dx - \int_0^{2R} \frac{\tau_{T,max}}{G} dx$$

$$= \int_0^{2R} \frac{M_B^1 x}{EI_B} dx - \int_0^{2R} \frac{V_B x^2}{EI_B} dx - \int_0^{2R} \frac{\tau_{B,max}}{G} dx$$

(I-6)

$$\int_0^{2R} \frac{M_T^1}{EI_T} dx - \int_0^{2R} \frac{V_T x}{EI_T} dx - \int_0^{2R} \frac{d\tau_{T,max}}{G}$$

$$= \int_0^{2R} \frac{M_B^1}{EI_B} dx - \int_0^{2R} \frac{V_B x}{EI_B} dx - \int_0^{2R} \frac{d\tau_{B,max}}{G}$$

(I-7)

The above equations, I-6 and I-7, can be rewritten in polar coordinates using Equations I-1, I-2 and I-5 as:

$$\int_{-\pi/2}^{\pi/2} \frac{M_T^1}{EI_T} R(\sin\theta + 1) R \cos\theta d\theta - \int_{-\pi/2}^{\pi/2} \frac{V_T}{EI_T} R^2 (\sin\theta + 1)^2 R \cos\theta d\theta$$

$$- \int_{-\pi/2}^{\pi/2} \frac{V_T k_T}{G} R \cos\theta d\theta$$

$$= \int_{-\pi/2}^{\pi/2} \frac{M_B^1}{EI_B} R(\sin\theta + 1) R \cos\theta d\theta - \int_{-\pi/2}^{\pi/2} \frac{V_B}{EI_B} R^2 (\sin\theta + 1)^2 R \cos\theta d\theta$$

$$- \int_{-\pi/2}^{\pi/2} \frac{V_B k_B}{G} R \cos\theta d\theta$$

(I-8)

$$\int_{-\pi/2}^{\pi/2} \frac{M_T^1}{EI_T} R \cos\theta d\theta - \int_{-\pi/2}^{\pi/2} \frac{V_T R(\sin\theta + 1)}{EI_T} R \cos\theta d\theta - \int_{-\pi/2}^{\pi/2} \frac{V_T}{G} dk_T$$

$$= \int_{-\pi/2}^{\pi/2} \frac{M_B^1}{EI_B} R \cos\theta d\theta - \int_{-\pi/2}^{\pi/2} \frac{V_B R(\sin\theta + 1)}{EI_B} R \cos\theta d\theta - \int_{-\pi/2}^{\pi/2} \frac{V_B}{G} dk_B$$

(I-9)

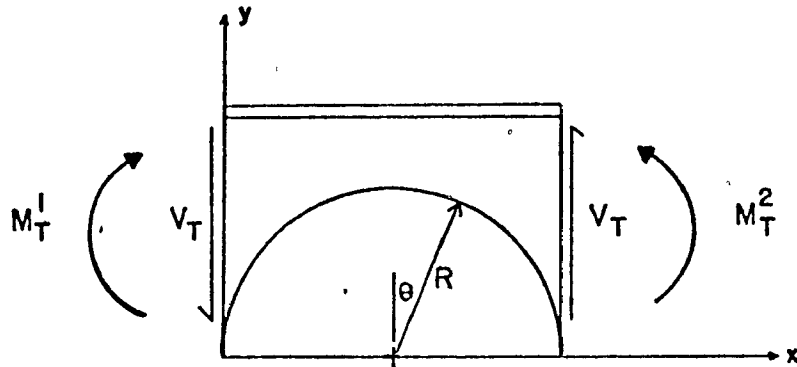
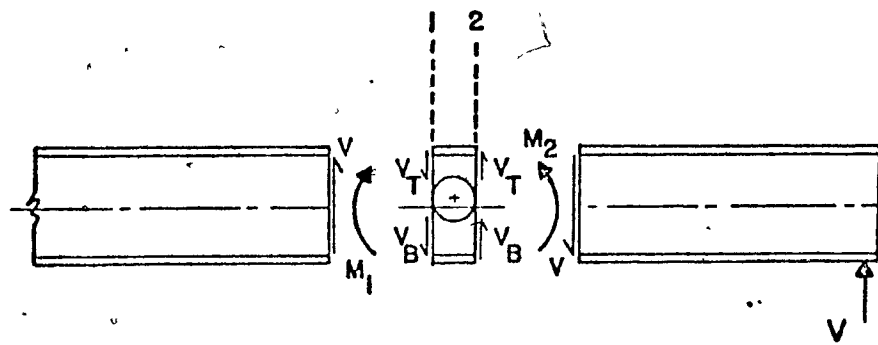
On expansion, many of the integrals are found to be odd functions, and therefore vanish. Rearrangement of these equations then leads to the following:

$$\begin{aligned}
 & \frac{M_T^1 R}{E} \int_0^\pi \frac{\cos \theta d\theta}{I_T} - \frac{V_T R^2}{E} \int_0^\pi \frac{\sin^2 \theta \cos \theta d\theta}{I_T} - \frac{V_T R^2}{E} \int_0^\pi \frac{\cos \theta d\theta}{I_T} \\
 & \quad - \frac{V_T}{G} \int_0^\pi k_T \cos \theta d\theta \\
 & = \frac{M_B^1 R}{E} \int_0^\pi \frac{\cos \theta d\theta}{I_B} - \frac{V_B R^2}{E} \int_0^\pi \frac{\sin^2 \theta \cos \theta d\theta}{I_B} - \frac{V_B R^2}{E} \int_0^\pi \frac{\cos \theta d\theta}{I_B} \\
 & \quad - \frac{V_B}{G} \int_0^\pi k_T \cos \theta d\theta \quad (I-10)
 \end{aligned}$$

and

$$\begin{aligned}
 & \frac{M_T^1 R}{E} \int_0^\pi \frac{\cos \theta d\theta}{I_T} - \frac{V_T R^2}{E} \int_0^\pi \frac{\cos \theta d\theta}{I_T} \\
 & = \frac{M_B^1 R}{E} \int_0^\pi \frac{\cos \theta d\theta}{I_B} - \frac{V_B R^2}{E} \int_0^\pi \frac{\cos \theta d\theta}{I_B} \quad (I-11)
 \end{aligned}$$

Equations I-10 and I-11 can thus be solved simultaneously to yield Equation 2-9, which can be integrated numerically to provide values of  $V_T/V_B$ .



BENDING MOMENT DIAGRAM

M/EI DIAGRAM

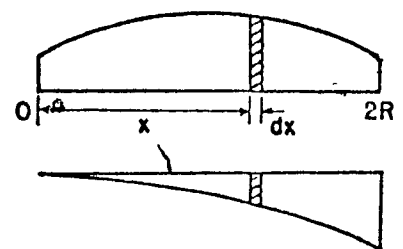
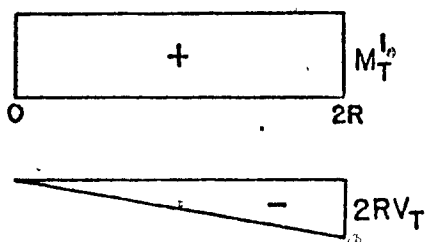


Figure I.1 Free Body Diagram For Shear Division

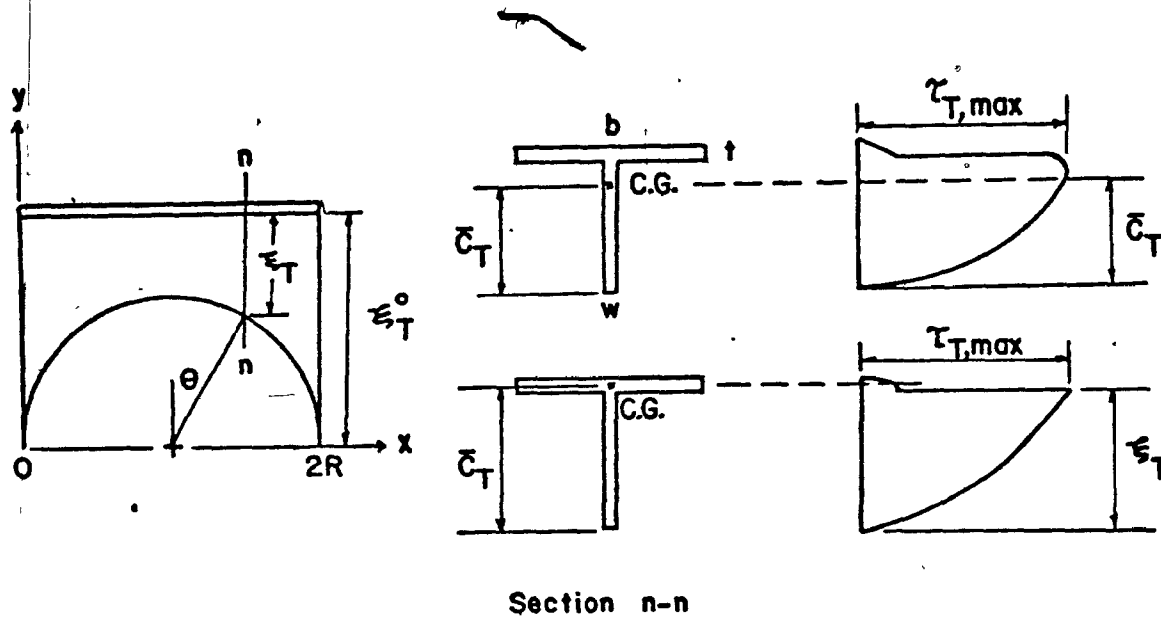


Figure I.2 Typical Vertical Tee-Section

APPENDIX II

THEORY OF ELASTICITY SOLUTION

## APPENDIX II

### THEORY OF ELASTICITY SOLUTION

In Ref. 6, the solution for stresses around a rectangular eccentric hole with round corners was given for the following cases, namely, pure bending, pure shear, eccentricity effect on pure bending and eccentricity effect on shear. If the radius of the round corner is taken as half the width of the hole and the height of the hole is taken as equal to its width, the solution for a circular hole can be obtained for the four cases mentioned above. Any combination of bending and shear can be solved by addition of the stresses given by the four separate solutions.

#### II.1 Pure Bending

For rectangular holes with round corners, the tangential stress on the edge of the hole is given as:

$$J_0^2 \left( \frac{\sigma_t}{MH} \right) = \frac{A}{Y_0} (\Delta_1 \sin \beta + \Delta_3 \sin 3\beta + \Delta_5 \sin 5\beta + \Delta_7 \sin 7\beta + \Delta_9 \sin 9\beta) \quad (\text{II-1})$$

In the case of circular holes,  $A = \frac{1}{2}$ ,  $\Delta_1 = \frac{1}{2}$ ,  $\Delta_3 = -\frac{1}{2}$ ,  $\Delta_5 = \Delta_7 = \Delta_9 = 0$ ,  $J_0^2 = \frac{1}{2}$ ,  $H = R$  and  $y_0 = \frac{1}{2}$ , therefore Equation II-1 is simplified to:

$$\left(\frac{\sigma_t}{MR}\right) \frac{1}{I} = \sin\beta - \sin 3\beta \quad (\text{II-2})$$

Furthermore, if  $F_b = \frac{M_{\text{all}} d}{2I}$ , then Equation II-2 can be rewritten as:

$$\frac{\sigma_t}{F_b} = \left(\frac{M}{M_{\text{all}}}\right) \left(\frac{2R}{d}\right) (\sin\beta - \sin 3\beta) \quad (\text{II-3})$$

## II.2 Pure Shear:

Similarly, for rectangular holes with round corners,

$$J_o^2 \left(\frac{\sigma_t}{MH}\right) \frac{1}{I} = \frac{4A^2 \left(\frac{\tau}{\sigma}\right) \left(\frac{h'}{y_o}\right) \Gamma}{1 + K_5} \left\{ (1 + 3K_5 + 6\frac{CE}{A^2} - 15\frac{D^2}{A^2}) \sin 2\beta \right. \\ \left. + (2K_3 - 21\frac{DE}{A^2}) \sin 4\beta + 2K_1 \sin 6\beta \right\} \quad (\text{II-4})$$

For circular holes,  $A = \frac{1}{2}$ ,  $B = C = D = E = 0$ ,  $K_1 = K_3 = K_5 = 0$ ,  $J_o^2 = \frac{1}{4}$ ,  $y_o = \frac{1}{2}$ ,  $H = R$  and  $h' = (d/2)/2R$ , then Equation II-4 reduces to:

$$\left(\frac{\sigma_t}{MR}\right) \frac{1}{I} = 4 \left(\frac{\tau}{\sigma}\right) \left(\frac{d}{2R}\right) \Gamma \sin 2\beta \quad (\text{II-5})$$

or:

$$\frac{\sigma_t}{F_b} = 4 \left( \frac{M}{M_{all}} \right) \left( \frac{\tau}{\sigma} \right) \Gamma \sin 2\beta \quad (\text{II-6})$$

where:

$$\Gamma = \frac{3}{2 \left( 1 - \frac{2t}{d} \right)} - \frac{A_w \left( \frac{d}{2} \right)^2}{2I} \frac{\frac{2A_f}{A}}{1 - \frac{2A_f}{A}}$$

$$\tau = \frac{V}{A_w}$$

$$\sigma = \frac{M_d}{I}$$

### II.3 Eccentricity Effect on Pure Bending

For rectangular holes with round corners,

$$J_o^2 \left( \frac{\sigma_t}{Me} \right) = \Delta_0 + \Delta_2 \cos 2\beta + \Delta_4 \cos 4\beta + \Delta_6 \cos 6\beta \quad (\text{II-7})$$

In the case of circular holes,  $\Delta_0 = \frac{1}{4}$ ,  $\Delta_2 = -\frac{1}{2}$ ,  $\Delta_4 = \Delta_6 = 0$   
and  $J_o^2 = \frac{1}{4}$ , then Equation II-7 is simplified to:

$$\left( \frac{\sigma_t}{Me} \right) = 1 - 2 \cos 2\beta \quad (\text{II-8})$$

or:

$$\frac{\sigma_t}{F_b} = 2 \left( \frac{M}{M_{all}} \right) \left( \frac{e}{d} \right) (1 - 2\cos 2\beta) \quad (II-9)$$

#### II.4 Eccentricity Effect on Shear

For rectangular holes with round corners,

$$\begin{aligned} J_0^2 \left( \frac{\sigma_t}{VLH} \right) = & - \frac{A}{y_0} \frac{e}{L} \{ \Delta_1' \cos \beta + \Delta_3' \cos 3\beta + \Delta_5' \cos 5\beta \\ & + \Delta_7' \cos 7\beta + \Delta_9' \cos 9\beta \\ & + 2e' (N_2' \sin 2\beta + N_4' \sin 4\beta + N_6' \sin 6\beta) \} \end{aligned} \quad (II-10)$$

In the case of circular holes,  $\Delta_1' = \frac{1}{4}$ ,  $\Delta_3' = -\frac{3}{4}$ ,  $\Delta_5' = \Delta_7' = \Delta_9' = 0$ ,  
 $N_2' = \frac{1}{2}$ ,  $N_4' = N_6' = 0$ ,  $e' = e/2R$ ,  $A = \frac{1}{2}$ ,  $y_0 = \frac{1}{2}$  and  $J_0^2 = \frac{1}{4}$ ,  
then Equation II-10 is simplified to:

$$\left( \frac{\sigma_t}{VLH} \right) = - \frac{e}{L} (\cos \beta - 3\cos 3\beta + 4\frac{e}{2R} \sin 2\beta) \quad (II-11)$$

or:

$$\frac{\sigma_t}{F_b} = - \frac{1}{2} \left( \frac{V}{M_{all}} \right) \left( \frac{F_v}{F_b} \right) \left( \frac{e}{d} \right) \left( \frac{A_w}{A_f} \right) \left( \frac{A_f d^2}{I} \right) \left( \frac{2R}{d} \right)$$

$$\{\cos\beta - 3\cos 3\beta + 4\left(\frac{e}{d}\right)\left(\frac{d}{2R}\right)\sin 2\beta\}$$

(II-12)

For mid-depth holes, the tangential stress on the hole edge is the sum of stresses due to bending and shear, i.e.,

$$\frac{\sigma_t}{F_b} = \left(\frac{M}{M_{all}}\right)\left(\frac{2R}{d}\right)(\sin\beta - \sin 3\beta) + 4\left(\frac{M}{M_{all}}\right)\left(\frac{\tau}{\sigma}\right)\Gamma\sin 2\beta$$

(II-13)

For eccentric holes, the tangential stress is the sum of stresses due to the four loading cases described previously, i.e.,

$$\begin{aligned} \frac{\sigma_t}{F_b} = & \left(\frac{M}{M_{all}}\right)\left(\frac{2R}{d}\right)(\sin\beta - \sin 3\beta) + 4\left(\frac{M}{M_{all}}\right)\left(\frac{\tau}{\sigma}\right)\Gamma\sin 2\beta \\ & + 2\left(\frac{M}{M_{all}}\right)\left(\frac{e}{d}\right)(1 - 2\cos 2\beta) - \frac{1}{2}\left(\frac{V}{V_{all}}\right)\left(\frac{F}{F_b}\right)\left(\frac{e}{d}\right)\left(\frac{A_w}{A_f}\right) \\ & \left(\frac{A_f d^2}{I}\right)\left(\frac{2R}{d}\right)\{\cos\beta - 3\cos 3\beta + 4\left(\frac{e}{d}\right)\left(\frac{d}{2R}\right)\sin 2\beta\} \end{aligned}$$

(II-14)

APPENDIX III

CURVED BEAM METHOD

## APPENDIX III

### CURVED BEAM METHOD

#### III.1 Unreinforced Holes

This Appendix describes how the axial force  $N_\phi$  and moment  $M_\phi$  of any inclined section at an angle  $\phi$  from the vertical are obtained. The stresses are then calculated by substituting these into Equation 2-6.

##### III.1.1 Sectional Properties

With reference to Figure III.1, the area, location of centroid and moment of inertia of an inclined section at an angle  $\phi$  from the vertical can be determined as follows:

$$A_\phi = A_f \sec\phi + s_\phi w \quad (\text{III-1})$$

$$c_\phi = \frac{A_f \sec\phi (s_\phi + \frac{1}{2} t \sec\phi) + \frac{1}{2} w s_\phi^2}{A_\phi} \quad (\text{III-2})$$

$$I_\phi = \frac{1}{12} \{ b (t \sec\phi)^3 + w s_\phi^3 \} + A_f \sec\phi (s_\phi + \frac{1}{2} t \sec\phi - c_\phi)^2 + w s_\phi (\frac{1}{2} s_\phi - c_\phi)^2 \quad (\text{III-3})$$

in which,

$$s_\phi = \left(\frac{d}{2} - e - t\right) \sec\phi - R \quad (\text{III-4})$$

### III.1.2 Bending and Shear Forces on Hole Centreline

The distance of the neutral axis from the top flange of the beam,  $y_n$ , and the moment of inertia,  $I_n$ , for a section through the hole centreline are given as:

$$y_n = \frac{A_f t/2 + A_f (d - t/2) + w(d - 2t)d/2 - w(2R)(d/2 - e)}{2A_f + (d - 2t - 2R)w}$$

(III-5)

$$\begin{aligned} I_n = & A_f t^2/6 + A_f (y_n - t/2)^2 + (A_w d^2/12) (h_T/d)^3 \\ & + A_w (h_T/d) (y_n - t - h_T/2)^2 + A_f (d - y_n - t/2)^2 \\ & + (A_w d^2/12) (h_B/d)^3 + A_w (h_B/d) (d - y_n - t - h_B/2)^2 \end{aligned}$$

(III-6)

in which,

$$h_T = d/2 - t - e - R \quad (III-7)$$

and

$$h_B = d/2 - t + e - R \quad (III-8)$$

If a linear distribution of bending stress is assumed, the normal force  $N_T$  and its line of action can be determined as:

when  $y_n \leq h_T + t + 2R$ ,

$$N_T = \int_{y_n-t}^{y_n} b \left( \frac{My}{I_n} \right) dy + \int_{y_n-h_T-t}^{y_n-t} w \left( \frac{My}{I_n} \right) dy \quad (\text{III-9a})$$

$$\bar{y} = \frac{\int_{y_n-t}^{y_n} b \left( \frac{My^2}{I_n} \right) dy + \int_{y_n-h_T-t}^{y_n-t} w \left( \frac{My^2}{I_n} \right) dy}{N_T} - R - e - \left( y_n - \frac{d}{2} \right) \quad (\text{III-10a})$$

or when  $y_n \geq h_T + t + 2R$ ,

$$N_T = \int_{y_n-t}^{y_n} b \left( \frac{My}{I_n} \right) dy + \int_{y_n-h_T-t}^{y_n-t} w \left( \frac{My}{I_n} \right) dy + \int_0^{y_n-h_T-t-2R} w \left( \frac{My}{I_n} \right) dy \quad (\text{III-9b})$$

$$\bar{y} = \frac{\int_{y_n-t}^{y_n} b \left( \frac{My^2}{I_n} \right) dy + \int_{y_n-h_T-t}^{y_n-t} w \left( \frac{My^2}{I_n} \right) dy + \int_0^{y_n-h_T-t-2R} w \left( \frac{My^2}{I_n} \right) dy}{N_T} - R - e - \left( y_n - \frac{d}{2} \right) \quad (\text{III-10b})$$

After integrating and rearranging terms, Equations III-9a, III-9b, III-10a and III-10b take the form respectively as:

$$N_T = \frac{M}{2I_n} \{ b[y_n^2 - (y_n-t)^2] + w[(y_n-t)^2 - (y_n-h_T-t)^2] \} \quad (\text{III-11a})$$

$$N_T = \frac{M}{2I_n} \{ b[y_n^2 - (y_n - t)^2] + w[(y_n - t)^2 - (y_n - h_T - t)^2] \\ + w(y_n - h_T - t - 2R)^2 \} \quad (\text{III-11b})$$

$$\bar{Y} = \frac{2}{3} \left\{ \frac{b[y_n^3 - (y_n - t)^3] + [w(y_n - t)^3 - (y_n - h_T - t)^3]}{b[y_n^2 - (y_n - t)^2] + [w(y_n - t)^2 - (y_n - h_T - t)^2]} \right\} \\ - R - e - y_n + \frac{d}{2} \quad (\text{III-12a})$$

$$\bar{Y} = \frac{2}{3} \left\{ \frac{b[y_n^3 - (y_n - t)^3] + [w(y_n - t)^3 - (y_n - h_T - t)^3]}{b[y_n^2 - (y_n - t)^2] + [w(y_n - t)^2 - (y_n - h_T - t)^2]} \right. \\ \left. + \frac{w(y_n - h_T - t - 2R)^3}{w(y_n - h_T - t - 2R)^3} \right\} - R - e - y_n + \frac{d}{2} \quad (\text{III-12b})$$

### III.1.3 Moment and Shear on an Inclined Section

Summing forces and taking moments about the centroid of the inclined section, the following equations are obtained:

$$N_\phi = V_T \sin \phi + N_T \cos \phi \quad (\text{III-13})$$

and

$$M_\phi = V_T (R + c_\phi) \sin \phi - N_T \{ \bar{Y} + R - (R + c_\phi) \cos \phi \} \quad (\text{III-14})$$

### III.1.4 Value of Z

From Equation 2-4,

$$Z = -1 + \frac{R+c_{\phi}}{A_{\phi}} \{ b \ln(R+c_{\phi}+u_1) + (w-b) \ln(R+c_{\phi}+u_2) - w \ln(R) \}$$

but  $R + c_{\phi} + u_1 = \left(\frac{d}{2} - e\right) \sec\phi$

and  $R + c_{\phi} + u_2 = \left(\frac{d}{2} - e - t\right) \sec\phi$

therefore,

$$Z = -1 + \frac{R+c_{\phi}}{A_{\phi}} \{ b \ln \left[ \left(\frac{d}{2} - e\right) \sec\phi \right] + (w-b) \ln \left[ \left(\frac{d}{2} - e - t\right) \sec\phi \right] - w \ln(R) \}$$

$$= -1 + \frac{R+c_{\phi}}{A_{\phi}} \left\{ b \ln \frac{\frac{d}{2} - e}{\frac{d}{2} - e - t} + w \ln \frac{\left(\frac{d}{2} - e - t\right) \sec\phi}{R} \right\}$$

(III-15)

### III.2 Reinforced Holes

The procedures in obtaining  $N_{\phi}$  and  $M_{\phi}$  are identical to that of unreinforced holes, except the section will be an I-section instead of a tee-section. This is taken into account in calculating the sectional properties.

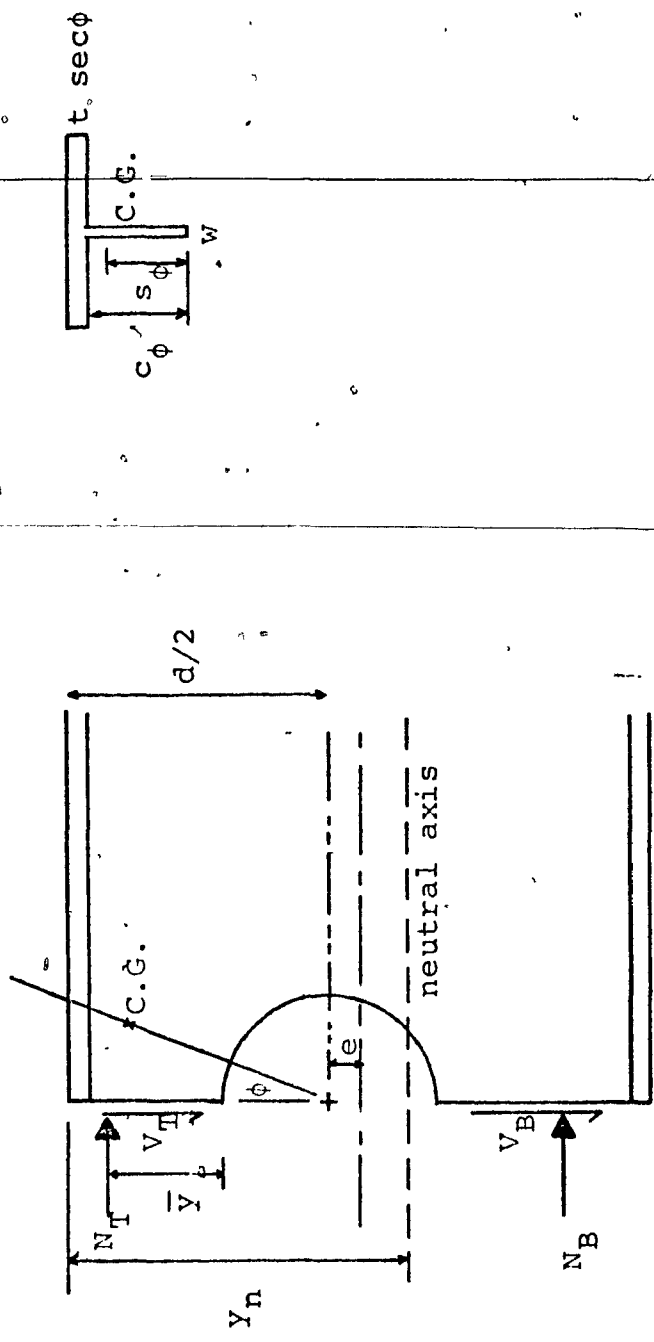


Figure III.1 Curved Beam Method

---

APPENDIX IV

EQUATIONS OF CURVED BEAM METHOD IN NON-DIMENSIONAL FORM

---

APPENDIX IV

EQUATIONS OF CURVED BEAM METHOD IN NON-DIMENSIONAL FORM

Equations III-1 to III-8 and III-11 to III-14 in

Appendix III can be non-dimensionalised as follows:

$$A'_{\phi} = \sec\phi + s'_{\phi} A'_{wf} \quad (IV-1)$$

$$c'_{\phi} = \frac{\sec\phi (s'_{\phi} + \frac{1}{2}t'\sec\phi) + \frac{1}{2}s'^2_{\phi} A'_{wf}}{A'_{\phi}} \quad (IV-2)$$

$$I'_{\phi} = \frac{1}{12} (t'^2 \sec^3\phi + A'_{wf} s'^3_{\phi}) + \sec\phi (s'_{\phi} + \frac{1}{2}t'\sec\phi - c'_{\phi})^2 + A'_{wf} s'_{\phi} (\frac{1}{2}s'_{\phi} - c'_{\phi})^2 \quad (IV-3)$$

$$s'_{\phi} = (\frac{1}{2} - e' - t') \sec\phi - \frac{1}{2}R' \quad (IV-4)$$

$$y'_n = \frac{1 + \frac{1}{2}A'_{wf}(1 - 2t') - A'_{wf}R'(\frac{1}{2} - e')}{2 + A'_{wf}(1 - 2t' - R')} \quad (IV-5)$$

$$I'_{nT} = \frac{1}{6}t'^2 + (y'_n - \frac{1}{2}t')^2 + \frac{1}{12}A'_{wf}h'^3_T + A'_{wf}h'_T(y'_n - t' - \frac{1}{2}h'_T)^2 + (1 + y'_n - \frac{1}{2}t')^2 + \frac{1}{12}A'_{wf}h'^3_B + A'_{wf}h'_B(1 - y'_n - t' - \frac{1}{2}h'_B)^2 \quad (IV-6)$$

$$h'_T = \frac{1}{2} - t' - e' - \frac{1}{2}R' \quad (IV-7)$$

$$h'_B = \frac{1}{2} - t' + e' - \frac{1}{2}R' \quad (\text{IV-8})$$

$$N'_T = M' \frac{I'_g}{I'_n} \left\{ \frac{(y'_n)^2 - (y'_n - t')^2}{t'} + A'_{wf} [(y'_n - t')^2 - (y'_n - h'_T - t')^2] \right\} \quad (\text{IV-11a})$$

$$N'_T = M' \frac{I'_g}{I'_n} \left\{ \frac{(y'_n)^2 - (y'_n - t')^2}{t'} + A'_{wf} [(y'_n - t')^2 - (y'_n - h'_T - t')^2] + A'_{wf} (y'_n - h'_T - t' - R')^2 \right\} \quad (\text{IV-11b})$$

$$\bar{y}' = \frac{2}{3} \left\{ \frac{\frac{(y'_n)^3 - (y'_n - t')^3}{t'} + A'_{wf} [(y'_n - t')^3 - (y'_n - h'_T - t')^3]}{\frac{(y'_n)^2 - (y'_n - t')^2}{t'} + A'_{wf} [(y'_n - t')^2 - (y'_n - h'_T - t')^2]} \right\} - \frac{1}{2}R' - e' - y'_n + \frac{1}{2} \quad (\text{IV-12a})$$

$$\bar{y}' = \frac{2}{3} \left\{ \frac{\frac{(y'_n)^3 - (y'_n - t')^3}{t'} + A'_{wf} [(y'_n - t')^3 - (y'_n - h'_T - t')^3]}{\frac{(y'_n)^2 - (y'_n - t')^2}{t'} + A'_{wf} [(y'_n - t')^2 - (y'_n - h'_T - t')^2]} \right\} + \frac{A'_{wf} (y'_n - h'_T - t' - R')^2}{A'_{wf} (y'_n - h'_T - t' - R')^2}$$

$$- \frac{1}{2}R' - e' - y_n' + \frac{1}{2} \quad (\text{IV-12b})$$

$$N'_\phi = \mu V' A'_{wf} F'_{vb} \sin\phi + N'_T \cos\phi \quad (\text{IV-13})$$

$$M'_\phi = \mu V' A'_{wf} F'_{vb} \left( \frac{1}{2}R' + c'_\phi \right) \sin\phi - N'_T \left\{ \bar{y}' + \frac{1}{2}R' - \left( \frac{1}{2}R' + c'_\phi \right) \cos\phi \right\} \quad (\text{IV-14})$$

in which  $A'_\phi = A_\phi / A_f$ ,

$$s'_\phi = s_\phi / d,$$

$$A'_{wf} = A_w / A_f,$$

$$c'_\phi = c_\phi / d,$$

$$t' = t / d,$$

$$e' = e / d,$$

$$R' = 2R / d,$$

$$y_n' = y_n / d,$$

$$h'_T = h_T / d,$$

$$h'_B = h_B / d,$$

$$N'_T = N_T / A_f F_b,$$

$$I'_g = I_g / A_f d^2,$$

$$I'_n = I_n / A_f d^2,$$

$$\frac{1}{2} \bar{y}' = \bar{y} / d,$$

$$V' = V / V_{\text{all}},$$

$$F'_{vb} = F_v / F_b \text{ and } \mu = V_T / V.$$

Similarly, Equations 2-4, 2-5, 2-6 can be rewritten

as:

$$Z' = -1 + \left(\frac{1}{2}R' + c'_\phi\right) \left\{ \frac{1}{t} \ln \frac{\frac{1}{2} - e'}{\frac{1}{2} - e' - t'} \right. \\ \left. + A'_{wf} \ln \frac{(\frac{1}{2} - e' - t') \sec \phi}{\frac{1}{2}R'} \right\} / A'_\phi \quad (\text{IV-15})$$

$$K' = \frac{I'_\phi}{A'_\phi \left( \frac{R'}{2} + c'_\phi \right) c'_\phi} \left( 1 - \frac{2c'_\phi}{Z'R'} \right) \quad (\text{IV-16})$$

$$\sigma'_\phi = K' \left( \frac{N'_\phi}{A'_\phi} + \frac{M'_\phi c'_\phi}{I'_\phi} \right) \quad (\text{IV-17})$$

APPENDIX V

COMPUTER PROGRAMS - EXPERIMENTS

## APPENDIX V

### COMPUTER PROGRAMS - EXPERIMENTS

#### V.1 Conversational Program for Automatic Recording of Strain

##### Gauge Readings

Most of this program is written in Fortran language except the subroutines which are written in Assembler. This program will record strain gauge readings automatically upon an instruction fed into the computer by an operator through a tele-typewriter. After each set of gauge readings for a particular loading is read, the program will be stopped to allow time for the operator to load the specimen to the next loading. By pressing the BREAK button, the program will be reactivated again and start recording the next set of gauge readings. All these readings will be stored on the disk for later analysis. The channel numbers and their readings will also be printed out on the tele-typewriter.

The program listing and some typical printouts are shown on Pages 117 to 122.

##### V.2 Program 1

This program computes the differences in strain between each load increment using the readings already stored on disk.

The program listing is shown on Page 123.

V.3 Program 2

This program fits linear regression lines on the strain readings obtained by the conversational program during the experiment and prints out the intercepts and slopes of these lines. Also calculated and printed out are the confidence interval of each reading. If any reading is outside this interval, the reading will be automatically discarded when fitting the regression line. A confidence limit of 90% is being used.

The program listing is shown on Page 124 to 127.

CONVERSATIONAL PROGRAM FOR AUTOMATIC RECORDING OF STRAINS

```

DIMENSION STRAIN(50,3),IC(14)(50),IC(50),VAL(50),RES(2),LARG(2)
IP=1X7X
IR=1X6X
CALL ACI
WRITE (IP,1)
1 FOR AT (6100,1) IN DISPLAY (0)
REAL (IR,2) TEST
2 FOR CI (IC)
ENTER VAL
DEL DATE
DEL TIME
LDA DATE+2
STA TIME+2
LEAVE VAL
DO 100 I=1,50
DO 101 J=1,3
100 STRAIN(I,J)=0
999 DO 101 J=1,30
ICNA(I)=0
101 IC(I)=0
DO 102 I=1,50
CALL RES(RES)
VAL(I)=RES(1)+1000
102 CONTINUE
MC=0
DO 103 I=1,50
IF (ABS(VAL(I))-1.2000) GO TO 104
IC(I)=1
GO TO 103
104 MC=MC+1
ICNA(MC)=I-1
103 CONTINUE
WRITE (IP,3)
3 FORMAT (100,4) WHILE FOLLOWING CHANNELS ARE NOT FUNCTIONING //
WRITE (IP,4) (IC(I),I=1,50)
4 FORMAT (IP,517)
WRITE (IP,5)
5 FORMAT (100,4) CHECK UNCHECKED GAUGES THAT ARE NOT RECORDING
WRITE (IP,6)
6 FORMAT (100,4) If any gauges are completed PRESS BREAK BUZZER
C (1110 C) (1105)
CALL ACN
CALL WAIT (1)
CALL ACS
WRITE (IP,7)
7 FOR AT (100,4) If any gauges are completed ALL TEST = 1 RECHECK RES(2) = 0
C (1110 C) (1105)
WRITE (IP,8) TEST = 0, 200 DISPLAY ALL CHANNELS = 3)
REAL (IR,3) TA
8 FORMAT (11)
IF (TA=0.0) GO TO 999
IF (TA=0.1) GO TO 1000
IF (TA=0.2) GO TO 1001

```

```

IF (IA.EQ.3) GO TO 105
105 WRITE (IP,12)
12 FORMAT (1H0,15H CHANNEL DISPLAY//)
DO 106 I=1,20
N=N+1
WRITE (IP,9) V(I), I(I)

```

```

9 FORMAT (1H ,12,22,10,3,2X,11)
106 CONTINUE

```

```

WRITE (IP,10)
10 FORMAT (1H0,12HCHUCK OUTPUT)
WRITE (IP,6)
CALL AC4

```

```

CALL AC1(15)
CALL AC3

```

```

WRITE (IP,11)
11 FORMAT (15H,41HPRODUCED WITH TEST = 1 RECHECK REQ'D = 0,
          21H TEST INAIL TEST = 0)
REAL (IX,22) IV

```

```

22 FORMAT (11)
IF (IV.EQ.0) GO TO 999
IF (IV.EQ.1) GO TO 1000
IF (IV.EQ.2) GO TO 1001

```

```

1000 WRITE (IP,13)

```

```

13 FORMAT (1H0,21HENTER NUMBER OF LOADING STEPS)
READ (IX,14) MEAS1

```

```

14 FORMAT (12)
DO 200 I=1,MEAS1
WRITE (IP,23)

```

```

23 FORMAT (1H0,10HAPPLY LO )
WRITE (IP,6)

```

```

CALL AC4
CALL RECALL (I)
CALL AC3
WRITE (I,19)

```

```

19 FORMAT (1H0,11HENTER LOAD IN KIIPS)
READ (IX,15) LOAD

```

```

15 FORMAT (F5.2)
DO 201 J=1,20
CALL MEAS(K)
STRTT(J,I) = S(I)*1000.

```

```

201 CONTINUE
WRITE (IP,16) STRTT

```

```

16 FORMAT (1H0,70H1 = ,F5.2,4X,4H IP)
DO 202 K=1,20
KK=K-1
WRITE (IP,17) KK,STRTT(K,1)

```

```

17 FORMAT (1H ,12,2X,F10.3)

```

```

202 CONTINUE

```

```

200 CONTINUE
ENTER PAL
SP= DTIC02
LEAVE PAL
SP= DFIC30
LEAVE PAL

```

1001 WRITE (IP,16)  
18 FORMAT (100,20HP PROGRAMME TERMINATED)  
CALL ACC  
STOP  
ENTER PAL

NIEST FSS 1

IOAT FSS 1

STRAIN FSS 400

FSS 100

XFR DEL 10/3500000

FOR 00/1000

DEL 00 TEST

DELC30 LIP

LEAVE PAL

END

SUBROUTINE INPES(RES)

DIMENSION IARG(2),RES(2)

CALL DIMO1(1,1)

CALL SCRB(IARG,RES)

ENTER PAL

IAI

LDA COST01

SRB 11

STA MOST01

OUT /4100

PAI

SRB DELC51

DEL 1.1

IAI

LDA MOST01

SRB 11

STA COST01

OUT /4100

PAI

LEAVE PAL

RETLK

ENTER PAL

MOST01 EQL /16464

IARG COE 0.0033032

CON 00-1

LEAVE PAL

END

\*4:47  
INIT  
U L P 126  
PROGRAM 30

TEST NUMBER  
17

THE FOLLOWING CHANNELS ARE NOT FUNCTIONING

44 45 46 47 48  
49

CHECK DISCONNECTED GAUGES THAT ARE NOT RECORDING

AFTER STEP COMPLETED PRESS BREAK BUTTON TO CONTINUE

PROCEED WITH TEST = 1 RECHECK REQ'D = 0 TERMINATE TEST = 2  
DI PLAY ALL CHANNELS = 3

ENTER NUMBER OF LOADING STEP  
00

APPLY LOAD

PRESS BREAK BUTTON TO CONTINUE

ENTER LOAD IN KIPS

2.0

LOAD = - 2.00 KIPS

0	-13.100
1	-7.300
2	-25.400
3	-7.900
4	5.400
5	0.900
6	-23.700
7	-39.200
8	-34.600
9	-0.900
10	0.900
11	-15.700
12	-45.600
13	-43.000
14	-37.000
15	-35.400
16	18.100
17	23.300
18	23.200
19	14.900
20	-27.500
21	-7.200
22	-32.100
23	-0.700
24	5.200
25	-12.300
26	-35.199
27	-32.200
28	-9.700
29	3.900
30	12.700
31	-7.900
32	-24.400
33	-33.900
34	-35.000
35	-30.300
36	-42.299
37	-39.799
38	18.300
39	20.000
40	27.100
41	25.900
42	-7.900
43	-0.900
44	-14901.375
45	-14901.250
46	-14901.000
47	-14900.875
48	-14900.750
49	-14900.625

APPLY LOAD

AFTER TEP COMPLETED PRESS BREAK BUTTON TO CONTINUE

ENTER LOAD IN KIPS

6.0

LOAD = 6.00 KIPS

0	-107.300
1	-12.300
2	-47.099
3	11.200
4	39.799
5	20.800
6	-37.599
7	-89.600
8	-70.899
9	7.000
10	44.100
11	-10.900
12	-121.699
13	-110.599
14	-80.899
15	-93.299
16	91.599
17	83.699
18	79.300
19	70.899
20	-56.000
21	15.200
22	-68.599
23	-3.500
24	40.699
25	-6.500
26	-74.699
27	-69.799
28	-6.100
29	38.200
30	44.399
31	-1.100
32	-57.399
33	-57.599
34	-89.800
35	-83.399
36	-100.299
37	-108.398
38	74.499
39	79.599
40	80.199
41	80.799
42	-43.899
43	-3.300
44	-1492.875
45	-1492.000
46	-1492.000
47	-1491.875
48	-1491.025
49	-1491.525

APPLY LOAD

PROGRAM 1

```

C
C
DIMENSION STRAIN(50,3),IDAT(3),NOPEN(20),WORK(7)
ENTER PAL
SP=DELC30
L=1
SP=DELC30
LEAVE PAL
WRITE(6,1) NTEST,(IDAT(1),I=1,3)
1 FOR AT(100,1) I=1 DO. = ,10000/(NDATE = ,3A3)
READ(5,2) N1,N2,N3,N4
2 FOR AT(100,1)
IF (N1.N2.N3) GO TO 1000
READ(5,3) (NOPEN(I),I=1,20)
3 FOR AT(100,1)
L=L+1
IOPEN=NOPEN(1)
WRITE(6,4)
4 FOR AT(100,1) (NOPEN(I),I=1,20) SEND DIFFERENCE IN STRAIN BETWEEN EACH LOAD
* 7)
DO 100 I=1,50
II=I-1
IF (II.EQ.IOPEN) GO TO 101
DO 110 J=2,3
J1=J-1
110 WORK(J1)=STRAIN(I,J)-STRAIN(I,J1)
NLD=NOPEN(I)-1
WRITE(6,5) II,(WORK(K),K=1,NLD)
5 FOR AT(100,1) (I,J) (F10.3)
GO TO 100
101 IF (L.GE.NOPEN) GO TO 100
L=L+1
IOPEN=NOPEN(I)
100 CONTINUE
GO TO 1001
1000 WRITE(6,6)
6 FOR AT(100,1) (NOPEN(I),I=1,20) SEND THE TEST NUMBER IN TAPE DOES NOT AGREE WITH THAT IN
* INPUT, PROGRAM IS TERMINATED)
1001 STOP
ENTER PAL
XPR DELC30,3555000
FOR 0,1000
DELC30,1151
NTEST HSS 1
IDAT HSS 1
STRAIN HSS 400
HSS 100
DELC30 LIH
LEAVE PAL
END

```

PROGRAM 2

```

DIMENSION STRAIN(50,8), IDAT(3), NOPEN(20), ALOAD(8), APS(8), NCHAN(50)
*, LS(8), T(6,4), CLOAD(8), SLOPE(50), LCHAN(50), VALUE(8)
DATA T/6 314, 2 420, 2 353, 2 132, 2 015, 1 943, 12 706, 4 303, 3 182,
*      2 776, 2 571, 2 447, 63 657, 9 925, 5 841, 4 604, 4 032, 3 707,
*636 619, 31 598, 12 941, 8 610, 6 859, 5 959/

```

```

ENTER PAL
  SPB DTRCOZ
  LDY XFR
  SPB DELC30

```

```
LEAVE PAL
```

```
WRITE(6,1)
```

```
1 FORMAT(1H0, 19HREGRESSION ANALYSIS)
```

```
WRITE(6,2) NTEST, (IDAT(I), I=1, 3)
```

```
2 FORMAT(1H0, 11HTEST NO = , 12, 5X, 7HDATE = , 3A3)
```

```
READ(5,3) NT, NDC, NLOAD
```

```
3 FORMAT(3I5)
```

```
NG=50-NDC
```

```
READ(5,3) MODE
```

```
IF(NT NE NTEST) GO TO 1000
```

```
IF(NDC EQ 0) GO TO 90
```

```
READ(5,4)(NOPEN(I), I=1, NDC)
```

```
4 FORMAT(16I5)
```

```
GO TO 92
```

```
90 NOPEN(1)=-1
```

```
92 READ(5,5)(ALOAD(I), I=1, NLOAD)
```

```
5 FORMAT(8F10 3)
```

```
READ(5,6) NSC
```

```
6 FORMAT(15)
```

```
IF(NSC EQ 0) GO TO 91
```

```
READ(5,4)(NCHAN(I), I=1, NSC)
```

```
GO TO 93
```

```
91 NCHAN(1)=-1
```

```
93 L=1
```

```
M=1
```

```
LL=1
```

```
IOPEN=NOPEN(1)
```

```
ICHAN=NCHAN(1)
```

```
DO 100 I=1, 50
```

```
  I1=I-1
```

```
  IF(I1 EQ IOPEN) GO TO 101
```

```
  IF(I1 EQ ICHAN) GO TO 102
```

```
  SUMX=0
```

```
  SUMXZ=0
```

```
  SUMY=0
```

```

SUMXY=0
DO 200 J=1, NLOAD
SUMX=SUMX+ALOAD(J)
SUMXZ=SUMXZ+ALOAD(J)**2
SUMY=SUMY+STRAIN(I, J)
SUMXY=SUMXY+STRAIN(I, J)*ALOAD(J)
CLOAD(J)=ALOAD(J)
VALUE(J)=STRAIN(I, J)
200 CONTINUE
SUMXX=SUMX**2
N=NLOAD
CALL REGRN(SUMX, SUMY, SUMXY, SUMXZ, SUMXX, N, A, B)
LCHAN(LL)=I1
SLOPE(LL)=B
LL=LL+1
WRITE(6, 7) I1, A, B, N
IF(MODE EQ 0) GO TO 204
CALL CL(N, SUMX, CLOAD, A, B, I, MODE, T, VALUE)
204 GO TO 100
102 READ(5, 4) NPS, (LS(I), I=1, NPS)
SUMX=0
SUMXZ=0
SUMY=0
SUMXY=0
I1=1
L1=1
IL=LS(I1)
DO 202 J=1, NLOAD
IF(J EQ IL) GO TO 203
SUMY=SUMY+ALOAD(J)
SUMY=SUMY+STRAIN(I, J)
SUMXZ=SUMXZ+ALOAD(J)**2
SUMXY=SUMXY+STRAIN(I, J)*ALOAD(J)
CLOAD(I1)=ALOAD(J)
VALUE(I1)=STRAIN(I, J)
I1=I1+1
GO TO 202
203 IF(L1 GE NPS) GO TO 202
L1=L1+1
IL=LS(L1)
202 CONTINUE
SUMXX=SUMX**2
N=NLOAD-NPS
CALL REGRN(SUMY, SUMY, SUMXY, SUMXZ, SUMXX, N, A, B)
LCHAN(LL)=I1
SLOPE(LL)=B
LL=LL+1
WRITE(6, 7) I1, A, B, N
7 FORMAT(1H0, I2, 5X, 12HINTERCEPT = , F8 2, 5X, 8HSLOPE = , F8 2, 5X, 16HNO
* OF POINTS = , I2)

```

```

      IF(MODE EQ 0) GO TO 205
      CALL CL(N, SUMY, CLOAD, A, B, I, MODE, T, VALUE)
205  IF(M GE NSC) GO TO 100
      M=M+1
      ICHAN=NCHAN(M)
      GO TO 100
101  IF(L GE NOC) GO TO 100
      L=L+1
      IOPEN=NOPEN(L)
100  CONTINUE

C
C    STRESS ANALYSIS
C
      READ(5, 3) IANLYS
      IF(IANLYS EQ 0) GO TO 1001
      IF(IANLYS NE 1) GO TO 1001
      WRITE(6, 11)
11  FORMAT(1H0, 25HANALYSIS OF LINEAR GAUGES)
      READ(5, 5) E, V
      WRITE(6, 9) E, V
9    FORMAT(1H0, 4HE = , E12 4, 2X, 4HV = , F8 2/)
      WRITE(6, 12)
12  FORMAT(1H0, 7HCHANNEL, 3X, 5HSLOPE, 6X, 6HSTRAIN, 9X, 6HSTRESS/)
      DO 300 I=1, NG
      S=SLOPE(I)*V*1 0E-6
      STRESS=E*S
      WRITE(6, 10) LCHAN(I), SLOPE(I), S, STRESS
10  FORMAT(1H , I5, F10 3, 2E15 5)
300  CONTINUE
      GO TO 1001
1000 WRITE(6, 8)
8    FORMAT(1H0, 79HTHE TEST NUMBER IN TAPE DOES NOT AGREE WITH THAT IN
*INPUT, PROGRAMME TERMINATED)
1001 STOP
      ENTER PAL
XFR   DEL 0, /3355000
      FOR 0, /1000
      DEL 0, NTEST
NTEST BSS 1
IDAT  BSS 3
STRAIN BSS 400*
      BSS 108
DELC30 LIB
      LEAVE PAL
      END
      SUBROUTINE REGRN(SX, SY, SXY, SX2, SXX, NDF, A, B)
      ADF=NDF
      A=(SX2*SY-SX*SXY)/(ADF*SY2-SXX)
      B=(ADF*SXY-SX*SY)/(ADF*SX2-SXX)
      RETURN

```

```

END
SUBROUTINE CL(NP, SX, CLOAD, A, B, I, ICL, T, VALUE)
INTEGER U
DIMENSION SDYI(8), YMAX(8), YMIN(8), CLOAD(8), T(6, 4), VALUE(8)
DOF=NP
XBAR=SX/DOF
U=NP-2
AU-U
RLZ=0
XMXBAR=0
DO 10 J=1, NP
Y=A+B*CLOAD(J)
RL=VALUE(J)-Y
RLZ=RLZ+RL**2
XMXBAR=XMXBAR+(CLOAD(J)-XBAR)**2
10 CONTINUE
SDYZ=RLZ/AU
DO 20 J=1, NP
V=(CLOAD(J)-XBAR)**2
SDYI(J)=SORT(SDYZ*(1 +1 /DOF+V/XMXBAR))
Y1=A+B*CLOAD(J)
YMAX(J)=Y1+T(U, ICL)*SDYI(J)
YMIN(J)=Y1-T(U, ICL)*SDYI(J)
20 CONTINUE
WRITE(6, 1) U, T(U, ICL), (YMAX(J), J=1, NP)
1 FORMAT(1H0, 4X, I2, 2X, 9F7.1)
WRITE(6, 2) (YMIN(J), J=1, NP)
2 FORMAT(1H , 15X, 8F7.1)
RETURN
END

```

APPENDIX VI

COMPUTER PROGRAM - THEORY OF ELASTICITY METHOD

## APPENDIX VI

### COMPUTER PROGRAM - THEORY OF ELASTICITY METHOD

#### VI.1 Program Abstract

This program computes the stresses at the edge of a hole in the web of a flanged beam using the theory of elasticity method described in Chapter 2. The stresses are calculated at  $10^0$  intervals for the whole circumference of the hole.

#### VI.2 Input Data Requirement

(a) First card: (FORMAT I5)

Read in the number of beams to be analysed.

NB = Number of beam sections.

(b) Second card: (FORMAT 8F10.2)

Read in the dimensions of beam section, radius of hole and eccentricity.

D = Beam depth;

B = Beam flange width;

T = Beam flange thickness;

W = Beam web thickness;

R = Radius of hole;

ECC = Eccentricity of hole centre with respect to the beam's mid-depth; equal to 0 for mid-depth holes.

(c) Third card: (FORMAT I5)

Read in the number of moment and shear combinations that stresses are to be computed.

NMSR = Number of moment-shear combinations.

(d) Read in different sets of moment and shear (M,V) (FORMAT 8F10.2)

One card for each set, that is, there will be NMSR number of cards.

(e) Repeat procedures (b), (c) and (d) for NB number of times.

### VI.3 Output Data

ANGLE = The angle at which the stress is calculated;

X,Y = The location in Cartesian coordinates in which the stress is calculated;

SIGA, SIGB, SIGC, SIGD = Represent the stresses calculated by each term of Equation 2-7;

SIGMA = Stresses at the edge of the hole.

### VI.4 Program Listing and Sample Output

A program listing and a sample output are shown on

Pages 130 to 132.

```

REAL P,I
PJ=3.1415927
READ 1,NB
1 FORMAT(J5)
DO 50 J=1,NB
  READ 2,D,R,I,W,I,R,ECC
2 FORMAT(F10.2)
  I=(B**3-(B-I)*(D-2*T)**3)/12.
  PRINT 3,J
3 FORMAT(11PROPERTIES OF BEAM NO',I3)
  PRINT 4,D,R,I,W,I,R,ECC
4 FORMAT(100= ,F6.2, ' B= ,F6.2, ' T= ,F6.2, ' W= ,F6.2,
* ' I= ,F8.2, ' R= ,F8.2, ' EC= ,F5.2)
  AFIG=2*I*T
  ATGT=AFIG*(D-2*I)*V
  K=AFIG/ATGT
  H=I/2.
  GAMMA=1.5/(1.-T/I)-((D-2.*T)*W**2*R1)/(2.*I*(1.-R1))
  READ 5,M,S,R
  DO 50 K=1,M,S,R
  READ 2,H,V
  PRINT 9,H,V
9 FORMAT(100= ,F8.2, ' V= ,F7.2)
  IF(H.EQ.0) GO TO 51
  RATIO=2*V*I/(I*M**2)
  PRINT 12
12 FORMAT(101,17,'ANGLE',T18,'IX',T28,'IY',T37,'SIGA',T50,'SIGB',T63,
* 'SIGC',T76,'SIGD',T89,'SIGMA')/
  P=100 II=1,361,10
  III=II-1
  BETA=III*PI/150.
  BETA2=2*BETA
  BETA3=3*BETA
  BETA6=6*BETA
  SINX=SIN(BETA)
  SIN2X=SIN(BETA2)
  SIN3X=SIN(BETA3)
  COSX=COS(BETA)
  COS2X=COS(BETA2)
  COS3X=COS(BETA3)
  COS6X=COS(BETA6)
  S16A=SINX-SIN3X
  SIGC=2*I*III**2*GAMMA*SIN2X/R
  SIGD=1-2*COS2X
  SIGB=-ECC*V/P*(COSX-3*COS3X+4*ECC*(SIN2X/(2*R)))
  SIGA=(SIGB+SIGD)*M**2/I+SIGC*M*ECC/I
  X1=.5*COSX
  Y1=.5*SINX
  X=2.*P*X1
  Y=2.*I*Y1
  A G=ATAN(Y1/X1)*180./PI
100 PRINT 11,A,G,X,Y,SIGB,SIGC,SIGD,SIGMA
11 FORMAT(1 ,F10.2,5E13.4)
  GO TO 50
51 PRINT 52
52 FORMAT('THIS METHOD FAILS FOR PURE SHEAR')
50 CONTINUE
STOP
END

```

PROPERTIES OF BEAM NO 1

D= 14.12 B= 6.78 T= 0.51 W= 0.31 I= 380.70 R= 2.50 EC= 2.50

M= 240.00 V= 10.00

ANGLE	X	Y	SIGA	SIGB	SIGC	SIGD	SIGMA
0.00	2.50	0.00	0.0000E 00	0.0000E 00	-0.1000E 01	0.2083E 00	-0.1249E 01
10.00	2.46	0.43	-0.3264E 00	0.2283E 01	-0.8794E 00	0.9679E-01	0.1850E 01
20.00	2.35	0.86	-0.5240E 00	0.4290E 01	-0.5321E 00	-0.7555E-01	0.4977E 01
30.00	2.17	1.25	-0.5000E 00	0.5780E 01	-0.1907E-05	-0.2706E 00	0.7495E 01
40.00	1.92	1.61	-0.2232E 00	0.6572E 01	0.6527E 00	-0.4412E 00	0.1034E 02
50.00	1.61	1.92	0.2660E 00	0.6572E 01	0.1347E 01	-0.5428E 00	0.1705E 02
60.00	1.25	2.17	0.8660E 00	0.5780E 01	0.2000E 01	-0.5450E 00	0.1277E 02
70.00	0.86	2.35	0.1440E 01	0.4290E 01	0.2532E 01	-0.4402E 00	0.1233E 02
80.00	0.43	2.46	0.1851E 01	0.2283E 01	0.2379E 01	-0.2456E 00	0.1067E 02
90.00	0.00	2.50	0.2000E 01	0.1672E-04	0.3000E 01	-0.1842E-05	0.7880E 01
-10.00	-0.43	2.46	0.1851E 01	-0.2283E 01	0.2879E 01	0.2456E 00	0.4245E 01
-20.00	-0.86	2.35	0.1440E 01	-0.4290E 01	0.2532E 01	0.4402E 00	0.1025E 00
-30.00	-1.25	2.17	0.8660E 00	-0.5780E 01	0.2000E 01	0.5450E 00	-0.3733E 01
-40.00	-1.61	1.92	0.2661E 00	-0.6572E 01	0.1347E 01	-0.5428E 00	-0.6060E 01
-50.00	-1.92	1.61	-0.2232E 00	-0.6572E 01	0.6527E 00	-0.4412E 00	-0.8086E 01
-60.00	-2.17	1.25	-0.5000E 00	-0.5780E 01	0.5120E-05	0.2706E 00	-0.9471E 01
-70.00	-2.35	0.86	-0.5240E 00	-0.4290E 01	-0.5321E 00	0.7555E-01	-0.8306E 01
-80.00	-2.46	0.43	-0.3264E 00	-0.2283E 01	-0.8794E 00	-0.9679E-01	-0.5450E 01
-90.00	-2.50	0.00	-0.5170E-05	-0.3334E-04	-0.1000E 01	0.2083E 00	-0.1004E 01
10.00	-2.46	-0.43	0.3263E 00	0.2283E 01	-0.8794E 00	-0.2379E 00	0.2140E 01
20.00	-2.35	-0.86	0.5240E 00	0.4290E 01	-0.5321E 00	-0.1923E 00	0.6445E 01
30.00	-2.17	-1.25	0.5000E 00	0.5780E 01	-0.8580E-05	-0.9021E-01	0.9755E 01
40.00	-1.92	-1.61	0.2232E 00	0.6572E 01	0.6527E 00	0.3000E-01	0.1179E 02
50.00	-1.61	-1.92	-0.2660E 00	0.6572E 01	0.1347E 01	0.1324E 00	0.1227E 02
60.00	-1.25	-2.17	-0.8660E 00	0.5780E 01	0.2000E 01	0.1842E 00	0.1119E 02
70.00	-0.86	-2.35	-0.1440E 01	0.4290E 01	0.2532E 01	0.1723E 00	0.8754E 01
80.00	-0.43	-2.46	-0.1851E 01	0.2283E 01	0.2379E 01	0.1031E 00	0.5381E 01
90.00	-0.00	-2.50	-0.2000E 01	0.2530E-04	0.3000E 01	0.1185E-05	0.1576E 01
-10.00	0.43	-2.46	-0.1851E 01	-0.2283E 01	0.2879E 01	-0.1031E 00	-0.2139E 01
-20.00	0.86	-2.35	-0.1440E 01	-0.4290E 01	0.2532E 01	-0.1723E 00	-0.5311E 01
-30.00	1.25	-2.17	-0.8660E 00	-0.5780E 01	0.2000E 01	-0.1842E 00	-0.7612E 01
-40.00	1.61	-1.92	-0.2661E 00	-0.6572E 01	0.1347E 01	-0.1324E 00	-0.8863E 01
-50.00	1.92	-1.61	0.2232E 00	-0.6572E 01	0.6527E 00	-0.3000E-01	-0.9027E 01
-60.00	2.17	-1.25	0.5000E 00	-0.5780E 01	0.7391E-05	0.9021E-01	-0.8179E 01
-70.00	2.35	-0.86	0.5240E 00	-0.4290E 01	-0.5321E 00	0.1923E 00	-0.6471E 01
-80.00	2.46	-0.43	0.3264E 00	-0.2283E 01	-0.8794E 00	0.2379E 00	-0.4092E 01
-90.00	2.50	-0.00	0.1968E-04	-0.4222E-04	-0.1000E 01	0.2083E 00	-0.1248E 01

M= 480.00 V= 10.00

ANGLE	X	Y	SIGA	SIGB	SIGC	SIGD	SIGMA
0,00	2,50	0,00	0,0000E 00	0,0000E 00	-0,1000E 01	0,1042E 00	-0,2824E 01
10,00	2,46	0,43	-0,3264E 00	0,1141E 01	-0,8794E 00	0,4840E -01	-0,5058E -01
20,00	2,35	0,86	-0,5240E 00	0,2145E 01	-0,5321E -00	-0,3777E -01	0,3313E 01
30,00	2,17	1,25	-0,5000E 00	0,2890E 01	-0,1907E -05	-0,1353E 00	0,7106E 01
40,00	1,92	1,61	-0,2732E 00	0,3286E 01	0,6527E 00	-0,2206E 00	0,1102E 02
50,00	1,61	1,92	0,2660E 00	0,3286E 01	0,1347E 01	-0,2714E 00	0,1459E 02
60,00	1,25	2,17	0,8660E 00	0,2890E 01	0,2000E 01	-0,2725E 00	0,1728E 02
70,00	0,86	2,35	0,1440E 01	0,2145E 01	0,2532E 01	-0,2201E 00	0,1859E 02
80,00	0,43	2,46	0,1851E 01	0,1141E 01	0,2879E 01	-0,1228E 00	0,1812E 02
90,00	0,00	2,50	0,2000E 01	0,0460E -05	0,3000E 01	-0,9243E -06	0,1576E 02
-80,00	-0,43	2,46	0,1851E 01	-0,1141E 01	0,2879E 01	0,1228E 00	0,1179E 02
-70,00	-0,86	2,35	0,1440E 01	-0,2145E 01	0,2532E 01	0,2201E 00	0,6452E 01
-60,00	-1,25	2,17	0,8660E 00	-0,2890E 01	0,2000E 01	0,2725E 00	0,7839E 00
-50,00	-1,61	1,92	0,2660E 00	-0,3286E 01	0,1347E 01	0,2714E 00	-0,4418E 01
-40,00	-1,92	1,61	-0,2732E 00	-0,3286E 01	0,6527E 00	0,2206E 00	-0,8309E 01
-30,00	-2,17	1,25	-0,5000E 00	-0,2890E 01	0,5127E -05	0,1353E 00	-0,1026E 02
-20,00	-2,35	0,86	-0,5240E 00	-0,2145E 01	-0,5321E 00	0,3778E -01	-0,9971E 01
-10,00	-2,46	0,43	-0,3264E 00	-0,1141E 01	-0,8794E 00	0,4840E -01	-0,7551E 01
0,00	-2,50	0,00	-0,5000E -05	-0,1622E -04	-0,1000E 01	-0,1042E 00	-0,3480E 01
10,00	-2,46	-0,43	0,3264E 00	0,1141E 01	-0,8794E 00	-0,1197E 00	0,1477E 01
20,00	-2,35	-0,86	0,5240E 00	0,2145E 01	-0,5321E 00	-0,9614E -01	0,6432E 01
30,00	-2,17	-1,25	0,5000E 00	0,2890E 01	-0,6581E -05	-0,4511E -01	0,1054E 02
40,00	-1,92	-1,61	0,2732E 00	0,3286E 01	0,6527E 00	0,1544E -01	0,1317E 02
50,00	-1,61	-1,92	-0,2660E 00	0,3286E 01	0,1347E 01	0,6621E -01	0,1399E 02
60,00	-1,25	-2,17	-0,8660E 00	0,2890E 01	0,2000E 01	0,9208E -01	0,1297E 02
70,00	-0,86	-2,35	-0,1440E 01	0,2145E 01	0,2532E 01	0,8617E -01	0,1049E 02
80,00	-0,43	-2,46	-0,1851E 01	0,1141E 01	0,2879E 01	0,5154E -01	0,7002E 01
90,00	0,00	-2,50	-0,2000E 01	0,1265E -04	0,3000E 01	0,5923E -06	0,3152E 01
-80,00	-0,43	-2,46	-0,1851E 01	-0,1141E 01	0,2879E 01	-0,5154E -01	-0,5178E 00
-70,00	-0,86	-2,35	-0,1440E 01	-0,2145E 01	0,2532E 01	-0,8617E -01	-0,3489E 01
-60,00	-1,25	-2,17	-0,8660E 00	-0,2890E 01	0,2000E 01	-0,9208E -01	-0,5825E 01
-50,00	-1,61	-1,92	-0,2660E 00	-0,3286E 01	0,1347E 01	-0,6621E -01	-0,7159E 01
-40,00	-1,92	-1,61	0,2732E 00	-0,3286E 01	0,6527E 00	-0,1544E -01	-0,7646E 01
-30,00	-2,17	-1,25	0,5000E 00	-0,2890E 01	0,7391E -05	0,4510E -01	-0,7491E 01
-20,00	-2,35	-0,86	0,5240E 00	-0,2145E 01	-0,5321E 00	0,9614E -01	-0,6433E 01
-10,00	-2,46	-0,43	0,3264E 00	-0,1141E 01	-0,8794E 00	0,1197E 00	-0,4964E 01
0,00	-2,50	-0,00	0,1968E -04	-0,2111E -04	-0,1000E 01	0,1042E 00	-0,2924E 01

---

APPENDIX VII

---

COMPUTER PROGRAM - CURVED BEAM METHOD

---

## APPENDIX VII

### COMPUTER PROGRAM - CURVED BEAM METHOD

#### VII.1 Program Abstract

This program computes the stresses at the edge of a hole in the web of a flanged beam using the curved beam method described in Chapters 2 and 3. This can be used for unreinforced and circularly reinforced holes. The stresses are calculated at  $5^\circ$  intervals for a region of  $\pm 45^\circ$  from the vertical centreline of the hole, for both the upper and lower portions of the beam. Flange stresses are also computed at the same intervals.

#### VII.2 Input Data Requirement

(a) First card: (FORMAT 8F10.3)

Read in the dimensions of beam section, radius of hole, eccentricity, reinforcement width and thickness.

D = Beam depth;

B = Beam flange width;

T = Beam flange thickness;

W = Beam web thickness;

R = Radius of hole;

ECC = Eccentricity of hole centre with respect to the beam's mid-depth; equal to 0 for mid-depth holes;

BR = Width of reinforcement;

TR = Thickness of reinforcement.

(b) Second card: (FORMAT 2F10.3)

Read in the elastic and shear moduli.

E = Elastic modulus;

G = Shear modulus.

(c) Third card: (FORMAT I5)

Read in the number of moment-shear combination that stresses are to be computed.

N = Number of moment-shear combinations.

(d) Read in different sets of moment and shear (M,V) (FORMAT 2F10.3)

One card for each set, that is, there will be N number of cards.

(e) Repeat procedures (a), (b), (c) and (d) for other beam sections, if any.

(f) Terminate the program by reading in a card with a zero or a negative number.

### VII.3 Output Data

$V_T$  = Shear force for the upper beam section at hole centreline;

$V_B$  = Shear force for the lower beam section at hole centreline;

EQUIVALENT BR = Reduced width of reinforcement;

BETA = The angle of a section measured from the vertical;

AREA = Area of a section;

$I^*$  = Moment of inertia of a section;

P. = Resulting axial force acting at the centroid of a section;

M = Resulting moment at a section;

CH = Distance of the centroid of a section from the hole edge;

CF = Distance of the centroid of a section from the edge of  
the flange;

FIF = Stresses at the flanges;

FIH = Stresses at the hole edge before multiplying by K  
factor;

K = Stress concentration factor;

FMS = Stresses at hole edge after multiplying by K factor.

#### VII.4 Program Listing and Sample Output

A program listing and a sample output are shown on  
Pages 136 to 141.

```

REAL IN,M
COMMON D,P,T,W,R,ECC,PI,F,G,BR,TR
1 FORMAT(8F10.3)
2 FORMAT('D= ',F7.3,5X,'R= ',F7.3,5X,'T= ',F7.3,5X,'W= ',F7.3,5X,
*      'P= ',F7.3,5X,'ECC= ',F7.3,5X,' BR= ',F7.3,5X,' TR= ',
*      F7.3)
3 FORMAT(I5)
4 FORMAT(2F10.2)
5 FORMAT('OM= ',F7.3,5X,'V= ',F7.3,5X,'VI= ',F7.3,5X,'VP= ',F7.3)
6 FORMAT('UPPER TFF'/' -----')
7 FORMAT('HIGH MOMENT SIDE')
8 FORMAT('LOW MOMENT SIDE')
9 FORMAT('LOWER TFF'/' -----')
PI=3.1415927
21 READ 1,D,B,T,W,R,ECC,BR,TR
IF(D.LE.0) GO TO 22
READ 4,F,G
PRINT 2,D,P,T,W,R,ECC,BR,TR
CALL EQUIV(BR,TR,R,W)
CALL SHOOTV(V1,V2)
PRINT 2000,BR
2000 FORMAT('O', 'EQUIVALENT BR =',1X,F6.3)
HT=(D-2.*T)/2.-(R+ECC+TR)
HR=(F-2.*T)/2.-(R-ECC+TR)
AY=B*T*(D-2.*T)/2.+B*T*(D-T/2.)+W*HT*(T+HT/2.)+W*HR*(D-T-HR/2.)
*      +BR*TR*(T+HT+TR/2.)+BR*TR*(T+HT+TR+2*R+TR/2.)
A=2*B*T+2*BR*TR+(HT+HR)*W
Y=AY/A
Y1=D-Y
IN=B*T**3/12.+B*T*(Y-T/2.)**2+W*HT**3/12.+W*HT*(Y-T-HT/2.)**2+B*T
*      **3/12.+B*T*(Y1-T/2.)**2+W*HR**3/12.+W*HR*(Y1-T-HR/2.)**2
*      +2*BR*TR**3/12.+BR*TR*(Y-T-HT-TR/2.)**2+BR*TR*(Y-T-HT-(R-2*R-T/
*      2.))**2
READ 3,M
DO 20 I=1,M
READ 4,M,V
VT=V1*V
VR=V2*V
PRINT 5,M,V,VT,VR
FT1=M*Y/IN
FT2=FT1*(Y-T)/Y
FT3=FT1*(Y-T-HT)/Y
FT4=FT1*(Y-T-HT-TR)/Y
PT1=B*T*(FT1+FT2)/2.
PT2=HT*W*(FT2+FT3)/2.
PT3=BR*TR*(FT3+FT4)/2.
ZT1=T/3.*(FT1+2*FT2)/(FT1+FT2)
ZT2=HT/3.*(FT2+2*FT3)/(FT2+FT3)
ZT3=TR/3.*(FT3+2*FT4)/(FT3+FT4)
IF(Y.LE.(T+HT+TR+2*R)) GO TO 900
IF(Y.GT.(T+HT+TR+2*R).AND.Y.LE.(T+HT+2*TR+2*R)) GO TO 901
IF(Y.GI.(T+HT+2*TR+2*R)) GO TO 902
900 PT4=0.
PT5=0.

```

```

7T4=0.
7T5=0.
GO TO 903
901 FT5=FT1*(Y-T-HT-TP-2*R)/Y
PT4=PR*(Y-T-HT-TR-2*R)*FT5/2.
PT5=0.
7T4=(Y-T-HT-TP-2*R)/3.
7T5=0.
GO TO 903
902 FT5=FT1*(Y-T-HT-TP-2*R)/Y
FT6=FT1*(Y-T-HT-2*TR-2*R)/Y
PT4=PR*TR*(FT5+FT6)/2.
PT5=PR*(Y-T-HT-2*TR-2*R)*FT6/2.
7T4=TP/3.*(FT5+2*FT6)/(FT5+FT6)
7T5=(Y-T-HT-2*TP-2*R)/3.
903 PT0=PT1+PT2+PT3+PT4+PT5
ZT=(PT1-ZT1+PT2*(ZT2+T)+PT3*(ZT3+T+HT)+PT4*(ZT4+T+HT+TR+2*R)
+PT5*(ZT5+2*TR+2*R+HT+T))/PT0
PRINT 6
PRINT 8
CALL STRESS(PT0,VT,7T,HT)
VT=-VT
PRINT 7
CALL STRESS(PT0,VT,7T,HT)
FB1=-R*Y1/IN
FB2=FP1*(Y1-T)/Y1
PB1=PR*T*(FB1+FB2)/2.
ZB1=T/3.*(FB1+2.*FB2)/(FB1+FB2)
IF((Y1-T-HB).LE.0) GO TO 1000
IF((Y1-T-HB).GT.0.AND.(Y1-T-HB-TR).LE.0) GO TO 1001
IF((Y1-T-HB-TR).GT.0) GO TO 1002
1000 PB2=(Y1-T)*W*FB2/2.
ZB2=(Y1-T)/3.
PB3=0.
GO TO 1003
1001 FB3=FP1*(Y1-T-HB)/Y1
PB2=PR*W*(FB2+FB3)/2.
ZB2=HB/3.*(FB2+2.*FB3)/(FB2+FB3)
PB3=(Y1-T-HB)*PR*FB3/2.
ZB3=(Y1-T-HB)/3.
GO TO 1003
1002 FB3=FP1*(Y1-T-HB)/Y1
FB4=FP1*(Y1-T-HB-TR)/Y1
PB2=PR*W*(FB2+FB3)/2.
PB3=PR*TR*(FB3+FB4)/2.
ZB2=HB/3.*(FB2+2*FB3)/(FB2+FB3)
ZB3=TR/3.*(FB3+2*FB4)/(FB3+FB4)
1003 PPO=PB1+PB2+PB3
ZE=(PB1*ZB1+PB2*(T+ZB2)+PB3*(T+HB+ZB3))/PPO
PRINT 9
PRINT 7
CALL STRESS(PPO,VR,ZB,HB)
VR=-VR
PRINT 8

```

```

CALL STRESS(P,VC,ZB,HR)
20 CONTINUE
GO TO 2)
22 STOP
END

```

```

SUBROUTINE STRESS(P0,VS,Z,HS)
REAL I,MS,K
COMMON D,R,T,W,R,ECC,PI,F,G,RR,TR
PRINT 1)
1 FORMAT ('SECTION',T13,'BETA',T23,'AREA',T34,'I',T44,'P',T54,'M',
* T64,'CH',T74,'CF',T83,'FIF',T93,'FIH',T104,'K',T113,'FMS')
DO 10 J=1,10
J1=J-1
X=J1*5
BETA=PI*X/180.
P=P0*COS(BETA)+VS*SIN(BETA)
H=(HS+P+TR+1)/COS(BETA)-R
TT=T/COS(BETA)
CALL M(D,PI,H,W,RR,TR,AR,Y,T)
EC=Y*COS(BETA)-Z
ARM=(P+H)*SIN(BETA)-Y*SIN(BETA)
MS=P0*EC-VS*ARM
CH=H-Y
CF=Y
FAXIAL=-P/AR
FBENDH=MS*CH/I
FBENDE=MS*CF/I
FIF=FAXIAL-FBENDE
FIH=FAXIAL+FBENDH
CALL FACTOR(CH,CF,AR,RR,GG,TT)
SIGCR=-HS*GG/(AR*RR)
K=-GG*I/(CF*AR*RR)
FMS=FIH*K
10 PRINT 2,J,X,AR,I,P,MS,CH,CF,FIF,FIH,K,FMS
2 FORMAT (' ',I5,11F10.2)
RETURN
END

```

```

SUBROUTINE SHRDIV(V1,V2)
COMMON D,R,T,W,R,ECC,PI,F,G,BR,TR
DIMENSION Z1(101),Z2(101)
H10=D/2.-T-ECC
CALL INTGR(H10,Z1,Z2,N)
T1=P**2*Z1(N)/F
T2=Z2(N)/G
T4=T1+T2
H10=D/2.-T+ECC
CALL INTGR(H10,Z1,Z2,N)
B1=R**2*Z1(N)/E
B2=Z2(N)/G
B4=B1+B2
V1=B4/(T4+B4)
V2=T4/(T4+B4)
RETURN
END

```

```

SUBROUTINE MI(SB1,ST1,SD,SW,SB2,ST2,SAREA,SY,SXI)
H=SD-ST1-ST2
A1=SB1*ST1
A2=H*SW
A3=SB2*ST2
SAREA=A1+A2+A3
X1=A1*ST1/2.
X2=A2*(H/2.+ST1)
X3=A3*(SD-ST2/2.)
SY=(X1+X2+X3)/SAREA
XI1=(SB1*ST1**3)/12.+A1*(SY-ST1/2. )**2
XI2=(SW*H**3)/12.+A2*(H/2.+ST1-SY)**2
XI3=(SB2*ST2**3)/12.+A3*(SD-ST2/2.-SY)**2
SXI=XI1+XI2+XI3
RETURN
END

```

```

SUBROUTINE EQUIV(BR,TR,P,W)
BP=(BR-W)/2.
RRR=R+TR/2.
XX=BP**2/(RRR*TR)
ALPHA=.093466-.5142517*XX+.1284400*XX**2-.01121116*XX**3
BR=2.*ALPHA*BP+W
RETURN
END

```

```

SUBROUTINE INTGR(H0,Z1,Z2,N)
COMMON D,B,T,W,R,ECC,PI,F,G,RR,TR
REAL I,K1
DIMENSION F(101),Z(101),Z1(101),Z2(101)
PI2=PI/2.
H=PI2/100.
DO 1 J=1,101
K=J-1
X=K*H
BETA=ARCSIN(R*SIN(X)/(R+TR))
XI=H0-(R+TR)*COS(BETA)
ETA=(R+TR)*COS(BETA)-R*COS(X)
A=B*T+XI**2+BR*ETA
Y=(B*T**2/2.+X*I**2*(T+XI/2.))+BR*ETA*(T+XI+ETA/2.)/A
HH=H0+T-R*COS(X)
Y1=HH-Y
I=B*T**3/12.+R*T*(T-T/2.）**2+W*XI**3/12.+W*XI*(T+XI/2.-Y)**2
* +BR*ETA**3/12.+BR*ETA*(T+XI+ETA/2.-Y)**2
F(J)=SIN(X)**2*COS(X)/I
IF(Y.LE.T) K1=(BR*ETA*(XI+ETA/2.)+W*XI**2/2.)/(I*W)
IF(Y.GT.T) K1=(BR*ETA*(Y1-ETA/2.)+W*(Y1-ETA)**2/2.)/(I*W)
Z(J)=K1*COS(X)
1 CONTINUE
N=101
CALL QSF(H,F,Z1,101)
CALL QSF(H,Z,Z2,101)
RETURN
END

```

```

SUBROUTINE FACTD(CH,CF,ARR,RR,GG,TT)
COMMON D,B,T,W,R,ECC,PI,F,G,RR,TR
U1=CF
U2=CH
U3=CH-TT
U4=U1-TT
RR=R+U2
Z71=PI*ALOG(RR+U1)
Z72=(U-B)*ALOG(RR+U4)
Z73=(RR-U)*ALOG(RR-U3)
Z74=RR*ALOG(RR-U2)
Z7=-1.+RR/ARR*(Z71+Z72+Z73-Z74)
GG=1.-U2/(Z7*(RR-U2))
RETURN
END

```

U= 14.120 R= 6.780 T= 0.513 W= 0.313 K= 2.250 ECC= 2.500 BR= 3.500 IR= 0.250

EQUIVALENT BR = 1.482

M= 480.000 V= 10.000 VT= 2.429 VS= 7.571

UPPER TEE

LOW MOMENT SIDE

SECTION	BETA	AREA	I	P	M	CH	CF	FIF	FIH	K	FMS
1	0.0	4.33	1.73	37.35	1.17	1.77	0.54	-8.98	-7.42	1.15	-8.57
2	5.00	4.35	1.76	37.42	0.36	1.79	0.54	-8.71	-8.24	1.15	-9.51
3	10.00	4.41	1.87	37.21	-0.36	1.83	0.55	-8.34	-3.90	1.16	-10.19
4	15.00	4.50	2.06	36.71	-1.07	1.90	0.57	-7.90	-9.10	1.16	-10.57
5	20.00	4.64	2.36	35.93	-1.62	2.01	0.59	-7.34	-9.13	1.17	-10.67
6	25.00	4.82	2.80	34.89	-2.18	2.15	0.63	-6.74	-8.91	1.18	-10.50
7	30.00	5.07	3.47	33.56	-2.73	2.34	0.67	-6.10	-8.47	1.19	-10.10
8	35.00	5.38	4.45	31.99	-3.31	2.59	0.72	-5.40	-7.97	1.21	-9.51
9	40.00	5.78	5.96	30.18	-3.95	2.90	0.80	-4.69	-7.14	1.23	-8.73
10	45.00	6.30	8.33	28.13	-4.71	3.30	0.90	-3.96	-6.33	1.26	-7.99

HIGH MOMENT SIDE

SECTION	BETA	AREA	I	P	M	CH	CF	FIF	FIH	K	FMS
1	0.0	4.33	1.73	37.35	1.17	1.77	0.54	-8.98	-7.42	1.15	-8.57
2	5.00	4.35	1.76	37.00	2.07	1.79	0.54	-9.14	-6.40	1.15	-7.39
3	10.00	4.41	1.87	36.36	3.08	1.83	0.55	-9.16	-5.24	1.16	-6.06
4	15.00	4.50	2.06	35.43	4.21	1.90	0.57	-9.04	-3.99	1.16	-4.63
5	20.00	4.64	2.36	34.27	5.46	2.01	0.59	-8.76	-2.73	1.17	-3.19
6	25.00	4.82	2.80	32.93	6.86	2.15	0.63	-8.34	-1.53	1.18	-1.81
7	30.00	5.07	3.47	31.13	8.43	2.34	0.67	-7.78	-0.45	1.19	-0.53
8	35.00	5.38	4.45	29.21	10.17	2.59	0.73	-7.09	0.48	1.21	0.58
9	40.00	5.78	5.96	27.05	12.13	2.90	0.80	-6.31	1.23	1.23	1.51
10	45.00	6.30	8.33	24.70	14.36	3.30	0.90	-5.47	1.77	1.26	2.24

APPENDIX VIII

SUPPLEMENTAL RESULTS

## APPENDIX VIII

### SUPPLEMENTAL RESULTS

This appendix provides additional results which were not included in the paper reproduced as Chapter 2.

Tangential normal stresses around the large holes (10½ inch and 8 inch diameters) of Beam A are shown in Figures VIII.1 and VIII.2 for M/V ratio of 48 inches. Also plotted on the same diagrams are the stresses obtained from theory of elasticity solution and the curved beam method. Similar to the case of M/V = 24 inches, the theory of elasticity solution underestimates the stresses considerably, and the curved beam method predicts the stresses accurately in most locations. This further indicates that the curved beam method is the appropriate method to use in analysing large holes.

Experimental results for shear stresses at the centreline of the hole was given only for the 8 inch diameter hole in Chapter 2. Similar plots for the other holes are shown in Figures VIII.3 to VIII.5. Fair agreement between the experimental stresses and the predicted stresses is observed in all cases.

The experimental shear stresses obtained by Fröst<sup>10</sup> for holes of diameters 6.5 inch and 6.4 inch with eccentricity

of 1.0 inch and 2.0 inch respectively are shown on Figure VIII.6. Plotted on the same diagram are the shear stress distribution based on the unequal shear force obtained by Equations 2-8 and 2-9. Good agreement is observed in both cases.

Results for flange stresses not presented in Chapter. 2 are shown in Figures VIII.7 to VIII.11.

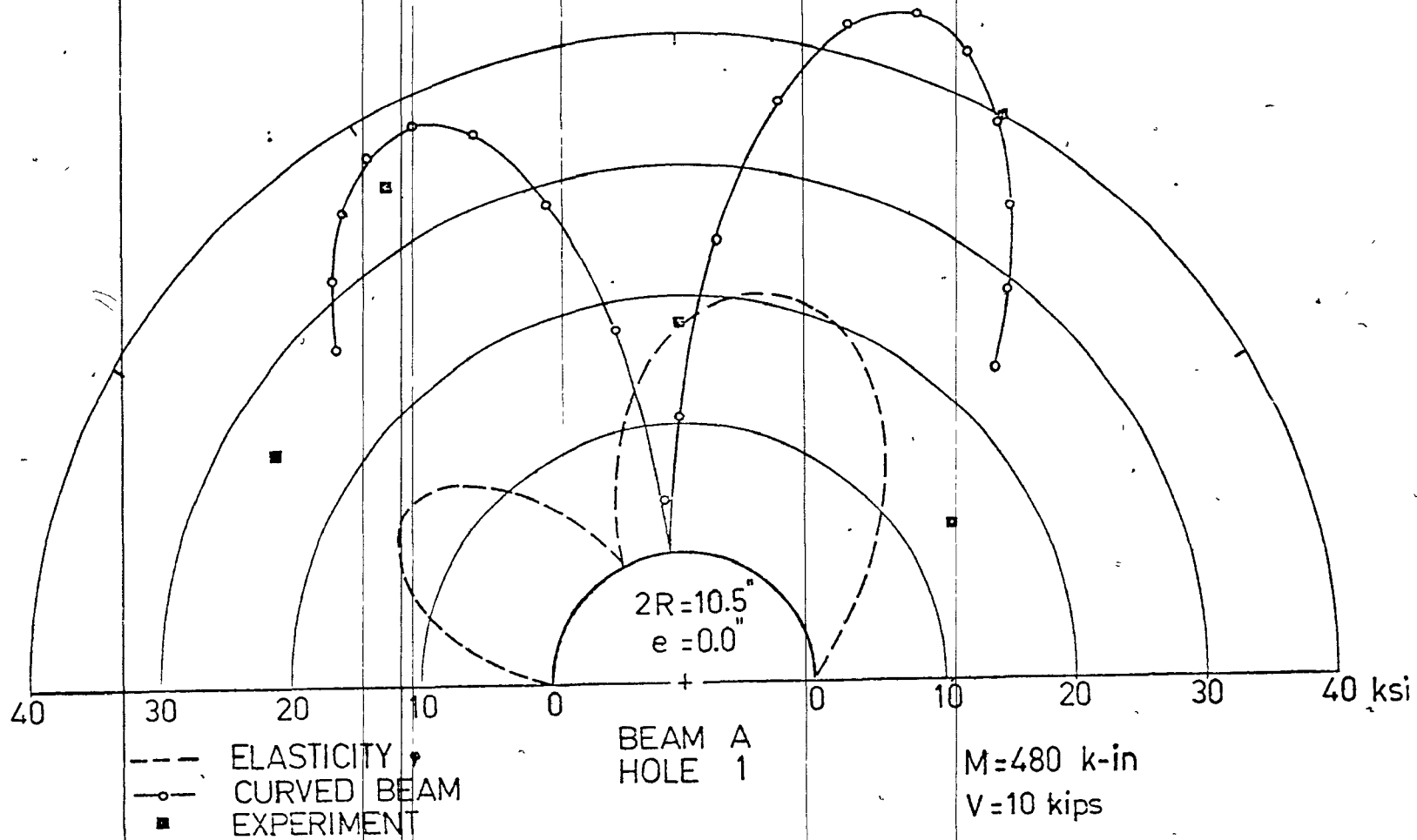
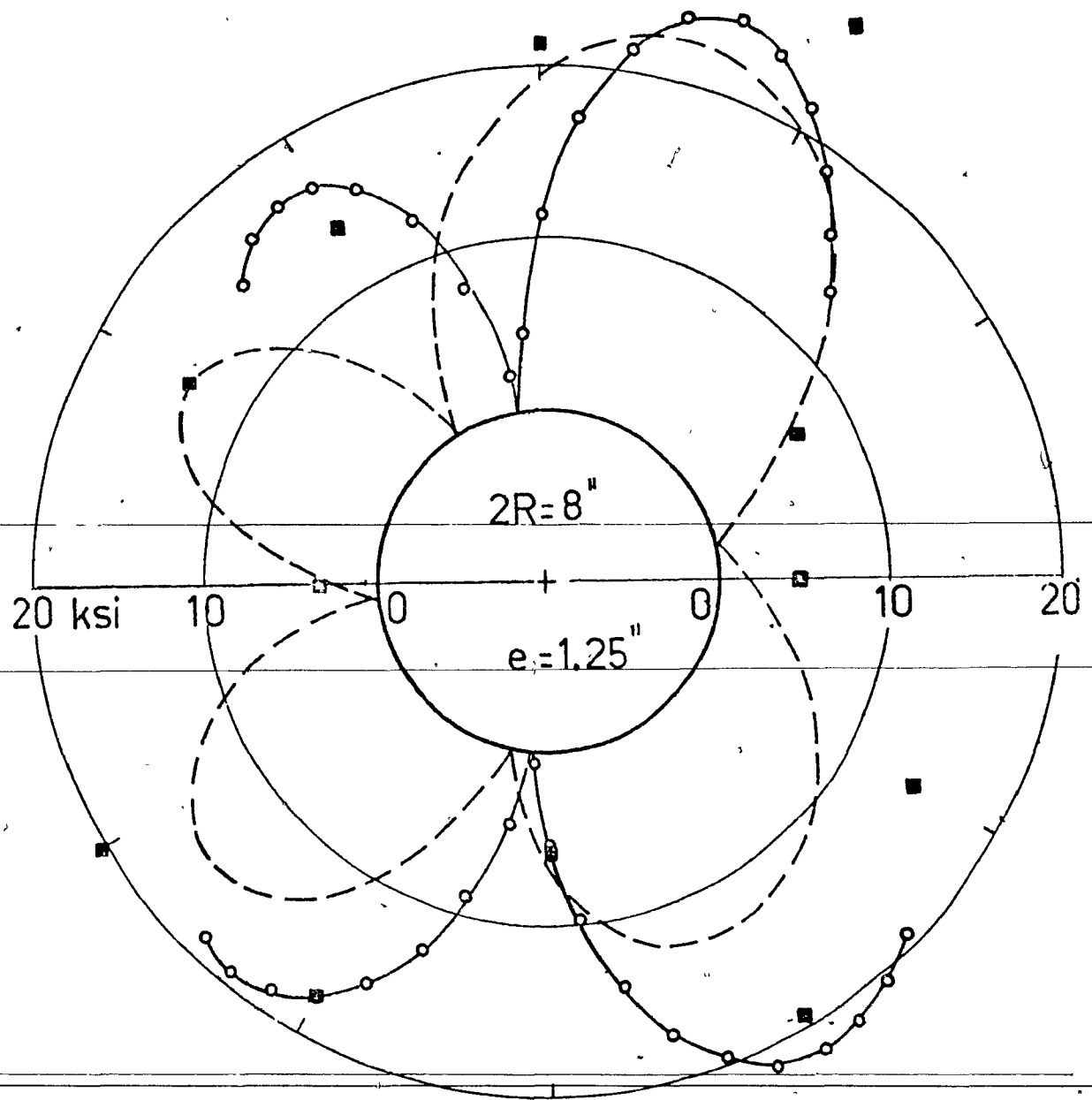


Figure VIII.1 Hole Edge Stresses For Hole 1, Beam A  
 ( $M/V = 48''$ )



---	ELASTICITY	BEAM A	M=480 k-in
—○—	CURVED BEAM	HOLE 2	V=10 kips
■	EXPERIMENT		

Figure VIII.2 Hole Edge Stresses For Hole 2, Beam A  
( $M/V = 48''$ )

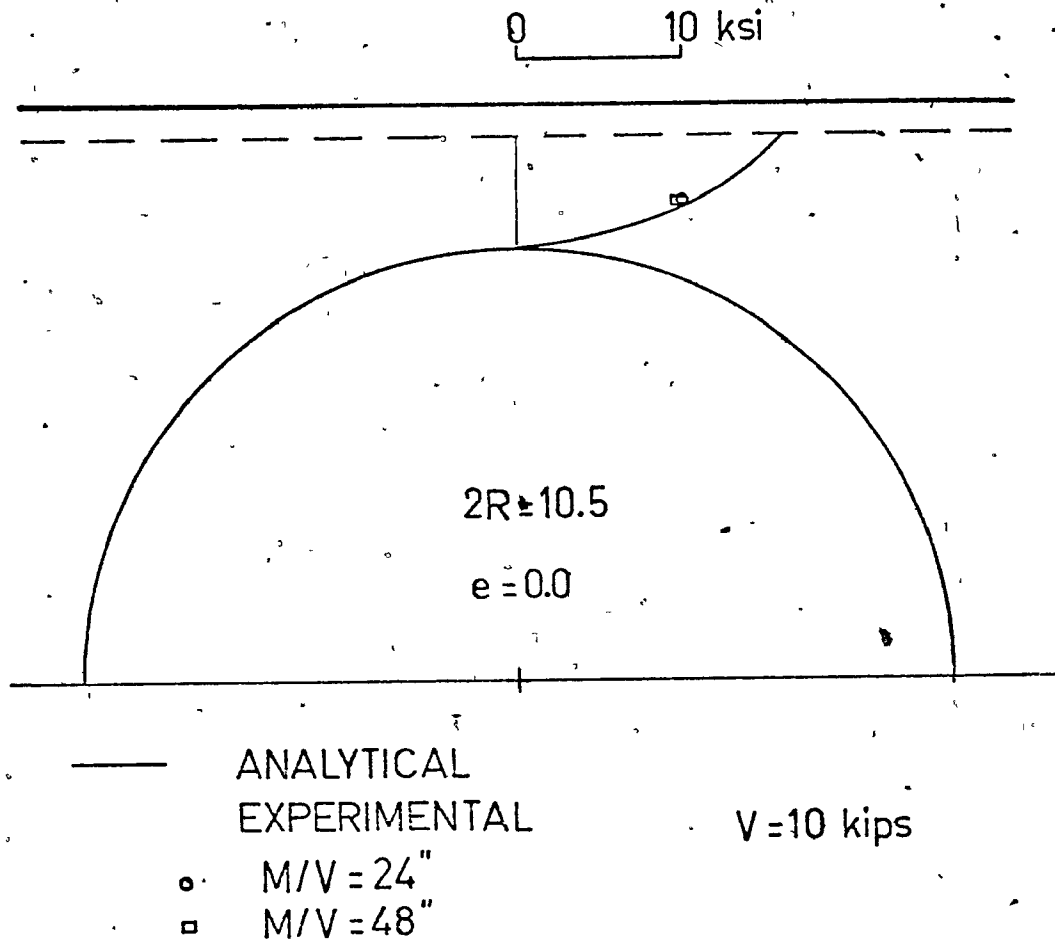


Figure VIII.3 Shear Stresses At Hole Centreline For Hole 1, Beam A

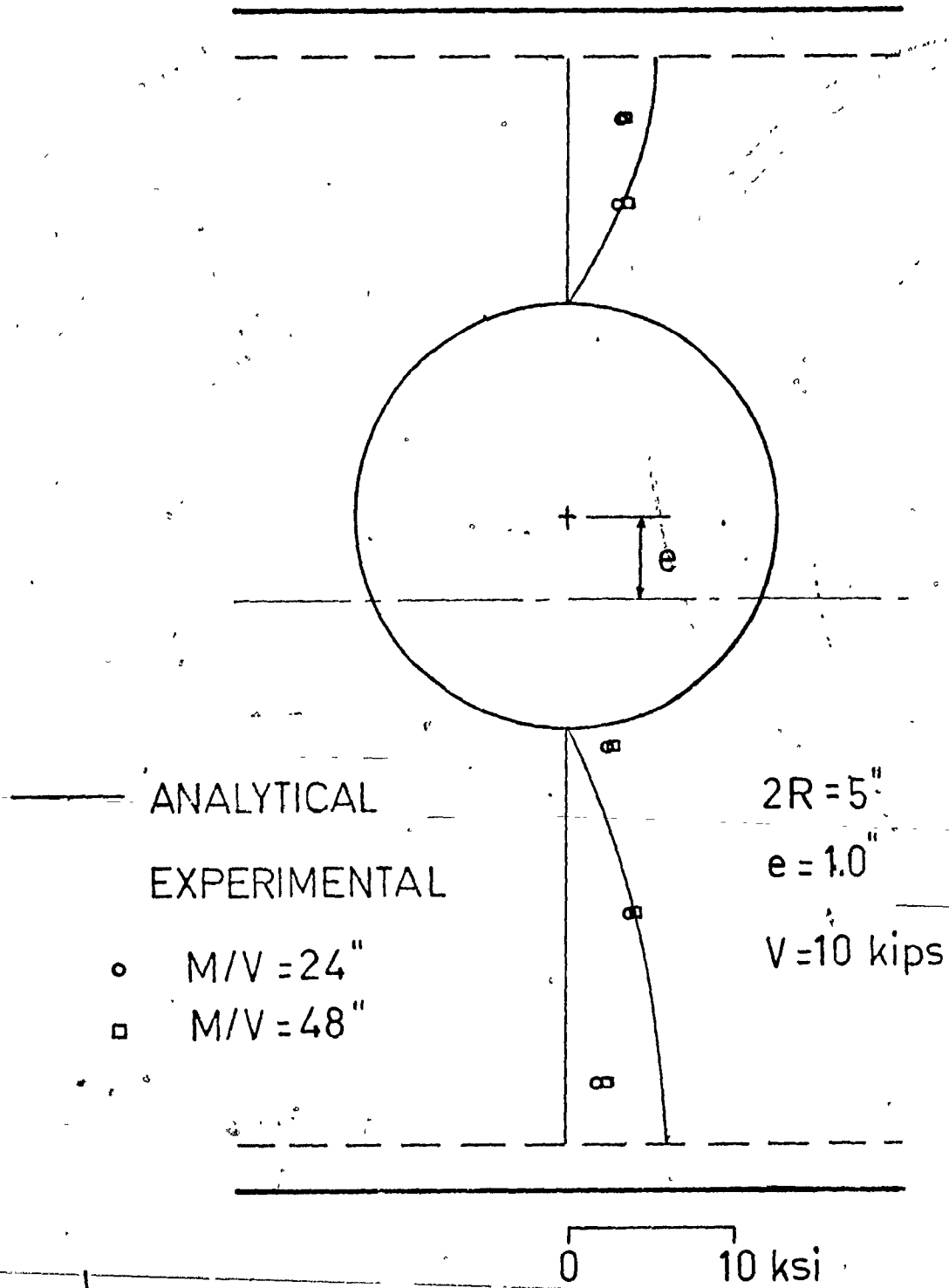


Figure VIII.4 Shear Stresses At Hole Centreline  
For Hole 3, Beam B

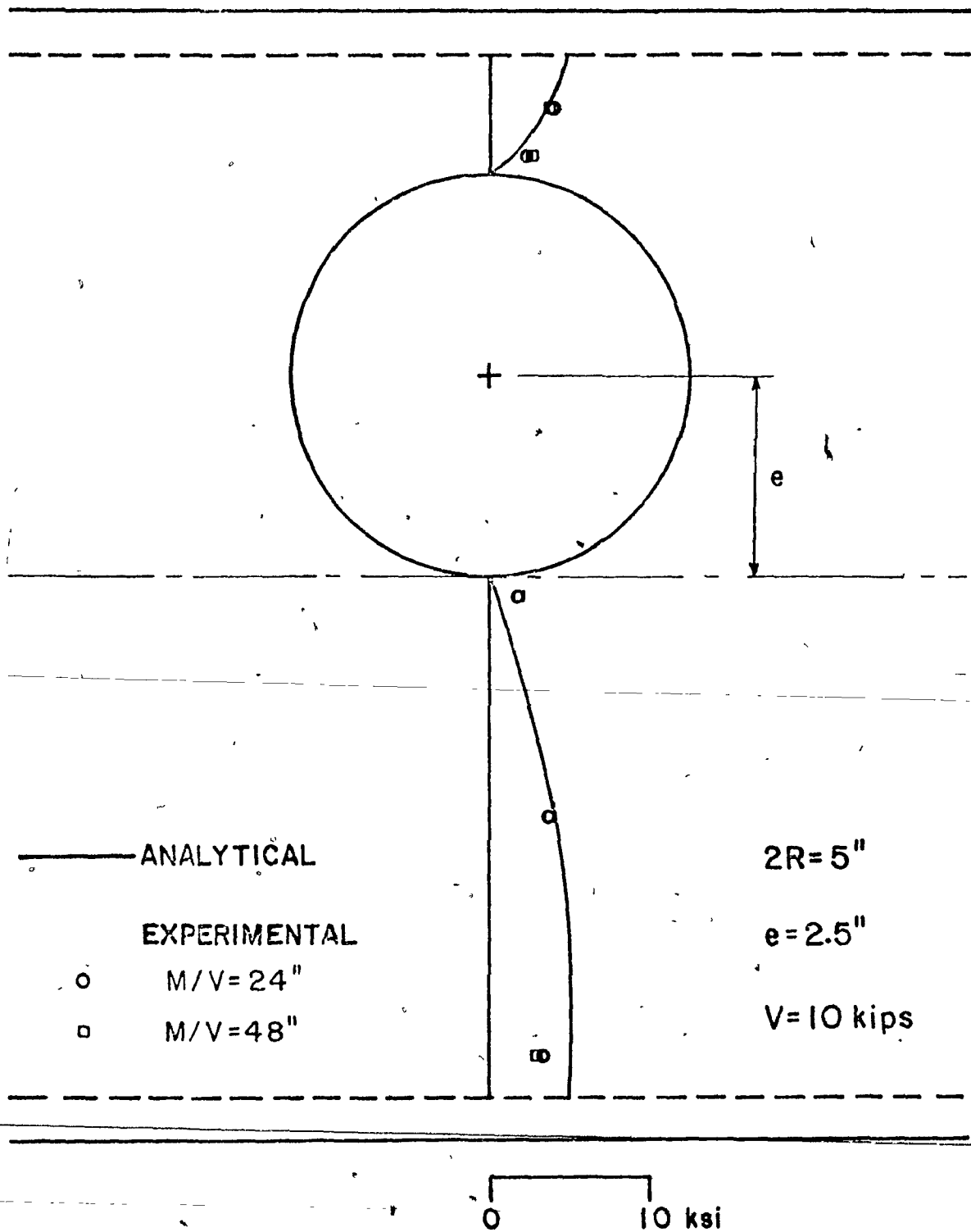


Figure VIII.5 Shear Stresses At Hole Centreline  
For Hole 4, Beam B

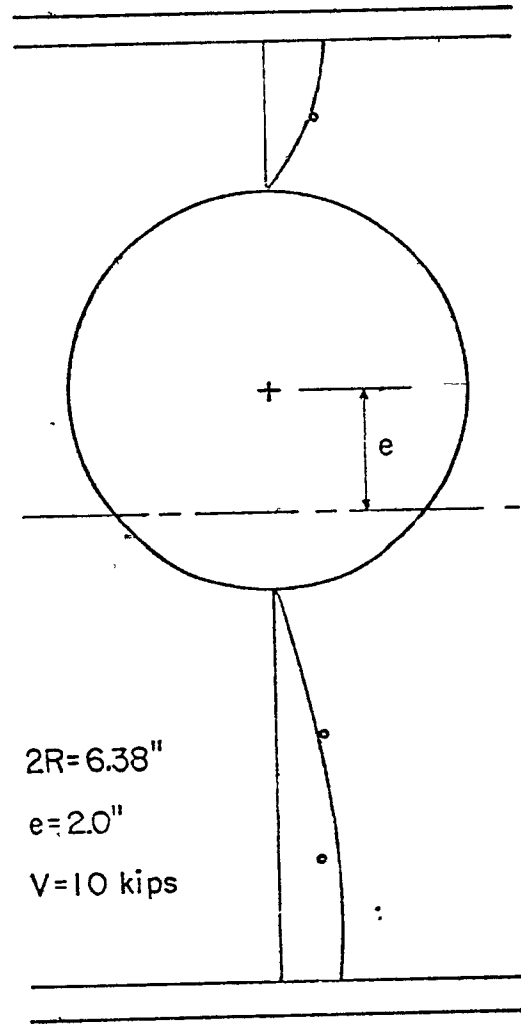
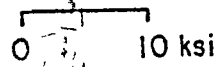
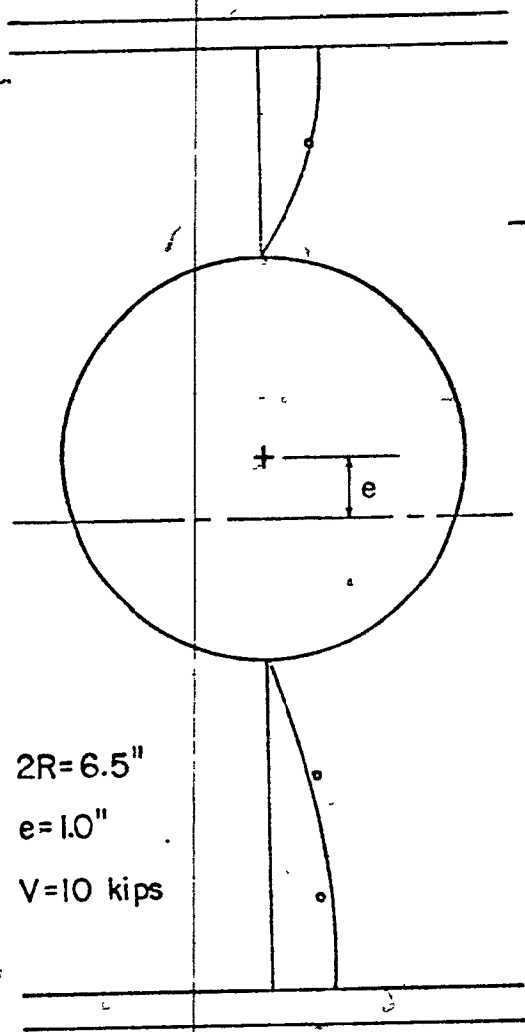
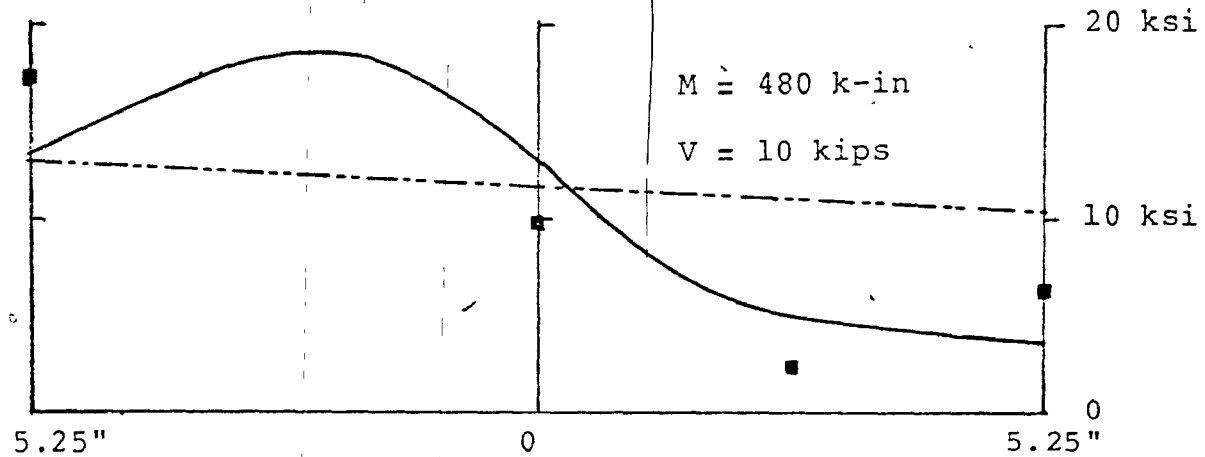
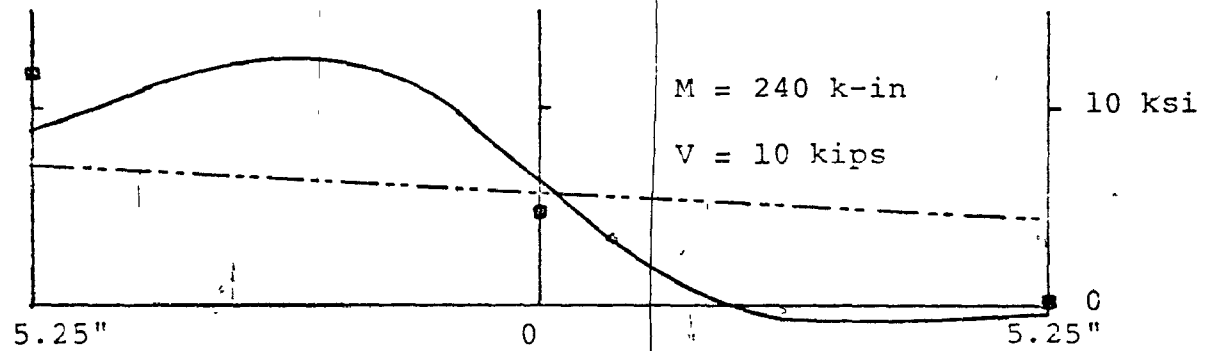


Figure VIII.6 Comparison of Results Obtained in Ref. 10

Figure VIII.7 Flange Stresses for Hole 1, Beam A



$10\frac{1}{2}$ " HOLE

$e = 0$

- SIMPLE BEAM
- CURVED BEAM
- EXPERIMENT

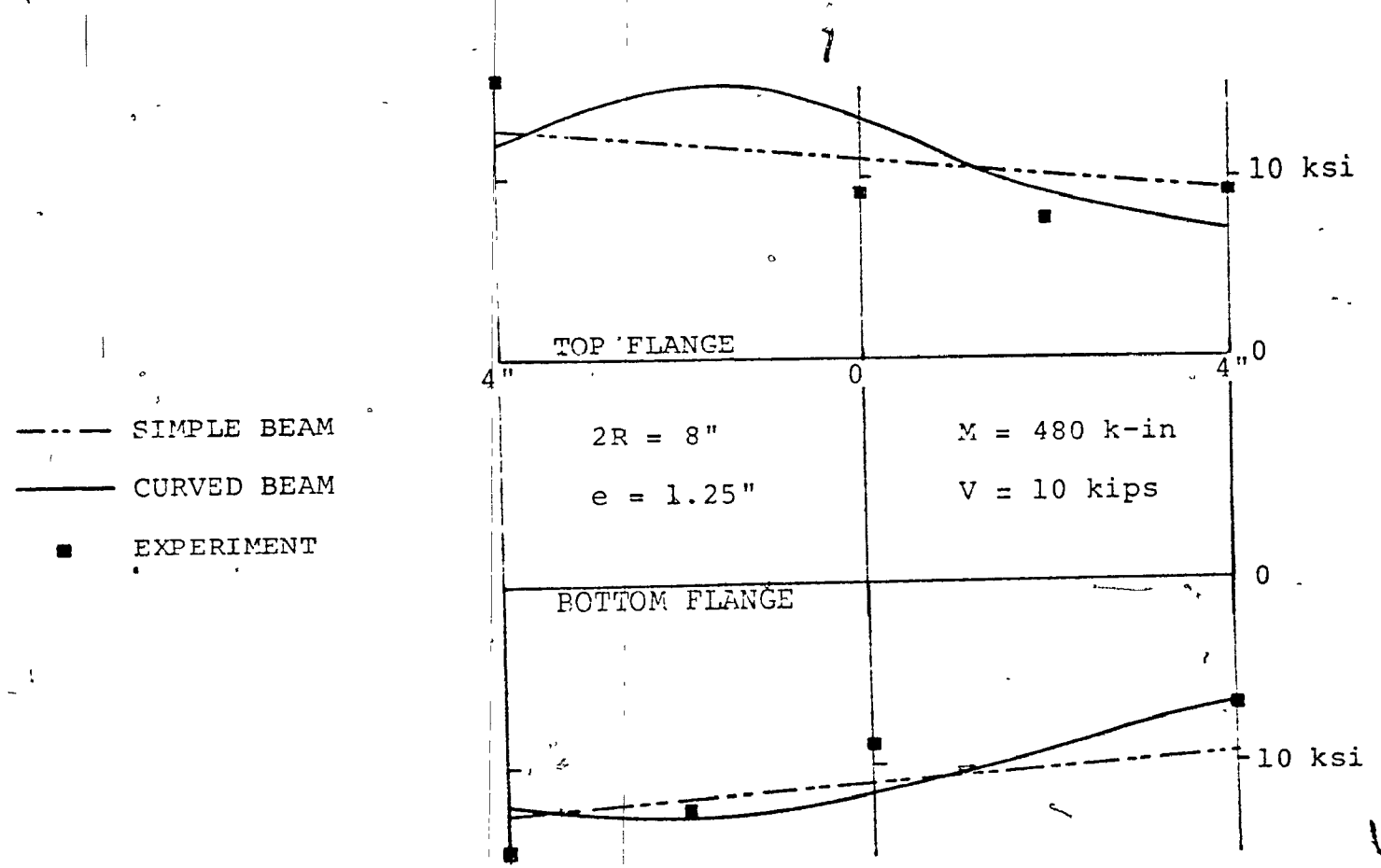


Figure VIII.8 Flange Stresses For Hole 2, Beam A  
( $M/V = 48"$ )

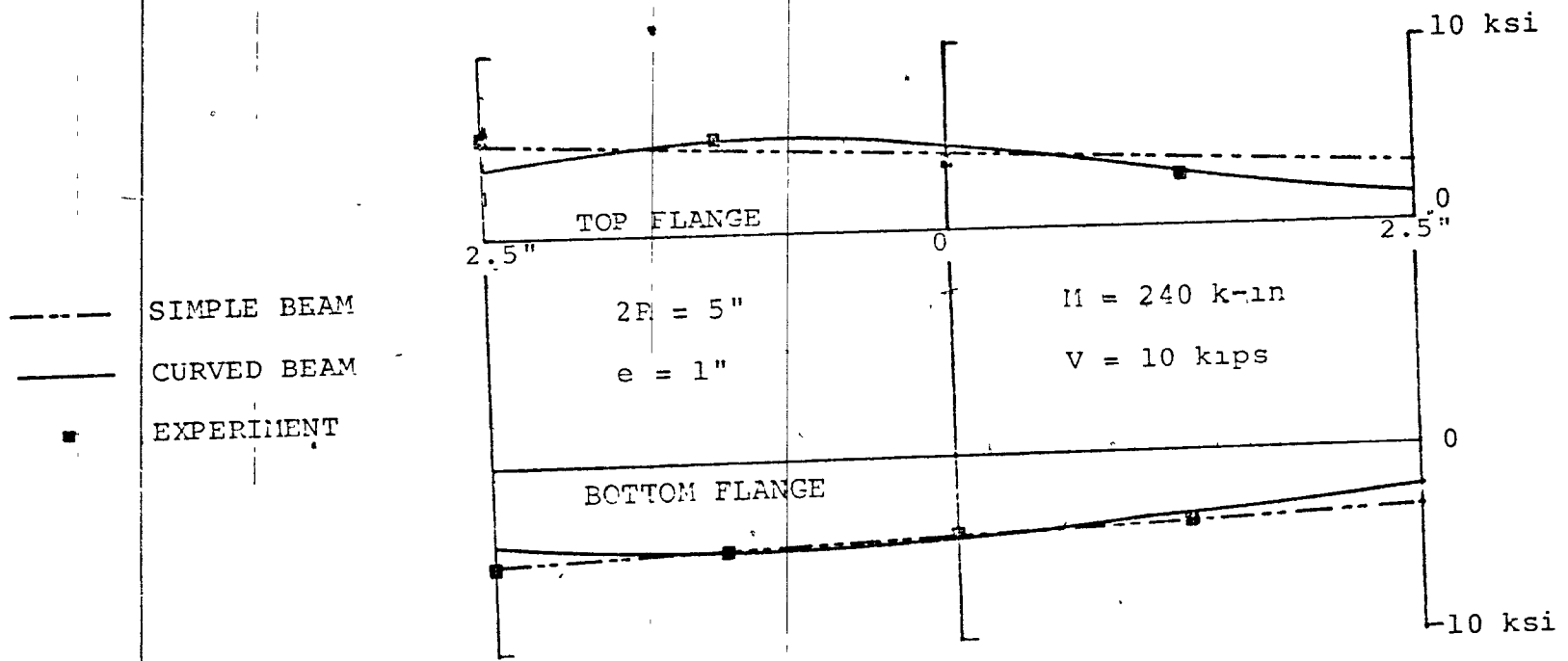


Figure VIII.9 Flange Stresses For Hole 3, Beam B<sup>o</sup>  
(M/V = 24")

--- SIMPLE BEAM  
— CURVED BEAM  
■ EXPERIMENT

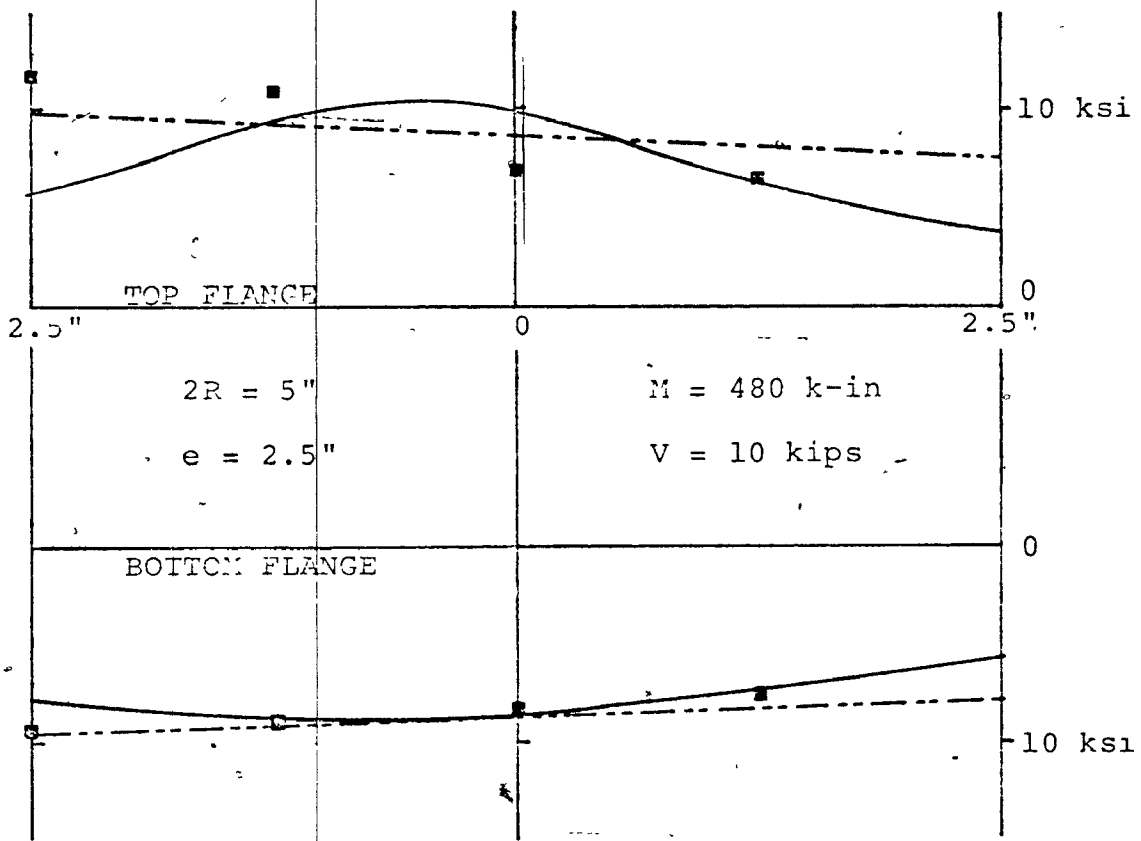


Figure VIII.10 Flange Stresses For Hole 4, Beam B  
(M/V = 48")

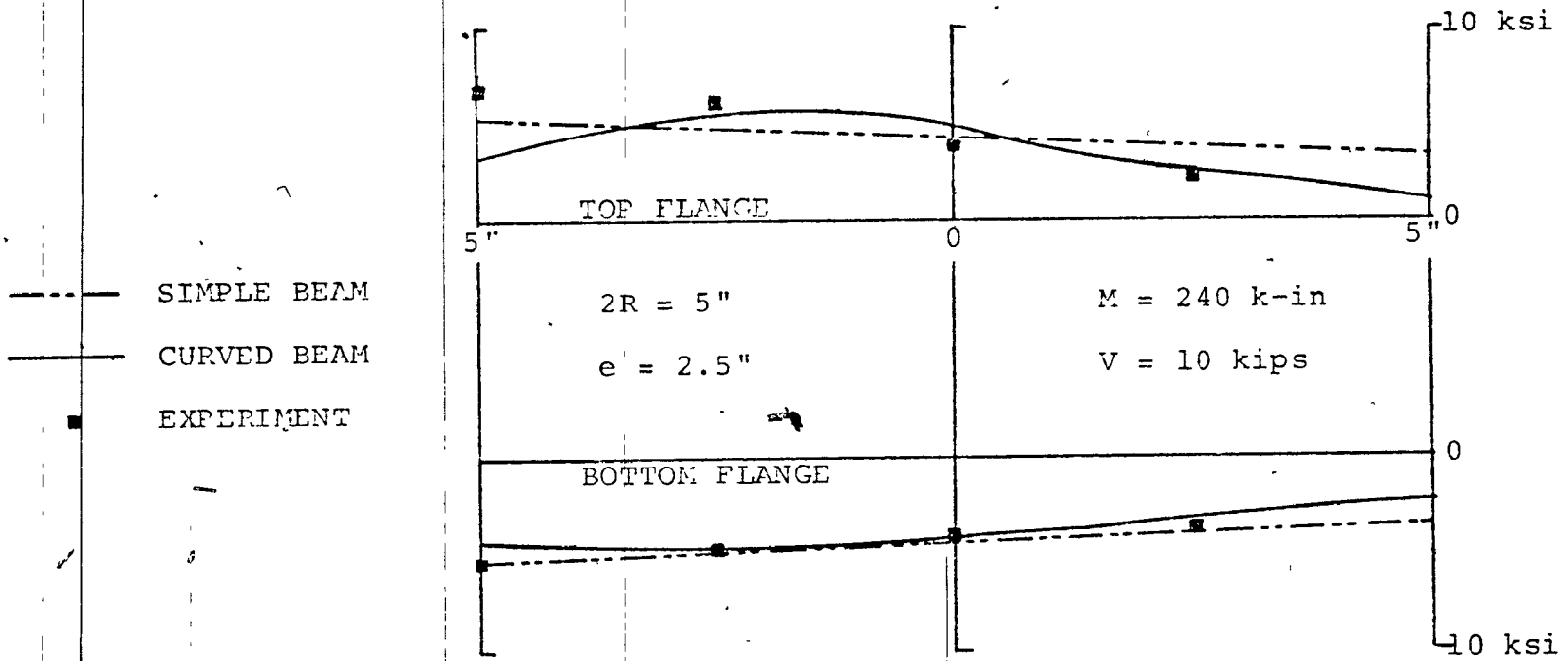


Figure VIII.11 Flange Stresses For Hole 4, Beam B.  
( $M/v = 24''$ )

BIBLIOGRAPHY

## BIBLIOGRAPHY

1. Bower, J.E., "Elastic Stresses Around Web Holes in Wide-Flange Beams", Journal of the Structural Division, ASCE, Vol. 92, No. ST2, Proc. Paper 4773, April, 1966, pp. 85-101.
2. Bower, J.E., "Experimental Stresses in Wide-Flange Beams With Holes", Journal of the Structural Division, ASCE, Vol. 92, No. ST5, Proc. Paper 4945, October, 1966, pp. 167-186.
3. Bower, J.E., "Design of Beams With Web Openings", Journal of the Structural Division, ASCE, Vol. 94, No. ST3, Proc. Paper 5869, March, 1968, pp. 783-807.
4. Bower, J.E., "Ultimate Strength of Beams With Rectangular Holes", Journal of the Structural Division, ASCE, Vol. 94, No. ST6, Proc. Paper 5982, June, 1968.
5. Chan, P.W., "Approximate Methods to Calculate Stresses Around Circular Holes", Report to Canadian Institute of Steel Construction, Project 695, November 1971.
6. Chan, P.W., and Redwood, R.G., "Stresses in Beams With Circular Eccentric Web Holes", Journal of the Structural Division, ASCE, Vol. 100, No. ST1, Proc. Paper 10291, January 1974, pp. 231-248.
7. Chmel, J., and Redwood, R.G., "Elastic Tests on Beams With Single Reinforced Circular Openings - Horizontal and

Circular Reinforcement", Report to Canadian Institute of Steel Construction, December, 1969.

8. Congdon, J.G., and Redwood, R.G., "Plastic Behavior Of Beams With Reinforced Holes", Journal of the Structural Division, ASCE, Vol. 96, No. ST9, Proc. Paper 7561, September, 1970, pp. 1933-1956.
9. Cooper, P.B., and Snell, R.R., "Tests On Beams With Reinforced Web Openings", Journal of the Structural Division, ASCE, Vol. 98, No. ST3, Proc. Paper 8791, March, 1972, pp. 611-632.
10. Frost, R.W., "The Behavior Of Steel Beams With Eccentric Web Holes", presented at the October 18-22, 1971, ASCE Annual and National Environmental Engineering Meeting, held at St. Louis, Missouri.
11. Heller, S.R., Jr., Brock, J.S., and Bart, R., "The Stresses Around A Rectangular Opening With Rounded Corners In A Uniformly Loaded Plate", Proc. 3rd U.S. National Congress of Applied Mechanics, ASME, 1958.
12. Heller, S.R., Jr., Brock, J.S., and Bart, R., "The Stresses Around A Rectangular Opening With Rounded Corners In A Beam Subjected To Bending With Shear", Proceedings, 4th U.S. National Congress of Applied Mechanics, ASME, Vol. 1, 1962, pp. 489-496.

13. Redwood, R.G., "Plastic Behaviour And Design Of Beams With Web Openings", Proceedings, First Canadian Structural Engineering Conference, Canadian Steel Industries Construction Council, Toronto, February 1968.
14. Redwood, R.G., "The Strength Of Steel Beams With Unreinforced Web Holes", Civil Engineering and Public Works Review, London, Vol. 64, No. 755, June, 1969, pp. 559-562.
15. Redwood, R.G., "Stresses In Webs With Circular Openings", Final Report to the Canadian Steel Industries Construction Council, Research Project 695, December 1971.
16. Redwood, R.G., and Chan, P.W., "Design Aids For Beams With Circular Eccentric Web Holes", Journal of the Structural Division, ASCE, Vol. 100, No. ST2, Proc. Paper 10331, February, 1974, pp. 297-303.
17. Sahmel, D., "Konstruktive Ausbildung Und Naeherungsberechnung Geschweisster Biegetrager Und Torsionsstabe Mit Grossen Stegausehnerungen", Schweissen and Schneider, 1969, No. 4, (The Design, Construction And Approximate Calculation Of Welded Transverse Beams And Torsion Bars Having Pronounced Web Clearance).
18. Seely, F.B., and Smith, J.O., Advanced Mechanics of Materials, 2nd ed., John Wiley and Sons, Inc., New York, N.Y., 1967.

19. "Steel Structures for Building", Standard S16, Canadian Standards Association, 1969.
  20. "Suggested Design Guides for Beams with Web Holes", by the Subcommittee on Beams with Web Openings of the Task Committee on Flexural Members of the Structural Division, John E. Bower, Chairman, Journal of the Structural Division, ASCE, Vol.97, No. ST11, Proc. Paper 8536, November, 1971, pp. 2707-2728.
-